NSF/CEE-81076

PB82-158494

REDUCTION OF OVERTURNING POTENTIAL OF SEISMICALLY EXCITED STRUCTURES

BY

ARTHUR A. HUCKELBRIDGE, JR

ROBERT M. FERENCZ

AND

SHYA-LING SHEIN

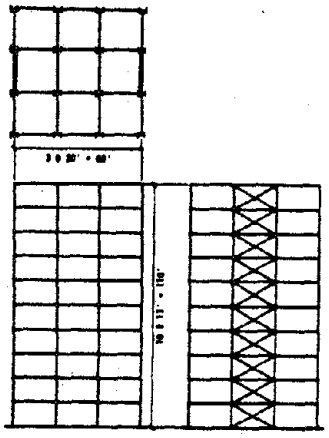

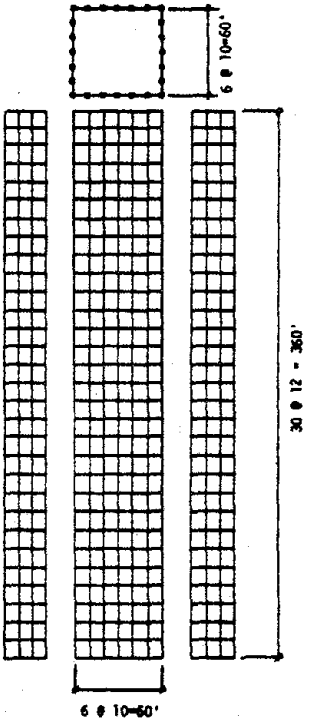

REPRODUCED BY
NATIONAL TECHNICAL
INFORMATION SERVICE
U.S. DEPARTMENT OF COMMERCE
SPRINGFIELD, VA 22161

REPORT NO.

PFR 78-08013

FINAL REPORT

MAY, 1981

DEPARTMENT OF CIVIL ENGINEERING

CASE INSTITUTE OF TECHNOLOGY

CASE WESTERN RESERVE UNIVERSITY

CLEVELAND, OHIO 44106

ABSTRACT

This report summarizes the results of a research effort directed toward a better understanding of the effects of large overturning moments upon the seismic response of structures. In particular, the influence of allowing transient foundation uplift was examined, and more efficient computational methods to treat such localized nonlinearity were incorporated into an existing general analysis program. A variety of commonly used structural types and configurations were studied, including moment frames, braced frames, shear walls and framed tubes.

For the structures examined, transient foundation uplift was found to be extremely effective in limiting response parameters governed by, or related to, overturning effects. For structures which maintained reasonable levels of ductility demand within the superstructure (and associated energy dissipation) there was little or no apparent loss in drift control associated with transient uplift.

Response parameters not arising from overturning, e.g. higher mode response effects, were not mitigated by transient foundation uplift. It was shown that, particularly for tall slender structures, story shears may be attributable to a significant degree to second or even higher mode response.

The use of substructuring techniques was shown to be computationally attractive for treating localized nonlinearity such as transient foundation uplift. The assumption of linearity within substructures obviously deserves careful consideration as to its appropriateness in a given situation.

ACKNOWLEDGEMENTS

The authors would like to express their appreciation to the Department of Civil Engineering of Case Western Reserve University which provided computational and graphics facilities. Ms. Margery O'Grady expertly and patiently typed the manuscript. Ms. Annette Messina cheerfully handled the administrtive and accounting details of the research.

Financial support of this research was provided by the National Science Foundation under Grant No. PFR-7808013. This support is gratefully acknowledged by the authors. The findings and conclusions presented, however, are those of the authors and do not necessarily reflect the views of the National Science Foundation.

TABLE OF CONTENTS

1. INTRODUCTION

Transient foundation uplift is believed to be one of the major contributing factors to the observed successful behavior of some structures during seismic events considerably more severe than those considered during the design process. Both experimental and analytical investigations have demonstrated that considerable reduction in seismic loading during severe earthquakes can potentially be realized by permitting transient uplift.

At the current time there are no completely satisfactory building code provisions which consider, in a rational manner, the extreme overturning effects associated with severe seismic excitation. Model building codes generally prescribe lateral load magnitudes which are unrealistically low for linear response to a severe seismic event. Special detailing requirements, however, intended to insure adequate available ductility for a structure's survival in case of an extreme event, are prescribed.

Model codes usually require that overturning effects associated with the prescribed loading be resisted in their entirety by the structural system, implying incorrectly that a static stability check is required to insure the safety of a structure during dynamic response. There are, in general, no provisions to insure "satisfactory" overturning behavior in the event of extreme seismic loading.

The extension of a static stability requirement to more severe lateral load cases, as required by the current California hospital code for example, may necessitate supplementary foundation anchorage for many medium and high-rise structures. The cost effectiveness of providing supplementary anchorage for increased overturning capacity is, however, suspect;

the end result may well be increased foundation and superstructure costs with only a questionable safety benefit.

In recent years a considerable interest has been shown in nonlinear seismic overturning effects for a variety of structures. Beck and Skinner investigated a slender bridge pier, (2) Meek investigated a core building, (13) Wolf and Skrikerud, (22) investigated containment vessels as well as building frames and Huckelbridge and Clough, (3,7) investigated two steel building frames. These investigations, the latter including experimental as well as analytical results, indicated that nonlinear overturning response, associated with transient uplift of the structure from the foundation, had potentially beneficial aspects. Seismic load levels were reduced in all cases, ductility demand was generally reduced and foundation overturning requirements were limited in all cases to that available from the dead weight of the structure. The experimental work, cited previously, demonstrated as well that nonlinearity of this type can be accurately predicted, at least for cases where the superstructure behavior is well understood.

1.1 Foundation Uplift as a Factor in Seismic Hazard Mitigation

In regions where seismic loadings have not historically been considered, structures have, nevertheless, been designed to resist lateral wind loading. The similarity of codified seismic and wind loads is illustrated schematically in Figure 1.1.1. For common magnitudes of codified seismic or wind loads, static overturning is readily maintained by dead weight resistance alone. Tensile foundation anchorage has therefore not generally been required for overturning resistance.

The absence of tensile foundation anchorage implies a potential for transient uplift during severe seismic excitation, along with attendant beneficial response modifications. A necessary condition to achieve such a response, however, is sufficient shear capacity in the superstructure to develop a base overturning moment at least as great as the gravity load resistance. This section discusses such a capacity requirement quantitatively for various aspect ratios, as well as implications for past and future designs.

CHARACTERIZATION OF LOADS

In order to examine in general terms the 2-dimensional overturning phenomenon it will be helpful to develop simple quantitative expressions for primary load resultants per unit width out of plane.

Gravity Loads: The gravity load resultant, G, can be written as:

$$G = \gamma\, b\, h = \frac{\gamma h^2}{\alpha} \qquad (1.1)$$

where γ is the effective weight density of the structure, b is the base width, h is the building height and α is the height/width or aspect ratio.

Seismic Loads: Assuming a uniform mass distribution and a triangular fundamental mode, the seismic load resultant E, can be written as:

$$E = 0.75\, G\, \frac{pSa}{g} \qquad (1.2)$$

where pSa is the pseudo spectral acceleration and g is the acceleration of gravity. This assumed mode shape will also dictate that the

seismic load resultant will act at 2/3 of the total height above the base, i.e. h_E is equal to $\frac{2}{3}$ h.

Wind Loads: Assuming a discretized wind pressure profile similar to that suggested in the Uniform Building Code, (25) a continuous power law expression such as:

$$\frac{p}{p_{max}} = \left[\frac{y}{1200}\right]^{\delta} \tag{1.3}$$

can be written which closely approximates the discrete profile. In this expression p is the pressure in psf as a function of the height in feet, y, and p_{max} is the pressure in psf at 1200 feet. A value of 0.213 for the exponent, δ, provides a least squares fit to the UBC profile; this curve is shown in Figure 1.1.2a.

If we utilize the pressure at 30 feet elevation, p_{30}, and assume it is 0.5 p_{max}, an expression for the wind load resultant, W, as a function of p_{30} and the building height in feet, h, can be written:

$$W = 0.364\ p_{30}\ h^{1.213} \tag{1.4}$$

The height of the wind load resultant, h_W, for this assumed profile will be 0.55 h.

COMPARISON OF WIND, SEISMIC, AND GRAVITY LOADS

Using units of pounds and feet, and an effective building weight density of 10 pcf, allows a comparison of wind and gravity loads as follows:

$$\frac{W}{G} = \frac{.0364\ p_{30}}{h^{.787}}\ \alpha \tag{1.5}$$

this relationship is plotted in Figure 1.1.2b. This expression for wind loads is in terms more familiar to earthquake engineers, namely a base shear coefficient.

Using this same assumed weight density one can also compare W and E by equating expressions for the two, leading to the following expression:

$$\frac{p_{30}}{pSa/g} = \frac{20.6\ h^{.787}}{\alpha} \tag{1.6}$$

for equivalent wind and seismic loads. Plots of this relationship are shown in Figure 1.1.3. Examination of Figure 1.1.3 indicates that slender buildings in particular, when designed for codified wind loads, do have a significant potential for seismic resistance as well.

INITIATION OF SEISMIC UPLIFT

In order to initiate a rigid body type of seismic uplift response the following inequality must be satisfied:

$$E\ h_E \geq \frac{1}{2} G\ b \tag{1.7}$$

which leads as well to the following requirement:

$$\frac{pSa}{g} \geq \frac{1}{\alpha} \tag{1.8}$$

The corresponding value per unit width out of plane of the seismic base shear, V_{max} to initiate rigid body motion is:

$$V_{max} = \frac{0.75\ G}{\alpha} = 7.5 \frac{h}{\alpha}^2 \tag{1.9}$$

assuming the same effective weight density of 10 pcf as before. A structure with a base shear capacity as indicated above would thus have the requisite lateral load capacity to anticipate potential benefits from transient seismic rigid body rocking or uplift.

Even though a structure may have been designed for lateral loads less than V_{max} as given above, there is nevertheless potential for uplift capacity due to the inherent conservatism of conventional design. There is a factor of safety applied to the nominal capacities of structural elements to obtain design capacities, and nominal material strengths are almost always significantly below actual mean material strengths. In addition reaching the capacity of one or more elements does not necessarily imply the capacity of the structure as a whole is exhausted; one can normally expect a considerable amount of load redistribution in a ductile structure.

Using Equations 1.4 and 1.9, the graphs of Figure 1.1.4 were prepared indicating requirements for significant seismic uplift potential. Examination of Figure 1.1.4 again indicates that slender structures may very reasonably be expected to uplift during severe seismic excitation and obtain the benefits of such response even though only designed for normal codified wind loads. This of course assumes no significant tensile capacity exists between superstructure and foundation.

1.2 Scope of this Study

A number of experimental and analytical studies have demonstrated the dynamic stability and the reduced lateral loading/ductility requirements associated with allowing transient uplift of portions of a structure

during extreme seismic response. (12,3,7,9). Verification of nonlinear analysis capabilities has also been accomplished.(3,7). There is, however, a scarcity of data describing the nonlinear overturning response of the various structural systems currently in popular usage. In addition, there are relatively few presented design details, intended to accommodate transient uplift response without foundation or superstructure damage.

While the concept of allowing uplift is attractive its implementation by the design community, and acceptance by regulatory agencies, would appear to rest in large part upon the ability to perform accurate analysis of this nonlinear dynamic phenomenon. While such analytic tools are available, the cost of using the available general purpose nonlinear analysis codes has restricted their use by design professionals. The use of linear substructures to simplify the analysis of locally nonlinear response, as is typical of many uplifting structures, has been suggested as one means of reducing computational costs.

The research herein reported addressed all of the above points. A linear substructuring capability was developed and put into place within a popular two-dimensional nonlinear analysis program, DRAIN-2D.[10] A variety of popular lateral load resisting systems were examined and their nonlinear overturning behavior documented. Foundation details intended to accommodate transient uplift without local distress are described. The results of the research are finally summarized, conclusions drawn and recommendations made for continued areas of exploration.

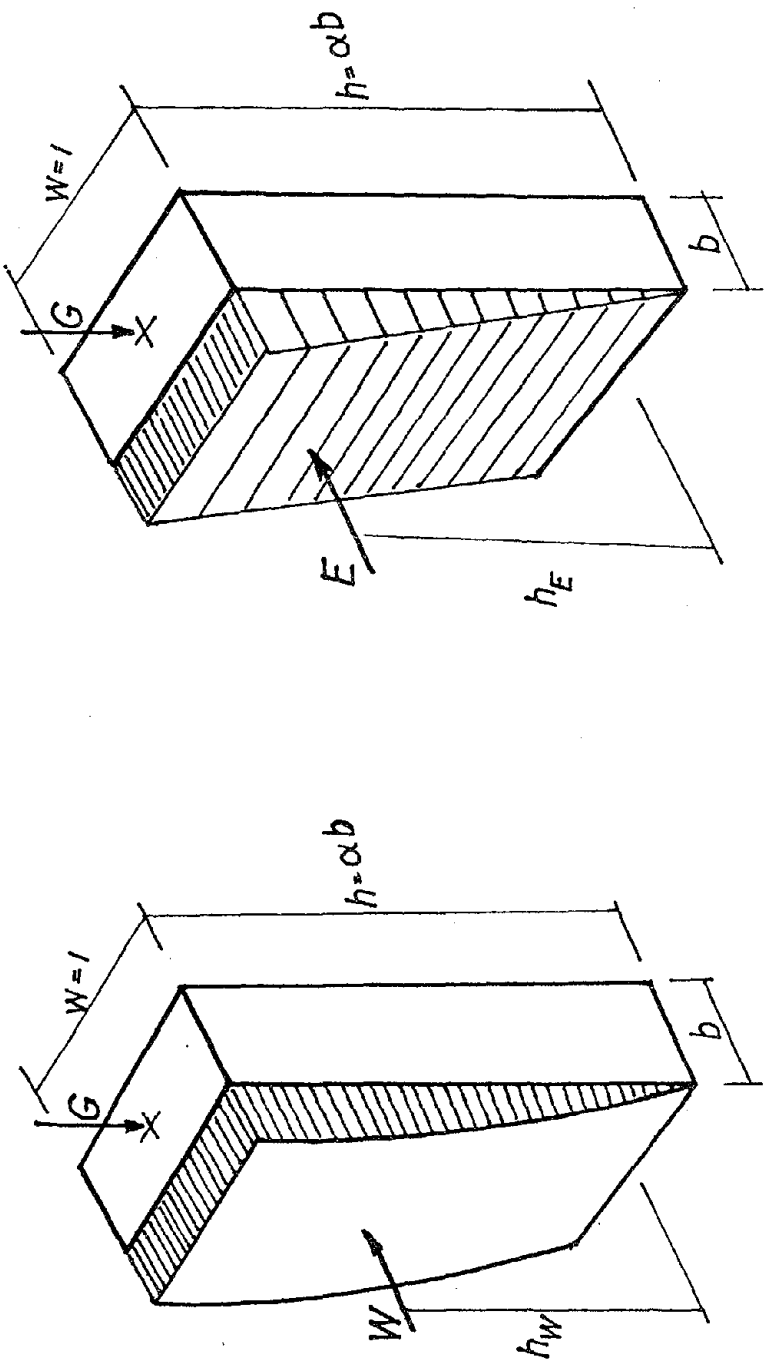

Figure 1.1.1. Overturning Effects; Wind vs Earthquake

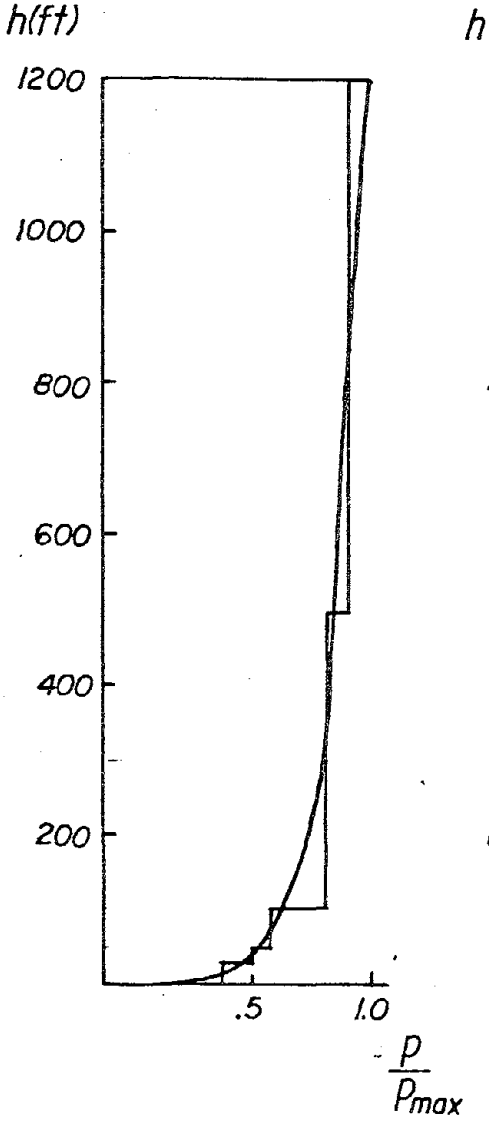

Figure 1.1.1a UBC Wind Pressure Profile

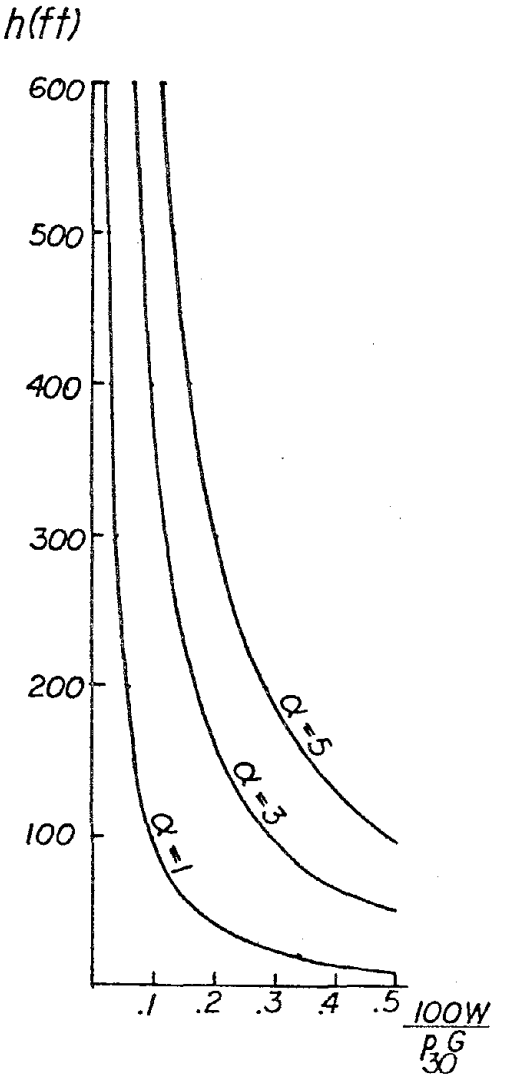

Figure 1.1.1b Comparison of Wind to Gravity Load

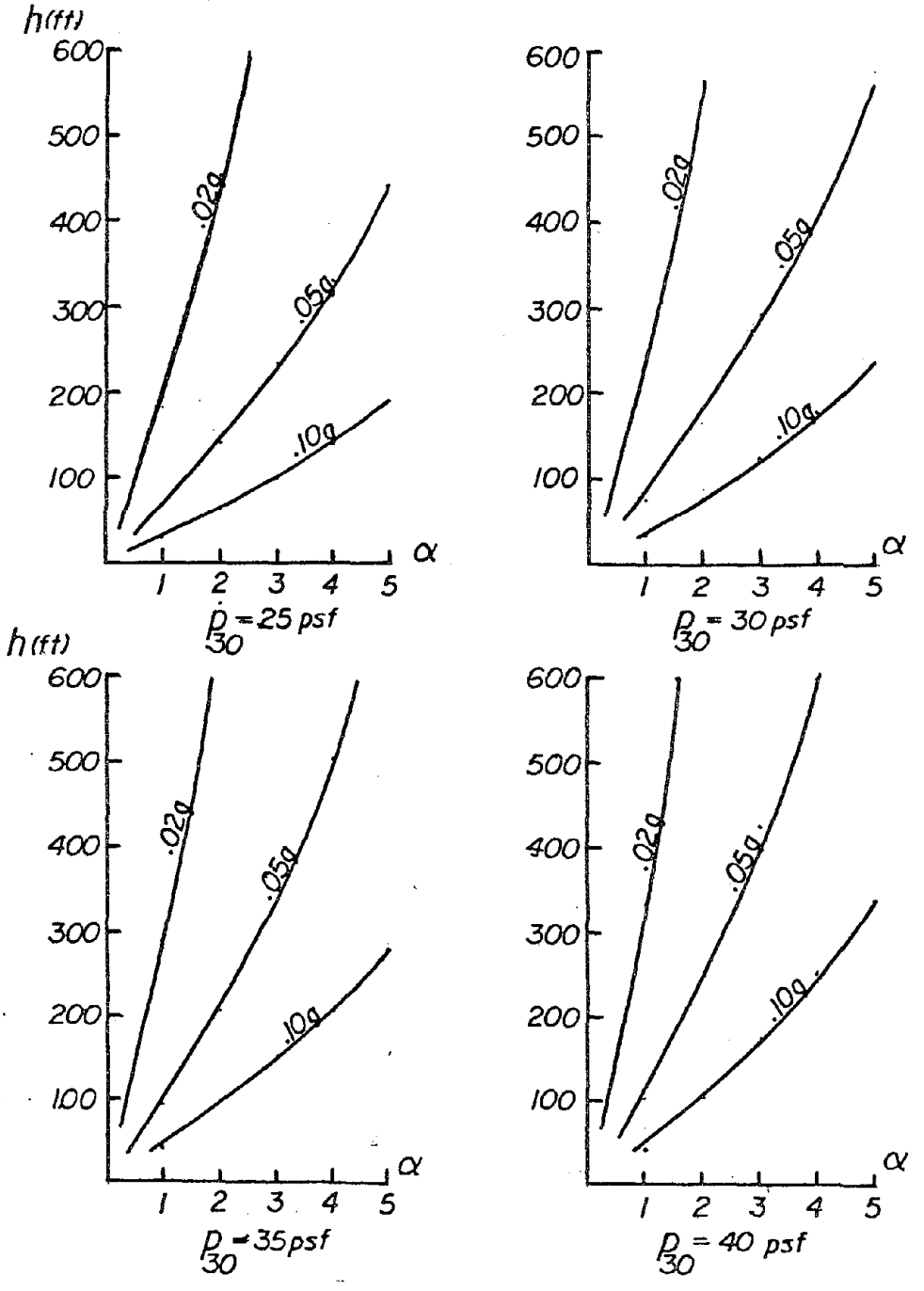

Figure 1.1.3: Comparison of Wind and Seismic Loads

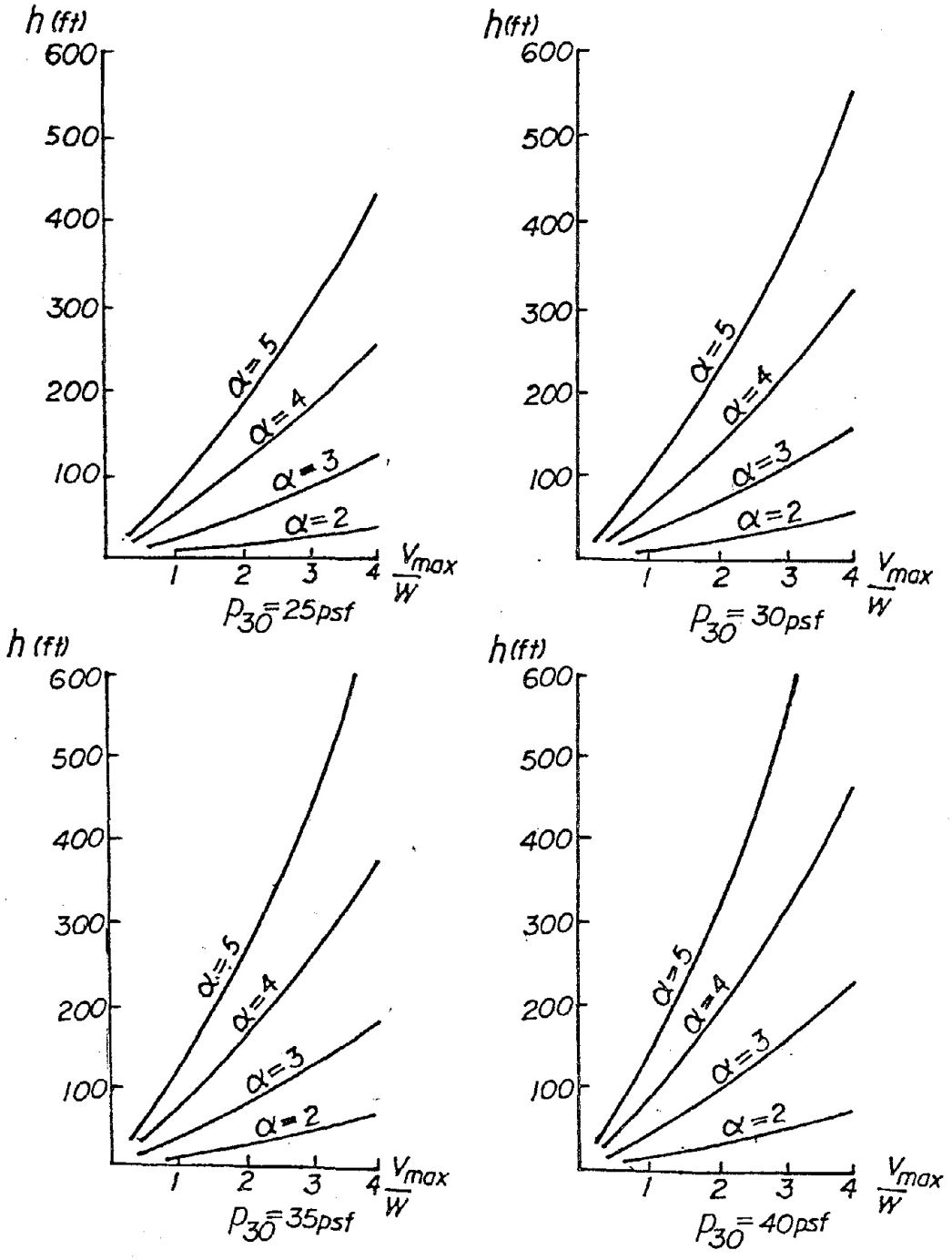

Figure 1.1.4: Shear Capacities Required to Initiate Uplift Compared to Design Wind Load

2. TRADITIONAL NONLINEAR ANALYSIS OF SEISMIC UPLIFT RESPONSE

Historically, analysis of structures exhibiting transient foundation uplift during seismic response can be divided generally into two categories: 1) relatively sophisticated two-dimensional finite element models which include nonlinear boundary and/or internal elements, thus attempting to simulate globally and locally the effects of transient loss of contact between foundation and superstructure as well as any superstructure material nonlinearity and 2) relatively simple single (rigid body) degree of freedom, or double (one elastic + rigid body) degree of freedom analytical models attempting only to simulate globally the effect of transient loss of contact between foundation and superstructure. Examples of the first technique can be found in References 3, 7, 9 and 19. Examples of the second technique can be found in References 2, 8, 12, 13 and 22.

The simple models, while computationally attractive, have some serious drawbacks. Local element behavior is not well predicted and all modes of the system, except possibly the fundamental one, are completely ignored.

The more sophisticated models, while analytically attractive (behavior is well predicted), are computationally unattractive. Although constant progress is being made in reducing the cost of computation, it is doubtful that complex nonlinear finite element analysis will be a routine design office tool in the immediate future.

It would seem that an intermediate approach between the above described extremes might be desirable. The following chapter describes an analysis

approach utilizing a linear substructure to represent the superstructure, or at least a linear portion thereof. Only the desired vibration modes of the linear substructure need be retained (usually only the first several) and subsequently combined with the nonlinear portion of the total system. This approach will eliminate to some extent the disadvantages of both the traditional approaches.

3. NONLINEAR DYNAMIC ANALYSIS WITH SUBSTRUCTURING

3.1 EQUATION OF MOTION

The principles of structural dynamics have been widely understood for many years, although practical analysis of all but the most elementary structures was impossible prior to the development of the digital computer and finite element methods. The equation of dynamic equilibrium, assuming linear viscous damping, can be expressed in the form (4)

$$[M]\{d\ddot{u}\} + [C]\{d\dot{u}\} + [K]\{du\} = \{dP\} \qquad (3.1)$$

where $\{du\}$,$\{d\dot{u}\}$ and $\{d\ddot{u}\}$ are differential increments of nodal displacement, velocity and acceleration, respectively. The matrices [M], [C] and [K] represent the mass, viscous damping and elastic stiffness properties of the structure, and $\{dP\}$ the effective applied load increment. This load term arises in seismic analysis because while the elastic and damping forces are proportional to relative displacements and velocities, the inertial term is proportional to the absolute accelerations. Examining the simple structural system of Fig. 3.1.1. the appropriate equation of motion can be written:

$$M(d\ddot{u} + d\ddot{u}_g) + Cd\dot{u} + Kdu = 0 \qquad (3.2.a)$$

Referencing the solution to the relative displacement and the associated derivatives results in the form

$$M\ddot{du} + C\dot{du} + Kdu = -M\ddot{du}_g = dP \tag{3.2b}$$

For multi-degree-of-freedom systems, the effective seismic loading can be calculated from

$$\{dP\} = -[M][B]\{\ddot{du}_g\} \tag{3.3}$$

where [B] is a Boolean matrix such that $B_{ij} = 1$ if dof i is in the direction of earthquake acceleration component j.

Consideration of dynamic equilibrium for two instants in time t_i and t_{i-1} where $t_i = t_{i-1} + \Delta t$ results in the approximate relationship

$$[M]\{\Delta\ddot{u}\} + [C]\{\Delta\dot{u}\} + [K]\{\Delta u\} = \{\Delta P\} \tag{3.4}$$

which becomes more accurate with decreasing time step Δt. Although [M] can normally be assumed constant, [C] and [K] must reflect the current structural properties, which will not be the same as the initial properties if nonlinear behavior is encountered. Although the best approximation could be made using the secant values $[C_s]$ and $[K_s]$, this would require an iterative solution at each time step during which a change in state occurred. For the sake of computational efficiency, therefore, a common procedure is to use the tangent values $[C_T]$ and $[K_T]$ determined at the beginning of the time step, and to apply a corrective load term at the beginning of the following step to account for any disequilibrium arising from a change of state.

While linear dynamic analysis, with its assumption of time-invariant structural properties, is usually performed using modal decomposition to uncouple the equations of motion, direct step-by-step integration methods are currently the most popular method of nonlinear dynamic analysis. These algorithms, such as the Newmark methods (15) and the Wilson θ-method (1), are founded upon the assumption of some simple variation of nodal acceleration within each time step. This assumption having been made, kinematics lead to expressions relating the incremental changes of acceleration and velocity to the incremental change in displacement and the values of these response quantities at the beginning of the time step. The incremental response of the system can then be found by solving the equation

$$[K_{eff}]\{\Delta u_i\} = \{\Delta P_{eff}\} \tag{3.5}$$

where:

$$[K_{eff}] = c_1\,[M] + c_2\,[C] + c_3\,[K]$$

$$\{\Delta P_{eff}\} = \{\Delta P_i\} + [M]\{f(\ddot{u}_{i-1}, \dot{u}_{i-1})\} + [C]\{g(\dot{u}_{i-1})\}$$

Equation 3.5 must be solved at each time step and the incremental changes in displacement, velocity and acceleration summed to the structure's response state at the beginning of the time increment to find the current response state. The behavior of all nonlinear elements within the structure must be monitored to determine if any structural properties have been altered. If such changes of state

do occur, the global matrices must be modified before solution for the next time step.

3.2 SUBSTRUCTURING

While the essential principle was known earlier (11), the technique of substructuring was not developed until the 1960's (17) in order to allow the analysis of large structural systems when the available computer facilities did not have sufficient memory capacity to store the entire global system of equations. Also, the process allows the design and local analysis of complex structures to be conveniently divided among multiple design groups. The substructuring process employs the following operations:

(1) The structural system is partitioned into two or more substructures.

(2) The stiffness properties and load vector of each substructure are formulated. The internal dof, those which are not directly coupled to dof in other substructures are eliminated or condensed out, to produce effective stiffness and load terms for the boundary nodes.

(3) The effective stiffness and load terms of all boundary nodes are assembled to produce a reduced global system of equations which can be solved to find the boundary node displacements.

(4) Substitution of the boundary node displacements into a transformation relationship derived as part of the condensation process in step 2 allows the internal node displacements to be calculated.

(5) Once all nodal displacements have been determined, the desired elastic force quantities can be computed.

While this process reduces the size of the global system of equations, it must be recognized that no computational effort has necessarily been saved. The condensation of the substructure's internal dof is computationally equivalent to the forward Gaussian elimination of those dof from the unreduced global system, and the calculation of internal displacements from those of the boundary corresponds to the back substitution phase. If the structure contains repeated modules which can be represented by the same substructure, however, then only one condensation is required to produce a "super-element" that can be utilized several times, resulting in a reduction of computational effort.

Although later increases in the capacity of computers available to structural analysts diminished the importance of the technique, recent years have seen a renewed interest in the substructuring as applied to nonlinear analysis (18, 5). The substructuring technique appears especially advantageous for the analysis of structures which exhibit nonlinearity in relatively small, predictable regions, such as uplifting building frames. Here, the linear dof need only be condensed once, while the state of only the limited regions of nonlinearity need to be continuously monitored and the properties updated when necessary. Such a strategy should allow considerable computational savings over the currently available programs which perform a totally nonlinear analysis.

Consider the unreduced substructure equations:

$$\begin{bmatrix} K_{\ell\ell} & K_{\ell b} \\ K_{b\ell} & K_{bb} \end{bmatrix} \begin{Bmatrix} u_\ell \\ u_b \end{Bmatrix} = \begin{Bmatrix} P_\ell \\ P_b \end{Bmatrix} \tag{3.6a}$$

where the subscripts ℓ and b denote linear and boundary degrees of freedom, respectively. This equation can either represent a static analysis, or the effective dynamic stiffness of equation 3.5. Consideration of the equations contained in the upper quadrants yields the relationship

$$\{u_\ell\} = [K_{\ell\ell}]^{-1}\{P_\ell - K_{\ell b}u_b\} \tag{3.6b}$$

which upon substitution into the lower equations produces

$$[K_{bb} - K_{b\ell}\, K_{\ell\ell}^{-1}\, K_{\ell b}]\{u_b\} = \{P_b - K_{b\ell}\, K_{\ell\ell}^{-1}\, P_\ell\} \tag{3.6c}$$

or,

$$[\bar{K}]\{u_b\} = \{\bar{P}\} \tag{3.7}$$

where the bar denotes a reduced set of equations. Equation 3.7 represents the final set of equations if only a single substructure is utilized. If multiple substructures are used, each of the local equations of this form must be assembled into the global system.

While equations 3.6 are exact for static analysis, hence the commonly used term static condensation, it is only an approximation

for dynamic analysis. This condensation fails to fully account for inertial effects, and slight distortions of the structure's vibration characteristics may occur (6). The relationships of 3.6 could be used in the pseudo-static step-by-step dynamic analysis of Eqn. 3.5, but this would require the computationally unfavorable operation of condensing the effective substructure loads at every time step. An alternate method, suggested by Clough and Wilson (5), is based upon using the constraint of Eqn. 3.6b with P_ℓ taken equal to zero:

$$\{u_\ell\} = [-K_{\ell\ell}^{-1} K_{\ell b}]\{u_b\} \tag{3.8}$$

and supplementing it with generalized coordinates corresponding to a few of the natural modes of vibration of the substructure, resulting in the coordinate transformation equation

$$\begin{Bmatrix} u_\ell \\ u_b \end{Bmatrix} = \begin{bmatrix} \Phi_{\ell m} & -K_{\ell\ell}^{-1} K_{\ell b} \\ 0 & I_{bb} \end{bmatrix} \begin{Bmatrix} u_m^* \\ u_b \end{Bmatrix} = [T]\{u_r\} \tag{3.9}$$

where the eigenvectors $[\Phi_{\ell m}]$ represent the assumed displacement patterns of the substructure and $\{u_m^*\}$ the corresponding generalized coordinates. The use of this transformation constitutes a Ritz analysis. Although approximate, it should yield excellent results if the chosen modes of vibration can closely model the response of the structure. In seismic analysis, the use of the few lowest modes of vibration would normally produce excellent approximate results,

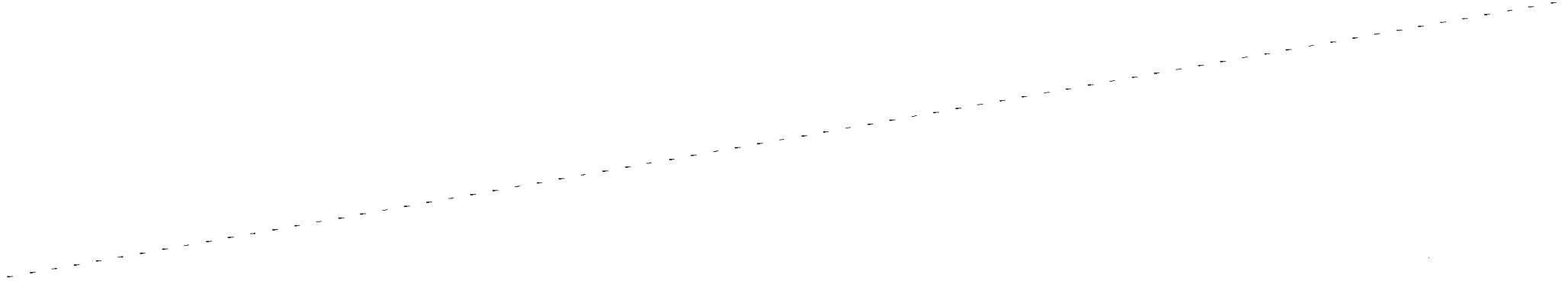

and should be adequate to model the dynamic behavior of a substructure. Clough and Wilson suggest a technique when higher modes may also be important (5).

Applying Eqn. 3.9 to the incremental equation of dynamic equilibrium in the form of a congruent transformation results in the reduced equation

$$[M_r]\{\Delta\ddot{u}_r\} + [C_r]\{\Delta\dot{u}_r\} + [K_r]\{\Delta u_r\} = [T]\{\Delta P\} \qquad (3.10)$$

where,

$$[M_r] = [T]^T[M][T]$$

$$= \left[\begin{array}{c|c} \Phi_{m\ell}^T M_{\ell\ell}\Phi_{\ell m} & -\Phi_{m\ell}^T M_{\ell\ell}K_{\ell\ell}^{-1}K_{\ell b} + \Phi_{m\ell}^T M_{\ell b} \\ \hline -K_{b\ell}K_{\ell\ell}^{-1}M_{\ell\ell}\Phi_{\ell m} + M_{b\ell}\Phi_{\ell m} & \begin{array}{l} M_{bb} + K_{b\ell}K_{\ell\ell}^{-1}M_{\ell\ell}K_{\ell\ell}^{-1}K_{\ell b} \\ -K_{b\ell}K_{\ell\ell}^{-1}M_{\ell b} - M_{b\ell}K_{\ell\ell}^{-1}K_{\ell b} \end{array} \end{array}\right]$$

$$[C_r] = [T]^T[C][T]$$

$$= \left[\begin{array}{c|c} \Phi_{m\ell}C_{\ell\ell}\Phi_{\ell m} & \Phi_{m\ell}^T C_{\ell\ell}K_{\ell\ell}^{-1}K_{\ell b} + \Phi_{m\ell}^T C_{\ell b} \\ \hline -K_{b\ell}K_{\ell\ell}^{-1}C_{\ell\ell}\Phi_{\ell m} + C_{b\ell}\Phi_{\ell m} & \begin{array}{l} C_{bb} + K_{b\ell}K_{\ell\ell}^{-1}C_{\ell\ell}K_{\ell\ell}^{-1}K_{\ell b} \\ -K_{b\ell}K_{\ell\ell}^{-1}C_{\ell b} - C_{b\ell}K_{\ell\ell}^{-1}K_{\ell b} \end{array} \end{array}\right]$$

$$[K_r] = [T]^T[K][T]$$

$$= \left[\begin{array}{c|c} \Phi_{m\ell}^T K_{\ell\ell} \Phi_{\ell m} & 0 \\ \hline 0 & K_{bb} - K_{b\ell} K_{\ell\ell}^{-1} K_{\ell b} \end{array}\right]$$

Although this reduction of variables is not quite as great as that produced by static condensation due to the addition of the modal coordinates, it should be recognized that the modal quadrant of all three matrices will be diagonal. Also, it will be shown in the following chapter that in general, the coupling quadrants will be far from fully populated, so that the total additional solution effort is usually minimal.

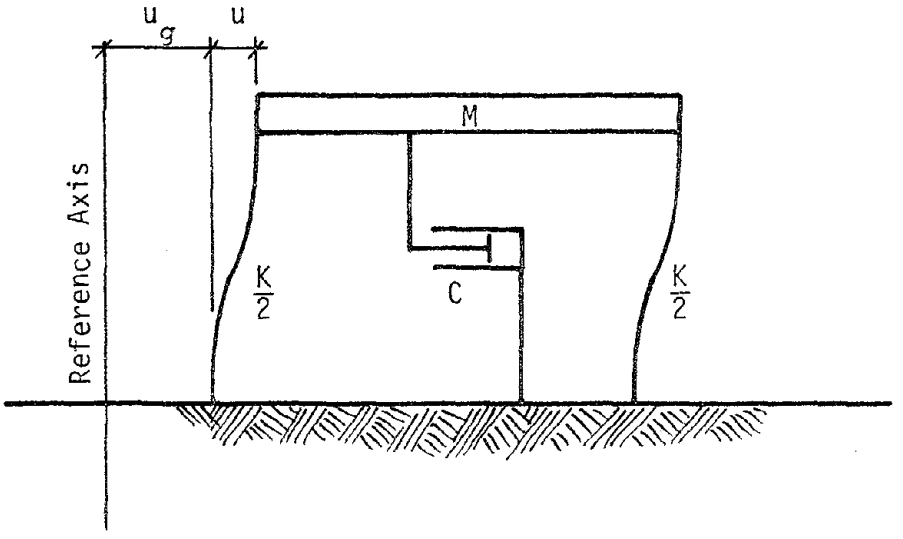

Figure 3.1.1 Structural Model

4. COMPUTER IMPLEMENTATION OF SUBSTRUCTURING

4.1 INTRODUCTION

In this chapter, the addition of a substructuring capability to the previously described program DRAIN-2D is outlined. Although the resulting program DRAINSUB-2D is limited to the consideration of a single linear substructure, it will be shown in the following chapter that it provides a useful tool for the analysis of structures uplifting under seismic loads. While the use of multiple substructures is certainly both feasible and desirable, it was beyond the scope of this work to develop such general capabilities. Also, such general capabilities would have required a massive alteration in the data input characteristics of the base program, which was considered undesirable from the standpoint of convenience. At least one general purpose nonlinear substructuring program is under development (18).

4.2 INTEGRATION METHOD

As stated previously, nonlinear dynamic analysis is most often performed using direct step-by-step integration methods. The integration method used in DRAIN-2D assumes a constant nodal acceleration in each time step. While this approximation is unconditionally stable, it is not accurate if Δt is not sufficiently small in comparison to the smallest period of vibration significant to the structure's

response. The required kinematic relationships are derived in Appendix 1 and substituted in Eqn. 3.4 resulting in the implicit equation of motion:

$$[\frac{4}{\Delta t^2} M + \frac{2}{\Delta t} C + K]\{\Delta u_i\} = \{\Delta P_i\} + [M]\{2\ddot{u}_{i-1} + \frac{4}{\Delta t} \dot{u}_{i-1}\} + [C]\{2\dot{u}_{i-1}\} \tag{4.1}$$

The assumption of Rayleigh damping,

$$[C] = \alpha[M] + \beta[K] \tag{4.2}$$

leads to the equation

$$[(\frac{4}{\Delta t^2} + \frac{2\alpha}{\Delta t})M + (\frac{2\beta}{\Delta t} + 1)K]\{\Delta u_i\} = \{\Delta P_i\} + [M]\{2\ddot{u}_{i-1} + (\frac{4}{\Delta t} + 2\alpha)\dot{u}_{i-1}\} + 2\beta[K]\{\dot{u}_{i-1}\} \tag{4.3}$$

The effective load term $2\beta[K]\{\dot{u}_{i-1}\}$ can be eliminated by introduction of the transformation developed by Wilson (20):

$$\{\Delta x_i\} = \{\Delta u_i\} + \beta\{\Delta \dot{u}_i\} = (\frac{2\beta}{\Delta t} + 1)\{\Delta u_i\} - 2\beta\{\dot{u}_{i-1}\} \tag{4.4}$$

resulting in the final form of the equation of motion:

$$[\gamma M + K]\{\Delta x_i\} = \{\Delta P_i\} + [M]\{2\ddot{u}_{i-1} + (\frac{4}{\Delta t} + 2\alpha - 2\beta\gamma)\dot{u}_{i-1}\} \tag{4.5}$$

where $$\gamma = (\frac{2\beta}{\Delta t} + 1)^{-1}(\frac{4}{\Delta t^2} + \frac{2\alpha}{\Delta t})$$

This equation is solved for the dummy variable $\{\Delta x_i\}$, and the incremental nodal displacements computed from the inverse of Eqn 4.4:

$$\{\Delta u_i\} = (\frac{2\beta}{\Delta t} + 1)^{-1}\{\Delta x_i + 2\beta\dot{u}_{i-1}\} \tag{4.6}$$

4.3 STRUCTURAL MATRICES

The structural property matrices [M] and [K] have several characteristics which allow the implementaion of efficient solution and storage techniques. Due to the symmetry of the matrices, which will be maintained for the unreduced degrees of freedom during Gaussian elimination, only the upper triangular half including the main diagonal terms need be assembled and stored. The banded nature of these matrices, assuming the structural dof's are assigned in an efficient manner, implies many zero off-diagonal terms. Only the diagonals containing nonzero coefficients would be held in memory with a banded storage scheme. DRAIN-2D utilizes an even more efficient technique in which the matrix is stored in a column vector and the position of the diagonal coefficients within this vector are stored in a second vector. The use of this "skyline" storage technique eliminates the need to store almost all zero terms that would remain unchanged by the solution process.

Due to its sparse nature, the unreduced global stiffness matrix can be represented as:

$$\begin{bmatrix} K_{\ell\ell} & K_{\ell b} & 0 \\ K_{b\ell} & K_{bb} & K_{bn} \\ 0 & K_{nb} & K_{nn} \end{bmatrix} \tag{4.7}$$

The subscript b represents the dof on the boundary of the linear substructure which couple it to the nonlinear region, and for typical structures b will be much smaller than ℓ. Both linear and

nonlinear element stiffnesses contribute to these global coupling terms, so these dof can not be condensed during the substructuring operation. The transformation of Eqn. 3.9 can now be written

$$\begin{Bmatrix} u_\ell \\ u_b \\ u_n \end{Bmatrix} = \begin{bmatrix} \Phi_{\ell m} & -K_{\ell\ell}^{-1}K_{\ell b} & 0 \\ 0 & I_{bb} & 0 \\ 0 & 0 & I_{nn} \end{bmatrix} \begin{Bmatrix} u_m^* \\ u_b \\ u_n \end{Bmatrix} = [T]\{u_r\} \tag{4.8}$$

If the congruent substructuring transformation developed in Chapter 3 is applied to Eqn. 4.5 using Eqn. 4.8 while noting that DRAIN-2D utilizes a lumped mass representation, the result is the reduced global system:

$$[\gamma M_r + K_r]\{\Delta u_r\}_i = [T]^T\{\Delta P_i\} + [M_r]\{2\ddot{u}_{r_{i-1}} + (\frac{4}{\Delta t} + 2\alpha - 2\beta\gamma)\dot{u}_{r_{i-1}}\} \tag{4.9}$$

where

$$[K_r] = \left[\begin{array}{c|c|c} \Phi_{m\ell}^T K_{\ell\ell}\Phi_{\ell m} & 0 & 0 \\ \hline 0 & K_{bb} - K_{b\ell}K_{\ell\ell}^{-1}K_{\ell b} & K_{bn} \\ \hline 0 & K_{nb} & K_{nn} \end{array}\right]$$

$$[M_r] = \left[\begin{array}{c|c|c} \Phi_{m\ell}^T M_{\ell\ell}\Phi_{\ell m} & -\Phi_{m\ell}^T M_{\ell\ell}K_{\ell\ell}^{-1}K_{\ell b} & 0 \\ \hline -K_{b\ell}K_{\ell\ell}^{-1}M_{\ell\ell}\Phi_{\ell m} & M_{bb} + K_{b\ell}K_{\ell\ell}^{-1}M_{\ell\ell}K_{\ell\ell}^{-1}K_{\ell b} & 0 \\ \hline 0 & 0 & M_{nn} \end{array}\right]$$

Upon solution of Eqn. 4.9, Eqn. 4.6 is used to find the incremental modal and nonlinear dof displacements. These quantities are then substituted into the transformation of Eqn. 4.8 to determine the incremental displacements of the linear substructure. Once the displacement response of the entire structure is determined, the elastic forces in the member elements can be determined by the base program. It should be noted that the velocities and accelerations of the substructure dof do not need to be computed, for only the modal velocities and accelerations are required to generate the effective load for the next time step.

Figure 4.3.1 illustrates the change in skyline of the effective stiffness matrix due to the substructuring transformation. Although the transformation has eliminated the substructure stiffness coupling terms, coupling is now present in the mass matrix. While these $[\Phi_{m\ell}^T M_{\ell\ell} K_{\ell\ell}^{-1} K_{\ell b}]$ coupling terms will in general be fully populated, the change in the skyline will not be critical if only a limited number of modal coordinates are used. Also, these terms will never need to be updated due to nonlinear behavior. Although the mass matrix is no longer diagonal, it can be easily stored using the original column vector for the diagonal terms and a small array for the interaction terms as shown in Fig. 4.3.2. This division is also computationally convenient for the calculation of mass-proportional effective loads for Eqn. 4.9.

4.4 SUBSTRUCTURING OPERATIONS

While the transformation of Eqn. 4.8 results in a desirable reduction in active degrees of freedom, the calculation of the required transformation terms involving $[K_{\ell\ell}]^{-1}$ would appear to be computationally expensive. It will be shown, however, that these transformation terms can be computed in a straightforward manner without resorting to the inversion of the potentially large matrix $[K_{\ell\ell}]$. Consider the original global stiffness equations:

$$\begin{bmatrix} K_{\ell\ell} & K_{\ell b} \\ K_{b\ell} & K_{bb} \end{bmatrix} \begin{Bmatrix} u_\ell \\ u_b \end{Bmatrix} = \begin{Bmatrix} 0 \\ P_b \end{Bmatrix} \tag{4.10}$$

where we ignore those nonlinear dof not coupled to the substructure, and P_ℓ is taken equal to zero in accordance with the assumption leading to Eqn. 3.8. The reduction of the first ℓ dof by Gaussian elimination (GE) results in the equation

$$\begin{bmatrix} U_{\ell\ell} & H_{\ell b} \\ 0 & K'_{\ell b} \end{bmatrix} \begin{Bmatrix} u_\ell \\ u_b \end{Bmatrix} = \begin{Bmatrix} 0 \\ P_b \end{Bmatrix} \tag{4.11}$$

where $U_{\ell\ell}$ is an upper triangular matrix. The row operations of GE are equivalent to a decomposition (18) such that:

$$\begin{bmatrix} K_{\ell\ell} & K_{\ell b} \\ K_{b\ell} & K_{bb} \end{bmatrix} = \begin{bmatrix} L_{\ell\ell} & 0 \\ M_{b\ell} & I_{bb} \end{bmatrix} \begin{bmatrix} U_{\ell\ell} & H_{\ell b} \\ 0 & K'_{bb} \end{bmatrix} \tag{4.12}$$

Eqn. 4.12 contains the following four identities:

$$K_{\ell\ell} = L_{\ell\ell} \cdot U_{\ell\ell} \tag{4.13a}$$

$$K_{\ell b} = L_{\ell\ell} \cdot H_{\ell b} \tag{4.13b}$$

$$K_{b\ell} = M_{b\ell} \cdot U_{\ell\ell} \tag{4.13c}$$

$$K_{bb} = M_{b\ell} \cdot H_{\ell b} + K'_{bb} \tag{4.13d}$$

These identities can be used to construct the following relationship:

$$K'_{bb} = K_{bb} - M_{b\ell} \cdot H_{\ell b} \tag{4.14a}$$

$$K'_{bb} = K_{bb} - (K_{b\ell}U_{\ell\ell}^{-1})(L_{\ell\ell}^{-1}K_{\ell b}) \tag{4.14b}$$

$$K'_{bb} = K_{bb} - K_{b\ell} \cdot K_{\ell\ell}^{-1} \cdot K_{\ell b} \tag{4.14c}$$

proving that the calculation of $[K_{\ell\ell}]^{-1}$ is not needed to determine the effective stiffness of the nonlinear degrees of freedom.

Inspection of Eqn. 4.8 reveals that the other stiffness quantity required in the substructuring transformation is the product $[K_{\ell\ell}^{-1}K_{\ell b}]$. Considering the upper quadrants of Eqn. 4.11:

$$[U_{\ell\ell}]\{u_\ell\} + [H_{\ell b}]\{u_b\} = \{0\} \tag{4.15}$$

Upward reduction of the first quadrant results in the equation:

$$[I_{\ell\ell}]\{u_\ell\} + [H'_{\ell b}]\{u_b\} = \{0\} \tag{4.16}$$

Comparison of this relationship to the constraint equation 3.8 reveals that:

$$[H'_{\ell b}] = [K_{\ell\ell}^{-1}K_{\ell b}] \tag{4.17}$$

so that again we find that a Gaussian elimination can be substituted for the inversion of $[K_{\ell\ell}]$ and the computation of the required matrix product.

4.5 VIBRATION ANALYSIS

The determination of the natural modes of vibration of the substructure used in the transformation equation requires the solution of the equation

$$[K_{\ell\ell}][\Phi_{\ell m}] = [M_{\ell\ell}][\Phi_{\ell m}][\Omega^2_{mm}] \tag{4.18}$$

where $[\Omega^2_{mm}]$ is a diagonal matrix containing the corresponding squared radial frequencies of vibration. Due to the importance of this equation in structural dynamics, considerable effort has been expended in developing efficient solution techniques. The method utilized in DRAINSUB-2D is a subspace iteration algorithm presented by Bathe and Wilson (1). In this particular routine, the eigenvectors are normalized to satisfy the constraint:

$$[\Phi^T_{m\ell}][M_{\ell\ell}][\Phi_{\ell m}] = [I_{mm}] \tag{4.19}$$

Premultiplying Eqn. 4.18 by the transposed matrix of eigenvectors:

$$[\Phi^T_{m\ell}][K_{\ell\ell}][\Phi_{\ell m}] = [\Phi^T_{m\ell}][M_{\ell\ell}][\Phi_{\ell m}][\Omega^2_{mm}] \tag{4.20}$$

we find:

$$[\Phi^T_{m\ell}][K_{\ell\ell}][\Phi_{\ell m}] = [\Omega^2_{mm}] \tag{4.21}$$

Therefore, the calculation of the modal stiffnesses required for

Eqn. 4.9 as a matrix triple product is not necessary and may simply be set equal to the corresponding natural frequencies of vibration.

4.6 ANALYSIS PROCEDURE

An outline of the analysis procedure utilized in DRAINSUB-2D is presented in Appendix 2, and a User's Manual in Appendix 3. A minimal amount of input beyond that required by the base program is necessary. Specifically, the user must specify the nodes which constitute the substructure boundary and the number of modal coordinates to be used as substructure displacement variables. Additionally, all flexural members in the substructure must be assigned as linear beam elements. All truss bars are tested and linearity automatically enforced if located in the substructure. Modification of the other available element types to enforce linearity as necessary has not been attempted, but could be readily accomplished.

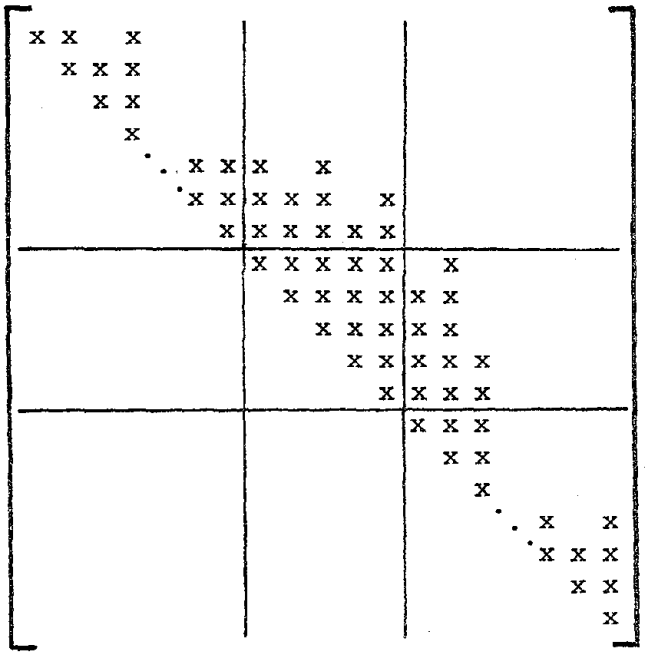

a) Prior to Reduction of Substructure Dof

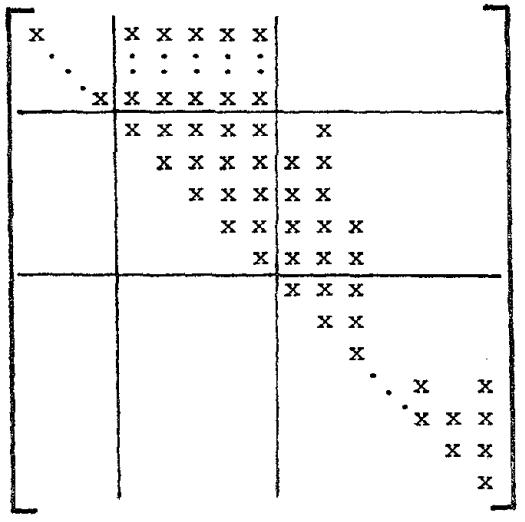

b) After Reduction

Figure 4.3,1. Effective Stiffness Matrix Skyline

$$[M_r] = \begin{bmatrix} I_{mm} & 0 & 0 \\ 0 & M_{bb} & 0 \\ 0 & 0 & M_{nn} \end{bmatrix} + \begin{bmatrix} 0 & -\Phi_{m\ell}^T M_{\ell\ell} K_{\ell\ell}^{-1} K_{\ell b} & 0 \\ -K_{b\ell} K_{\ell\ell}^{-1} M_{\ell\ell} \Phi_{\ell m} & K_{b\ell} K_{\ell\ell}^{-1} M_{\ell\ell} K_{\ell\ell}^{-1} K_{\ell b} & 0 \\ 0 & 0 & 0 \end{bmatrix}$$

Reduced Mass Matrix = Modal and Nonlinear DOF Lumped Masses + Mass Coupling Terms

Figure 4.3.2. Reduced Mass Matrix Storage Scheme

5. EXAMPLE STRUCTURES

In order to gain a greater understanding of the basic phenomenon of transient foundation uplift, a number of example structures were examined under conditions of severe seismic response. The structural types considered include a 20 story "slender" moment frame, a 10 story "stocky" moment frame, a 10 story braced frame, a 20 story core-wall building, a 15 story coupled shear wall building and a 30 story framed tube. All of the structures were designed for "typical" levels of lateral loading. The analysis performed considered both material nonlinearity in the structural elements and the transient uplift phenomenon. Comparative "fixed-base" analyses were performed to better isoltate the response effects attributable to foundation uplift.

The program utilized was DRAIN 2D, augmented by the previously described substructuring capability. Unless indicated otherwise, all superstructure nonlinearities were included in the following analytical results.

Two recorded ground motions were utilized primarily as excitations to the example structures. These ground motions were the 1971 Pacoima Dam SI6E and an amplified version of the 1940 El Centro N-S accelerograms. The ground acceleration time histories and 5% damped response spectra are shown in Figures 5.1 and 5.2. As indicated in the introductory section, foundation uplift will be an "extreme event" seismic phenomenon for almost all conventional structural configurations. For this reason only ground motions representative of extreme seismic events were utilized in the study.

5.1 Moment Frames

Moment frames of two different heights and aspect ratios were examined in detail; the 20 story frame will be discussed first, followed by a discussion of the 10 story frame.

TWENTY STORY FRAME

As the first example a 20 story, slender moment frame ($\alpha = 4$), designed for a 30 psf nominal wind pressure at 30 ft. elevation was subjected to a severe seismic excitation. The structure and design wind loads are indicated in Figure 5.1.1. As determined from Figure 1.1.2b this wind load is equivalent to a base shear coefficient of approximately 6% for an aspect ratio of 4. As determined from Figure 1.1.3, this design load is similarly equivalent to a spectral acceleration of approximately 8% gravity. From Figure 1.1.4 it can be seen a base shear somewhat over three times the design lateral load would be required to initiate rigid body uplift motion, i.e. a base shear coefficient of approximately 18%.

It was assumed that, although comprised of A36 steel, the actual average yield strength was 42 ksi for all sections, typical of A36 mill test results. It was assumed that no tensile capacity existed between superstructure and foundation.

The periods of the first three modes of the structure are 2.18 seconds, 0.84 seconds and .50 seconds, respectively. The corresponding effective masses in these two modes expressed as a percentage of the total mass are 72%, 14% and 5%. In order to bring the natural periods of the "bare frame" to the levels given above, which were considered representative of actual structures, it was necessary to use an artificially high value for the modulus of elasticity of the members. Due to the participation of non-structural elements in actual structures, such a stiffening effect at low response levels is usually to be anticipated. The columns of this structure ranged from W14 x 30 at the top to W14 x 264 at the bottom; the girders ranged from W18 x 35 to W24 x 94. Gravity loading was assumed to be 120 psf on the floor area, consistent with a weight density of 10 pcf. The assumed lateral spacing of frames was 20 ft.

Examination of the vertical reactions indicated in Figure 5.1.1 indicate that the outermost columns will tend to uplift considerably prior to onset of a "complete" or rigid body type of uplift motion. This is due to the fact the outer columns have less gravity load and greater overturning loads. Making use of a cantilever beam analogy, there is not sufficient shear stiffness in the lateral system to force a "plane section" bending behavior; i.e. instantaneous uplift of all but one column. Thus there will be a piecewise loss of lateral stiffness as column lines progressively uplift, until finally rigid body rotation is initiated when only the most "leeward" column is in contact with the foundation. It can therefore be anticipated that there will be an influence due to column uplift even prior to developing the base shears indicated by Figure 1.1.4. It is of interest to note that for this frame outermost column uplift is associated with a 33% loss at lateral stiffness, which might reasonably be expected as the available base lever arm is cut from 60 feet to 40 feet.

Seismic Response

Selected displacement response time histories are indicated in Figure 5.1.2. As can be seen the maximum roof displacement was 21 inches for the response with uplift allowed, and the maximum amount of column uplift was 1.28 inches. It is of interest to note that restraining uplift, which would require an anchorage force in excess of 600^{k}, actually increased lateral roof displacement by approximately one inch.

Story shear envelopes are plotted in Figure 5.1.3. From this diagram it is apparent that story shears considerably in excess of the design levels were developed. The shape of the seismic shear envelope also indicates a considerable influence of higher modes; a first mode only shear envelope

would have very little gradient in the lower floors. There is also comparatively little difference between the response cases with and without uplift allowed. This similarity is due largely to the importance of higher mode response. Uplift, being a phenomenon governed by base overturning moment, has little effect on response modes not themselves producing base overturning moment. For typical building frames all modes except the fundamental one produce a nearly negligible base overturning effect.

Maximum girder plastic hinge rotations are plotted in Figure 5.1.4. Again there is comparatively little difference with and without uplift. A reasonably well detailed ductile frame should be able to easily accommodate plastic hinge rotations of this magnitude.

Some additional insight into the behavior of this structure can be obtained by examination of response spectra for the ground motion utilized. Figure 5.1.5 indicates the conventional 2% damped spectrum along with generated nonlinear acceleration and displacement spectra for a simplified bilinear uplifting model having a similar aspect ratio.

If one assumed completely linear behavior and included the first three modes the usual SRSS base shear prediction would be approximately 36% of the total superstructure weight. (The actual model breakdown of base shear coefficients would be 29% in the first mode, 20% in the second mode and 10% in the third mode.)

For the bilinear uplifting model, the first mode base shear coefficient would be reduced to only 17% compared to 29% for linear response. In addition to this reduction due to uplift in the fundamental mode, there will be additional reductions due to observed ductility in all modes. The ductility related reduction is difficult to quantify, but undoubtedly is substantial.

The uplift reduction in the actual structure may be somewhat different than the spectral plot as well, due to its piecewise linear rather than bilinear response characteristic. (In the actual structure the observed maximum base shear coefficient was 18%).

TEN STORY FRAME

This hypothetical office building structure, illustrated in Figure 5.1.6 meets the design provisions of the ATC-3 model seismic code (24) for Zone 7 and a site founded on a shallow layer of stiff soil. Doubly symmetric in plan to reduce torsional loadings, the design relies upon rigid diaphragm action by the composite floor slabs to distribute lateral loads to the structural system. The braced frames are designed to carry all lateral loads along the weak axes of the columns. Per ATC-3 requirements, the structural elements were proportioned to have an ultimate capacity of 120 percent of the design dead load, full live load and an equivalent static lateral seismic load given as a function of the fundamental period of free vibration. This seismic design load represents a base shear coefficient of 6.5 percent for the moment frames. The mode shapes and periods of the first four modes are shown in Figure 5.1.7.

Seismic Response

The lateral roof displacement responses of the moment frame during the Pacoima acceleration record are shown in Figure 5.1.8. Allowing uplift resulted in only a minor increase in drift from 17.6 to 18.2 inches. A rather small shift in response frequency can be attributed to the change in stiffness after uplift. The time histories in Figure 5.1.9. show very little uplift; column-foundation separation did not exceed 1.0 in. The many small

amplitude uplifts of the columns bases can be interpreted as rocking of the base plates rather than actual uplift. The fixed-base response revealed that no more than a 50^k tie-down force was required to prevent uplift.

The small uplift response of the frame is reflected in comparatively little reduction of interstory shear forces. The shear envelopes in Figure 5.1.10 reveal that only a 12 percent reduction in base shear took place when uplift was permitted. Even these rather modest decreases accounted for a beneficial reduction in ductility demands upon the girders of the moment frame. Figure 5.1.11 illustrates the magnitude of greatest plastic hinge rotation of the girders in one of the exterior bays. Only near the base of the structure do the rotations during uplift, none of which were greater than .021 radians, exceed the corresponding fixed-base deformations. The average change in maximum and cumulative hinge rotations as a percentage of the fixed-base rotations are plotted in Figure 5.1.12.

The moment frame did not exhibit any more extreme behavior during the El Centro excitation. The roof displacement time histories in Figure 5.1.13. show the same changes between fixed-base and uplift response previously noted for the Pacoima earthquake. The maximum roof displacement only increased from 13.3 to 14.5 inches. No true column-foundation separation took place, but the time histories of the column bases in Figure 5.1.14. do show rocking of the base plates. Such rocking resulted in only a 6 percent reduction in the peak base shear, as illustrated in Figure 5.1.15. Changes in plastic hinge rotations from uplifting follow the same trend illustrated in Figure 5.1.12. for the Pacoima excitation; the maximum hinge rotation in the first story girders during uplift was only .016 radians.

In order to examine the behavior of the moment frame when highly excited, another set of analyses were performed using the Pacoima acceleration record. The modulus was doubled to 60,000 ksi, resulting in a reduction of the first mode period from 1.56 to 1.10 seconds. Also, only 1 percent critical damping was specified. A maximum roof displacement of 27 in. was predicted for the fixed-base structure; this was reduced to only 15 in. by allowing uplift. It should be noted, however, that the fixed-base response is probably overestimated: The analysis in no way accounted for the increase in damping resulting from nonstructural damage that would no doubt take place with such large deformations. Figure 5.1.16. shows the peak interstory shear forces predicted by the two analyses. The maximum base shear was reduced from 820^{k} to 491^{k} when uplift was permitted. Ductility demands were similarly reduced as illustrated by Figure 5.1.17. Although the maximum hinge rotations in the lower stories increased with uplift, nowhere did they exceed .025 radians, and the cumulative hinge rotations were decreased for every girder.

5.2 Braced Frame

The 10 story braced frame of Figure 5.1.6. was also analyzed; it was assumed that only the braced columns were free to uplift since this bay carried the dominant share of the lateral loading.

Figure 5.2.1 shows the analytic model used to determine the response of the braced frame. The girders and columns are modeled as rigidly connected beam and beam-column elements, while the bracing is represented by truss bars. Nominal values of 30,000 and 36 ksi were specified for the modulus and yield stress respectively. Stiffness and capacity of the

flexural members were scaled to reflect the properties of both the braced frame and the interior weak-axis moment frame. Inertial properties of the structure are described by lumped masses at the nodes, and the action of the rigid floor slabs represented by linking the horizontal dof of all nodes at each story level. Tangent stiffness proportional damping of 5 percent critical damping was assumed. The undamped first four periods and mode shapes of the braced frame are shown in Figure 5.2.2.

Seismic Response

Figure 5.2.3 shows the time histories of the lateral roof displacements during the ten seconds of the Pacoima record analyzed. The maximum displacement when uplift was permitted was 19.7 in. compared to 10.3 in. for the fixed-base response; the uplift drift index of 1.67 is large, but acceptable given the intense excitation. The shift in frequency response of the structure corresponds to the reduced lateral stiffness of the system once uplift of the brace bay occurs. The uplift behavior of the braced bay for this earthquake is recorded in the time histories shown in Figure 5.2.4. A maximum column-foundation separation of 3.6 in. took place; restraining this uplift would require an anchorage force of 2500 kips.

The substantial reduction in force levels resulting from uplift is illustrated in the shear envelopes shown in Figure 5.2.5. Computed as the sum of individual element envelope forces, these maximum story shears are conservative. The overestimation should not be great, however, for in most cases the extreme element forces at any one story occurred within one or two time steps of each other. Allowing uplift led to a 36 percent reduction in the maximum base shear; the forces carried by the bracing members

in the lower stories decreased 50 percent. In addition to reduced force levels, ductility demand on the bracing was altered from a maximum ductility factor of 5 to the elimination of plastic behavior in the bracing with uplift allowed. The rocking of the braced bay did result in plastic hinge formation in the lower story girders of the exterior bays at their connections with the braced bay. These hinges did not exceed rotations of 0.025 radians; hinge rotations of this magnitude represent a more desirable energy dissipation mechanism than yielding of the lateral bracing members.

Although the magnitude of the response for the magnified El Centro earthquake was lower, the structure exhibited the same changes in behavior observed with the Pacoima excitation. The time histories of the roof displacement in Figure 5.2.6 show a peak response of 8.7 and 12.5 inches for the fixed-base and uplift responses, respectively. The uplift rocking of the braced bay displayed in Figure 5.2.7 was more irregular than that from the Pacoima earthquake, but a maximum column separation of only 1.9 in. is recorded. The fixed-base analysis predicted a 2500^{k} anchorage force would be required to restrain uplift.

The shear envelopes for the El Centro record, shown in Figure 5.2.8 again exhibit the reduction in force levels attained through uplift behavior. The peak base shear of 1006^{k} decreased to 576^{k}: 43 percent reduction due to uplift. This reduction of load eliminated the plastic behavior in the bracing of the lowest three floors that took place during the fixed-base response. Plastic hinges in the beams connected to the braced bay did not experience any rotations greater than 0.01 radians.

Comparison of Braced Frame to Moment Frame

The seismic responses of the 10 story moment frame and the 10 story braced frame differ substantially. These differences can be explained by examining the load-deflection curves shown in Figure 5.2.9, which were generated by applying incremental lateral loads to the frames distributed in the shape of their first mode displacement pattersn. The braced frame shows an abrupt loss of stiffness once uplift takes place; near rigid-body overturning of the braced bay is only prevented by the stiffness of the exterior bays. For this particular frame, uplift results in an 84 percent reduction in lateral stiffness. Stiffness reduction of the moment frame is more gradual, being only 40 percent upon uplift of an exterior column. Further loss of stiffness would not occur until uplift of an interior column or plastic hinge formation in the superstructure. Therefore, while there is less increase in drift due to uplift of the moment frame, there is correspondingly less reduction in force levels.

The greater stiffness of braced frames relative to moment frames makes their use desirable to limit or eliminate damage to nonstructural components during moderate excitations. Loss of drift control due to poor nonlinear behavior of the bracing during extreme seismic events, however, has raised concern over using braced frames in highly seismic areas(16). Allowing transient uplift of the braced bay during extreme excitation has been shown to limit ductility demands upon the bracing, while relying upon reasonable plastic rotations of the connecting girders to partially dissipate the structure's vibrational energy. Moment frames also benefit from transient uplift, reducing force levels and ductility demands upon all girders but those in the lowest stories.

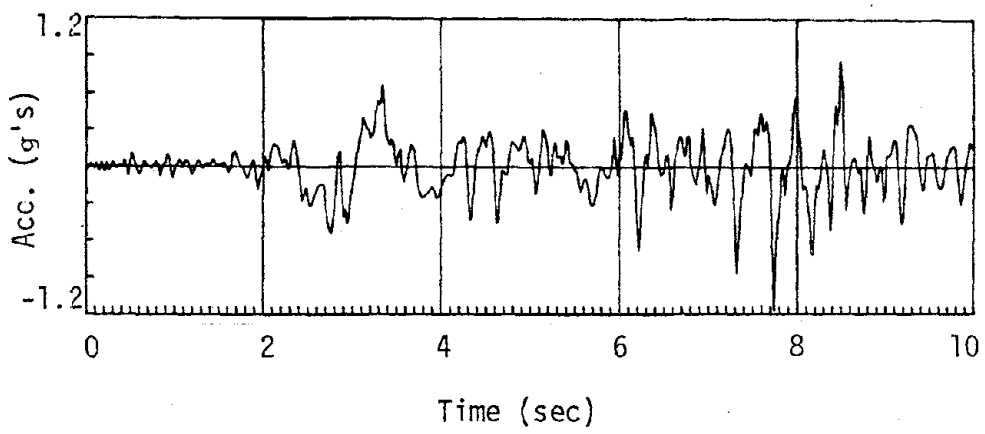

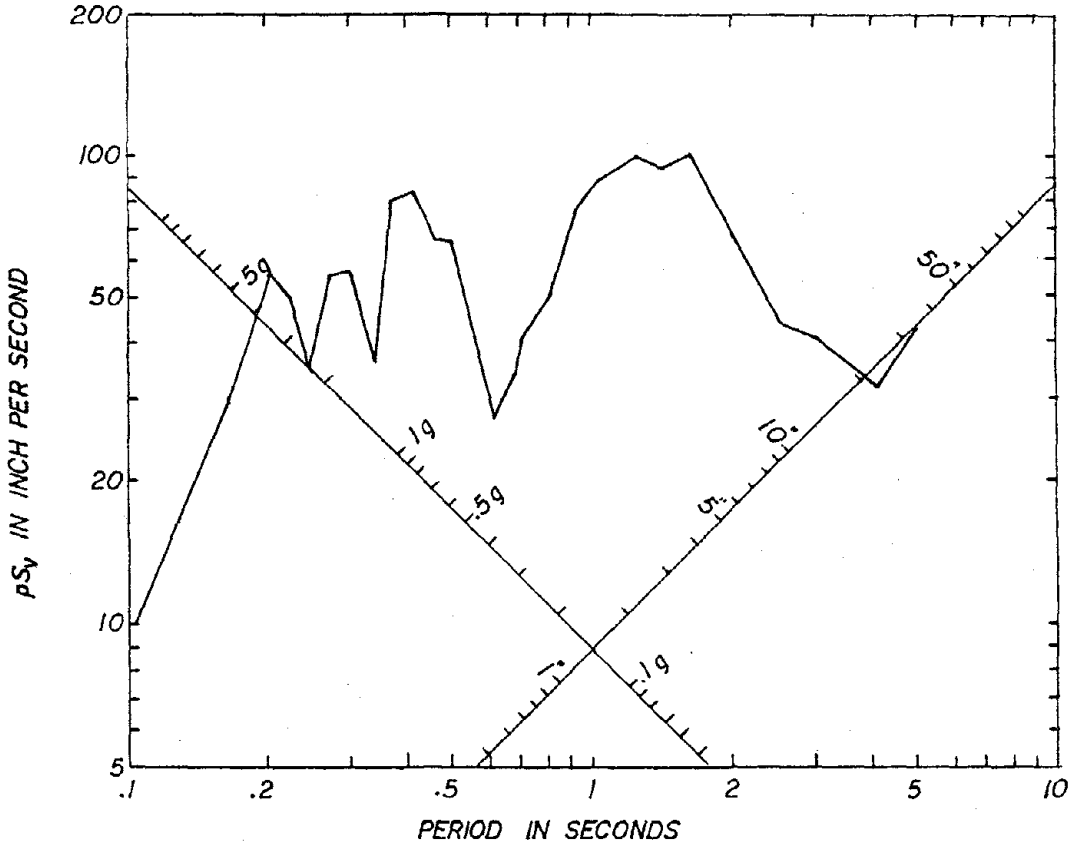

Figure 5.1.Accelerogram and 5 percent Damped Response Spectra, Pacoima Dam S-16-E Ground Motion

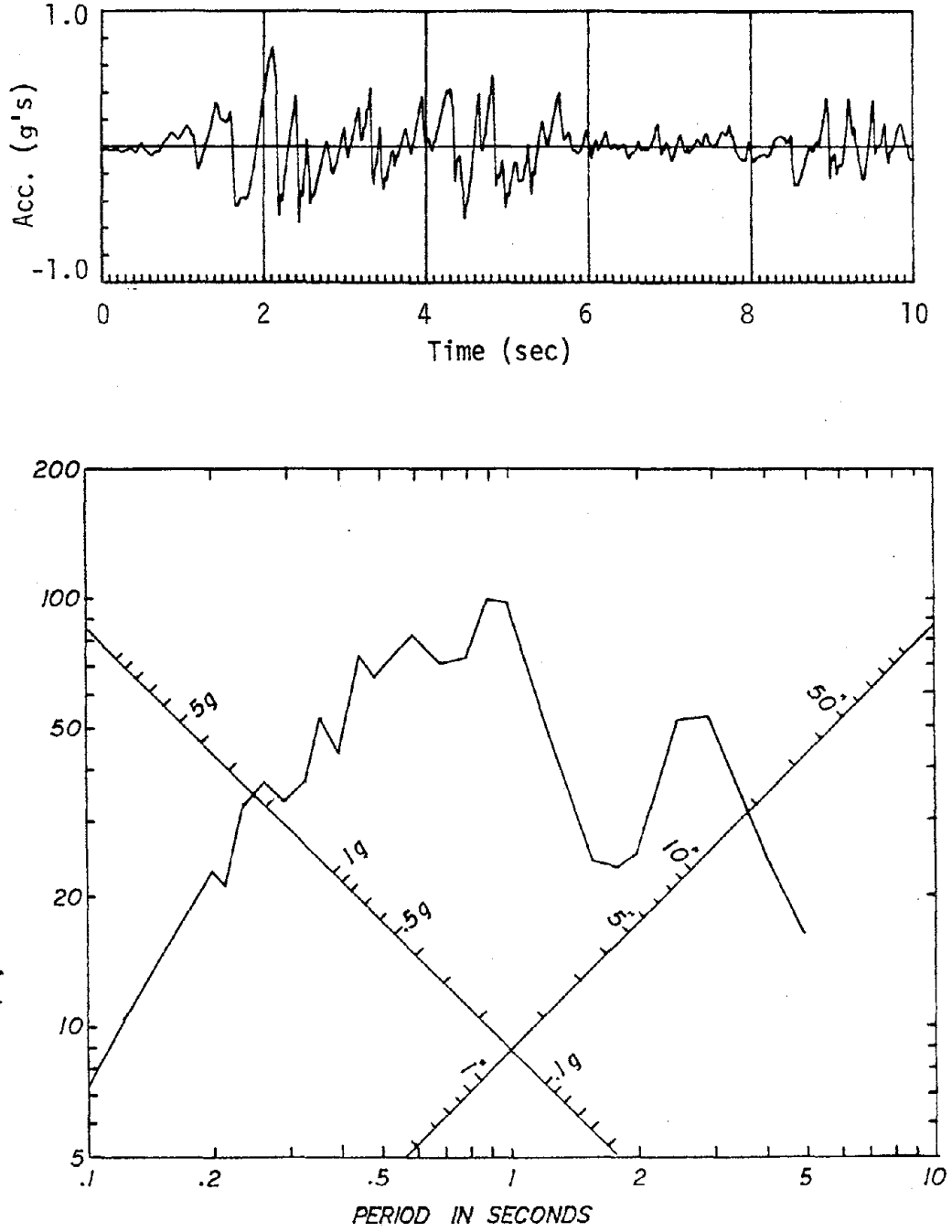

Figure 5.2. Accelerogram and 5 percent Damped Response Spectra, Magnified 1940 El Centro N-S Ground Motion

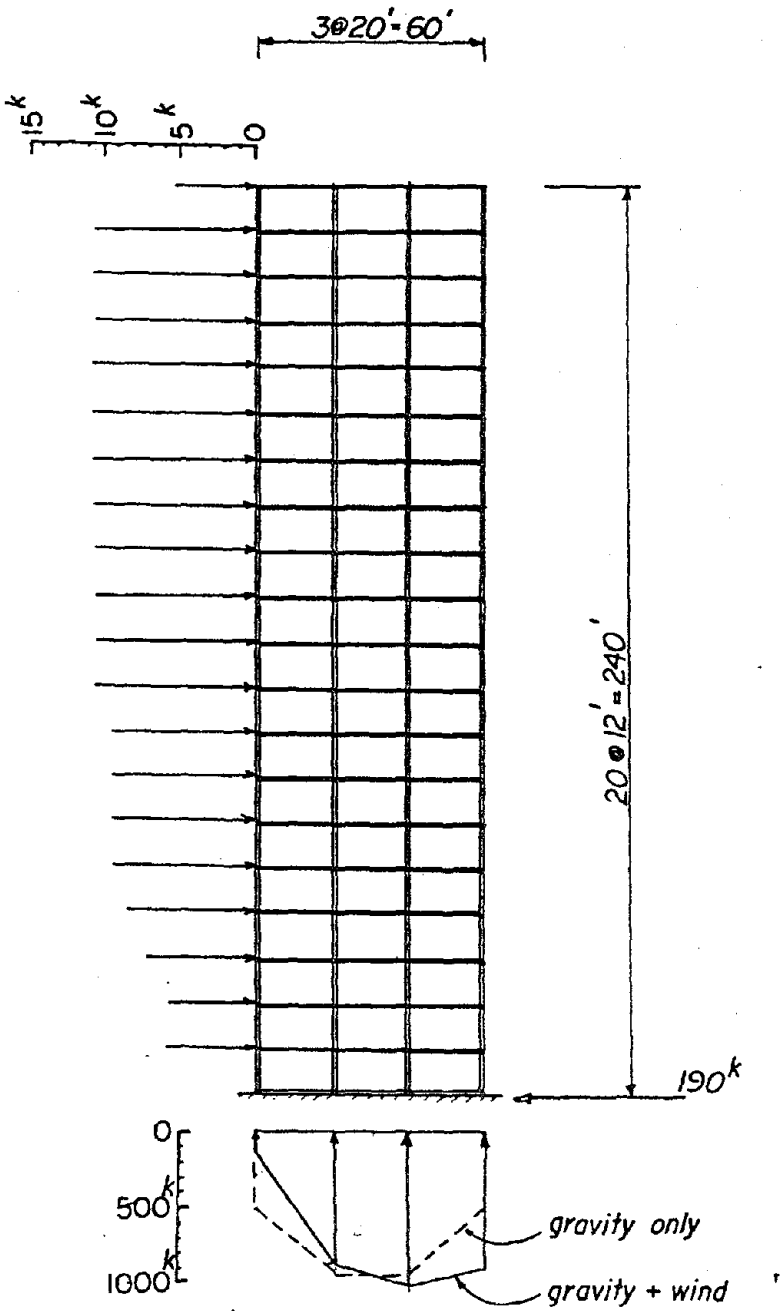

Figure 5.1.1. Twenty Story Moment Frame

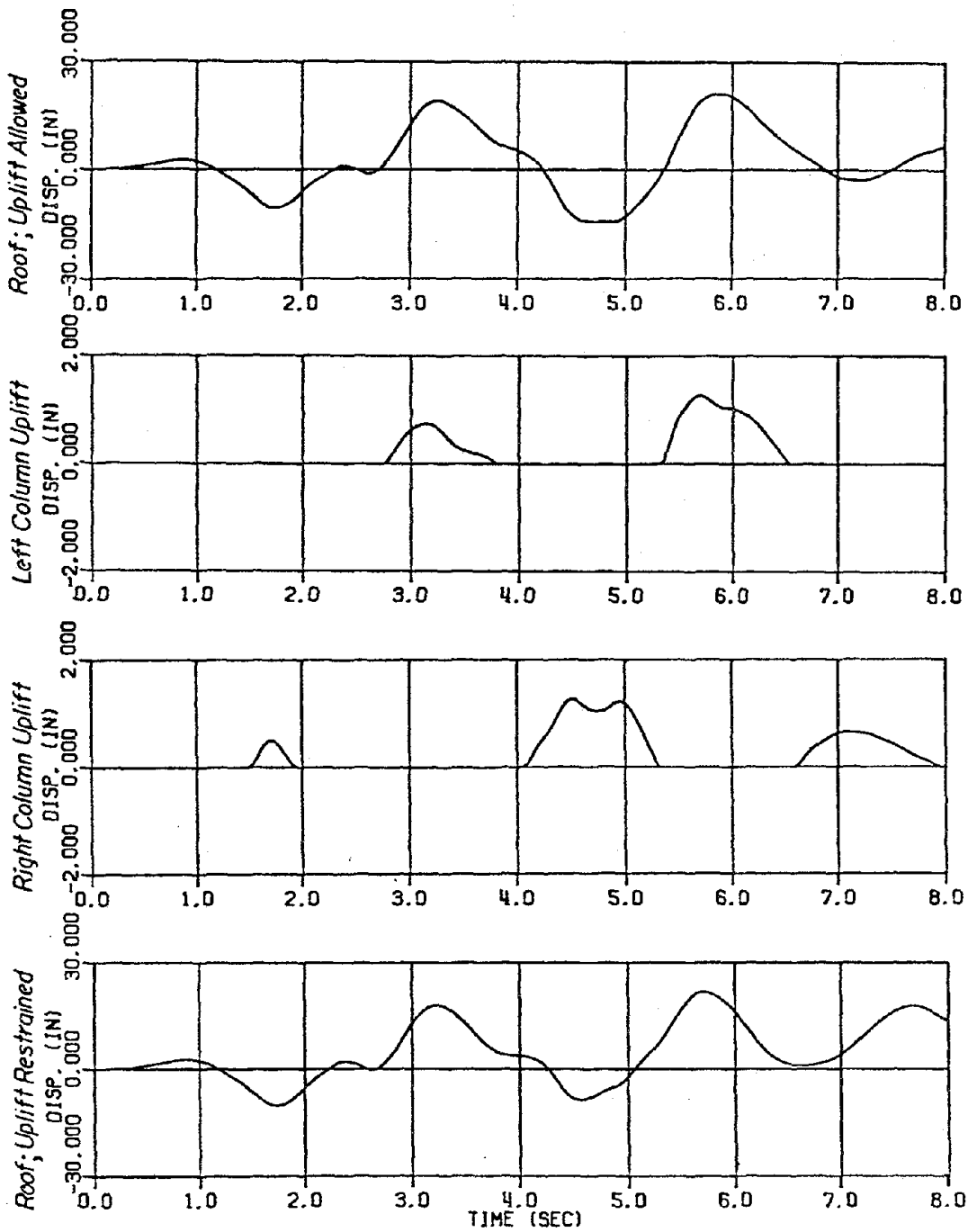

Figure 5.1.2. Uplift Displacements

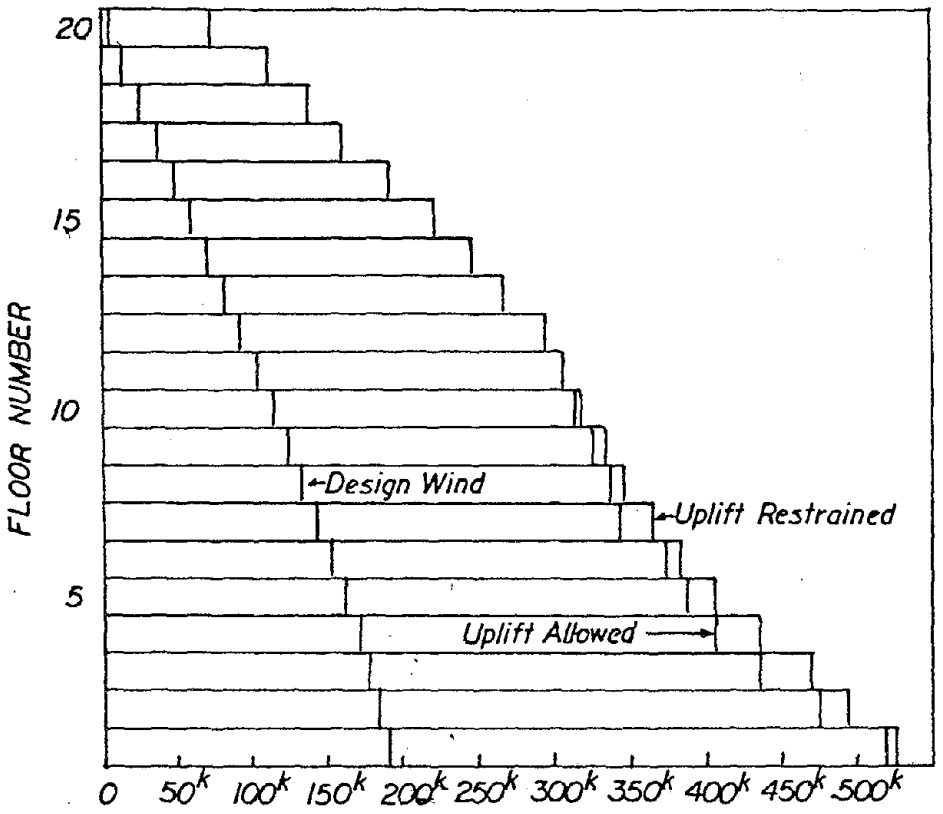

Figure 5.1.3. Story Shear Envelopes

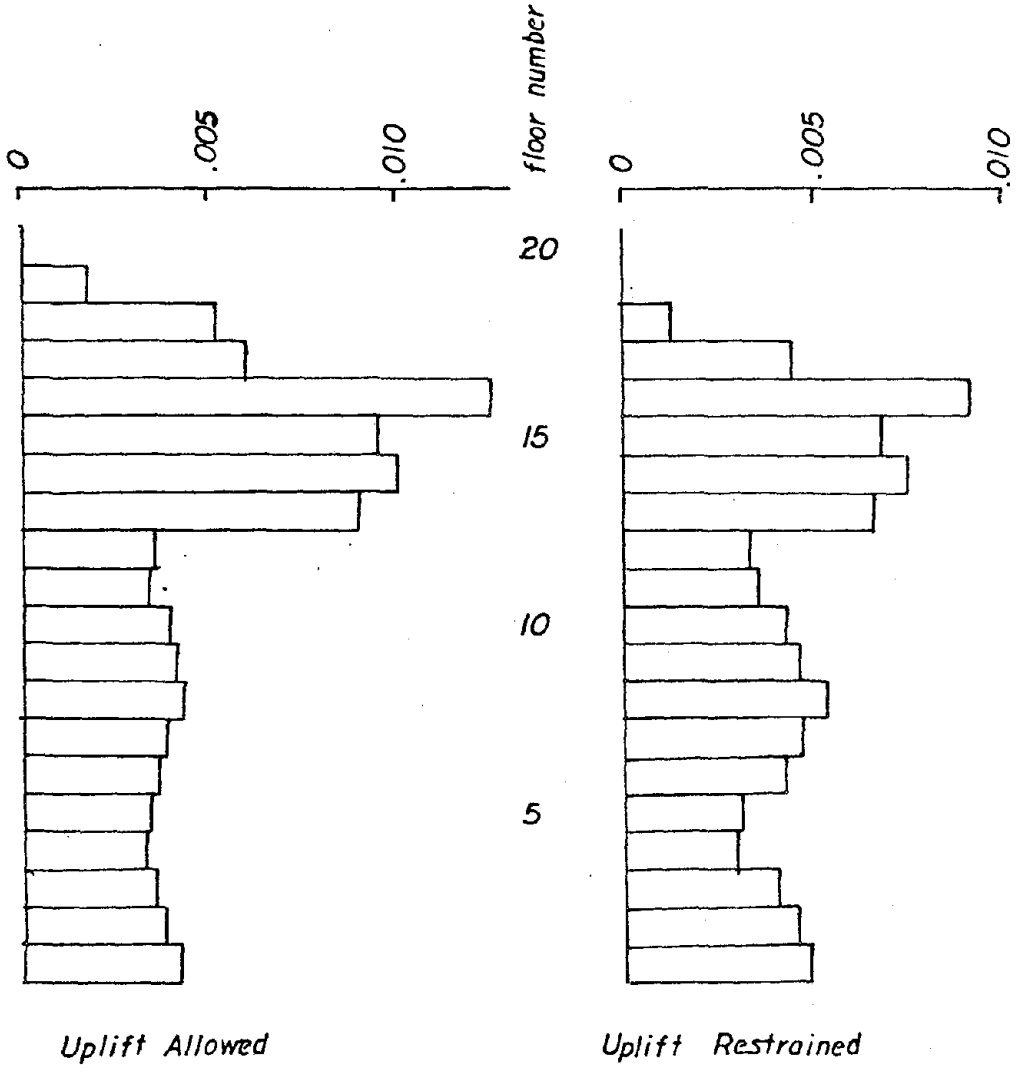

Figure 5.1.4. Maximum Girder Plastic Hinge Rotations (radians)

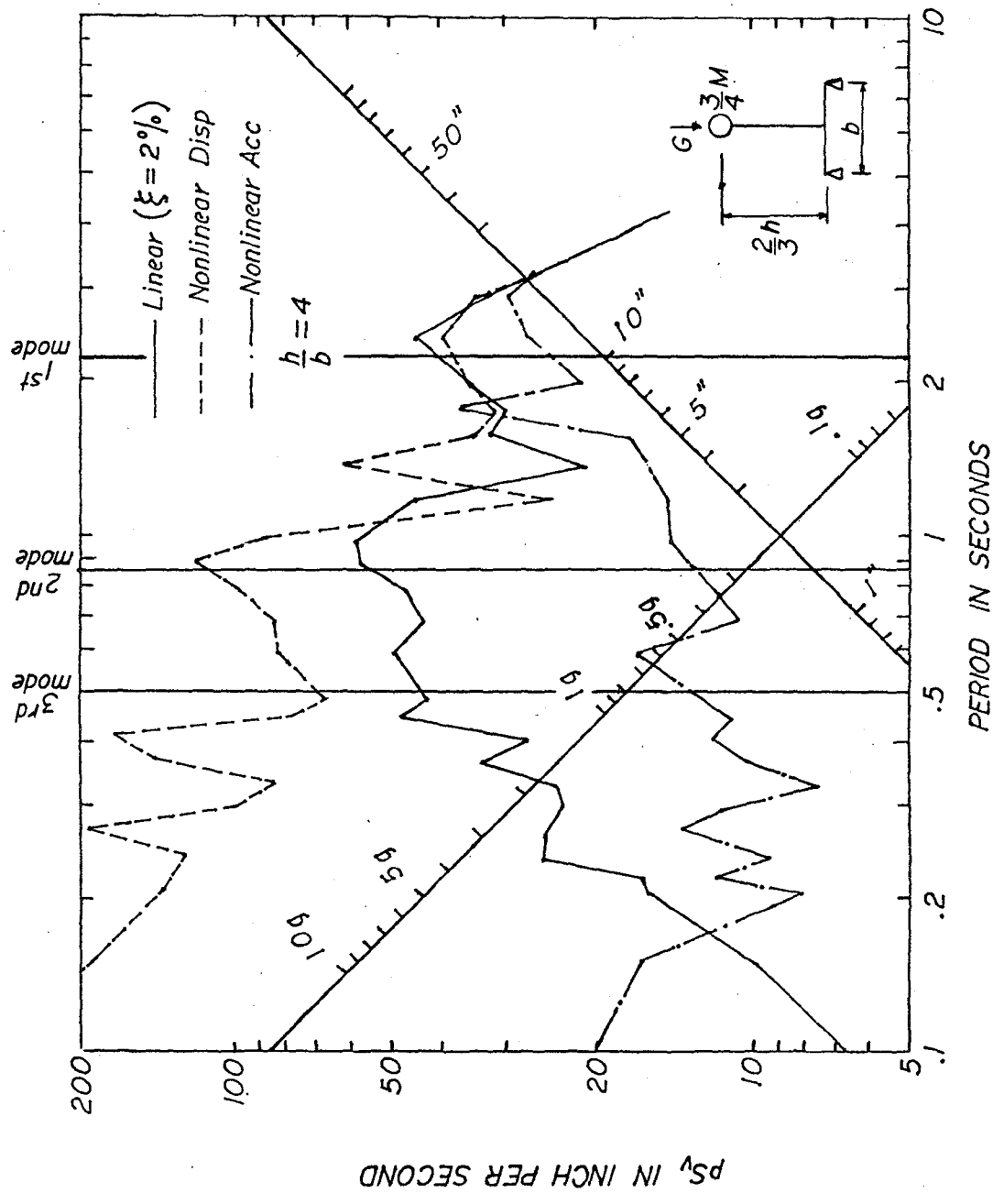

Figure 5.1.5. Linear and nonlinear response spectra

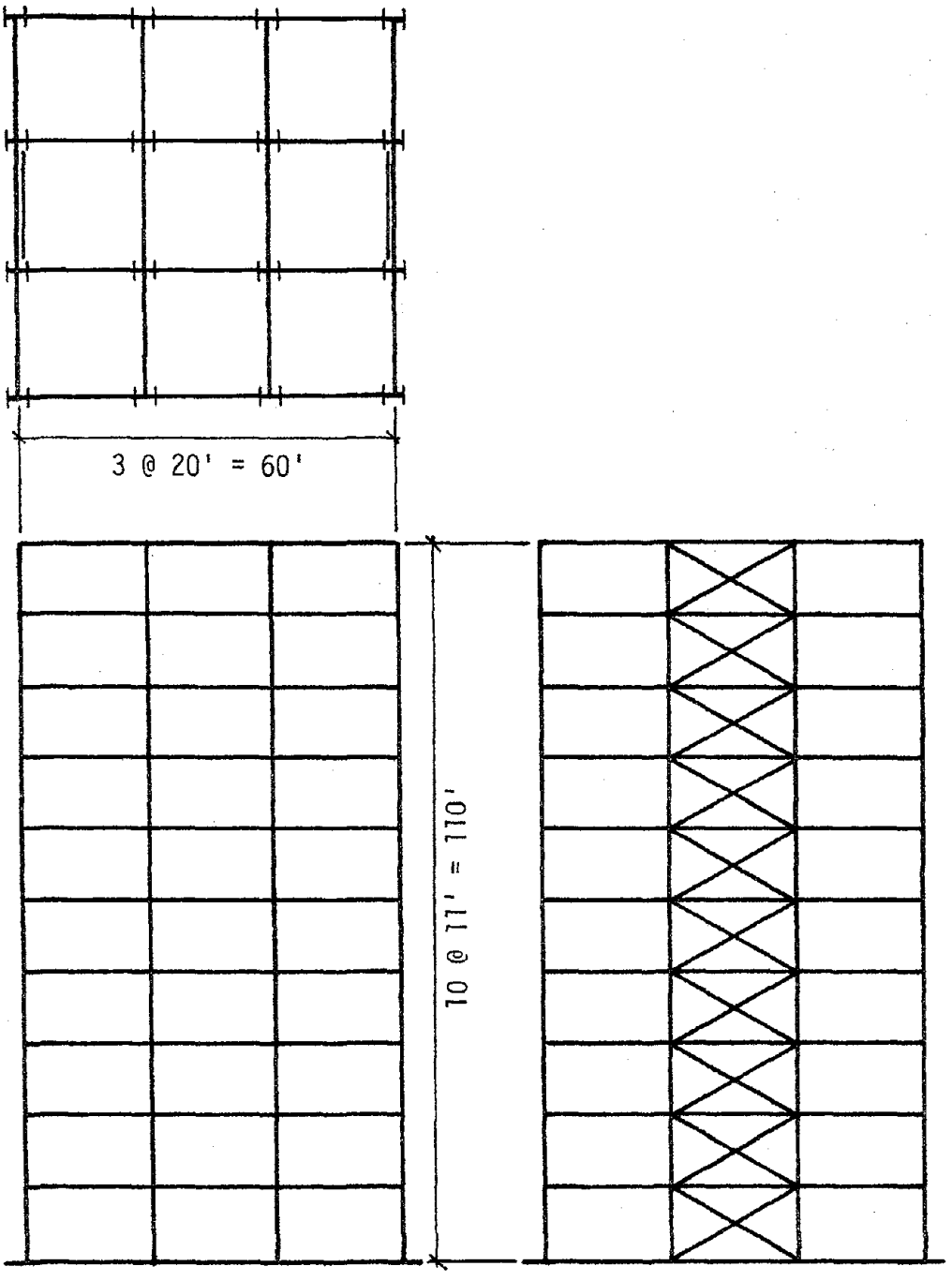

Figure 5.1.6. 10 Story Steel Frame

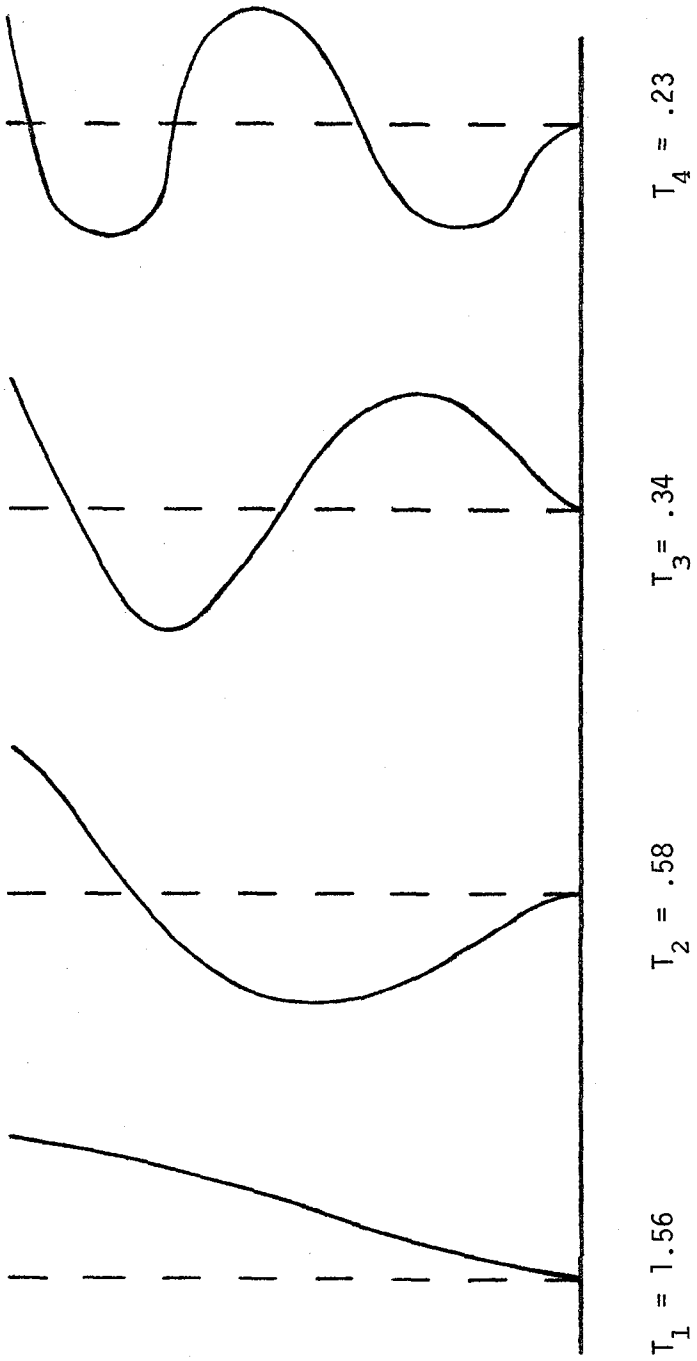

Figure 5.1.7. First Four Periods (sec) and Modes of Vibration, *Moment Frame*

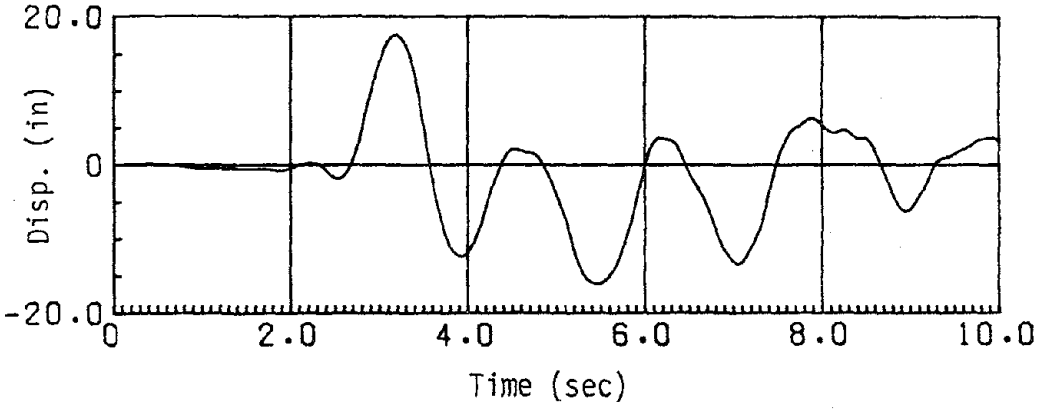

a) Fixed-Base Response

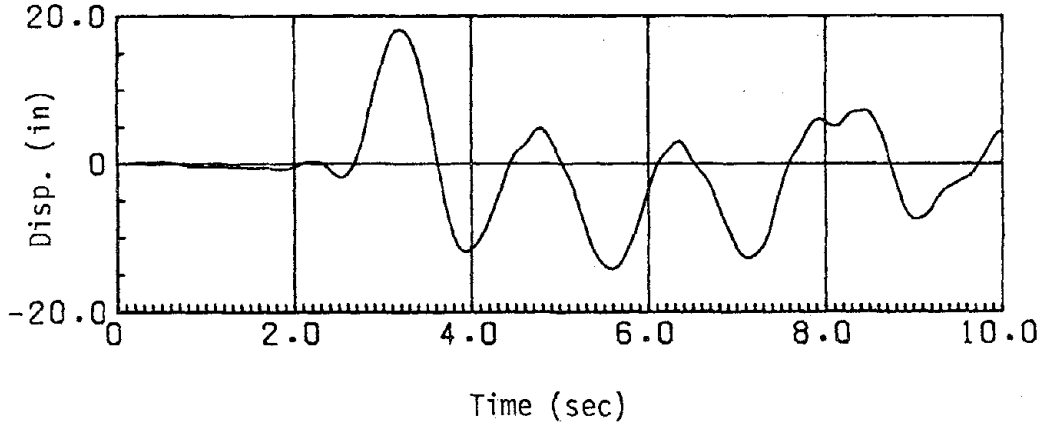

b) Uplift Response

Figure 5.1.8. Moment Frame Lateral Roof Displacements, Pacoima Dam Record

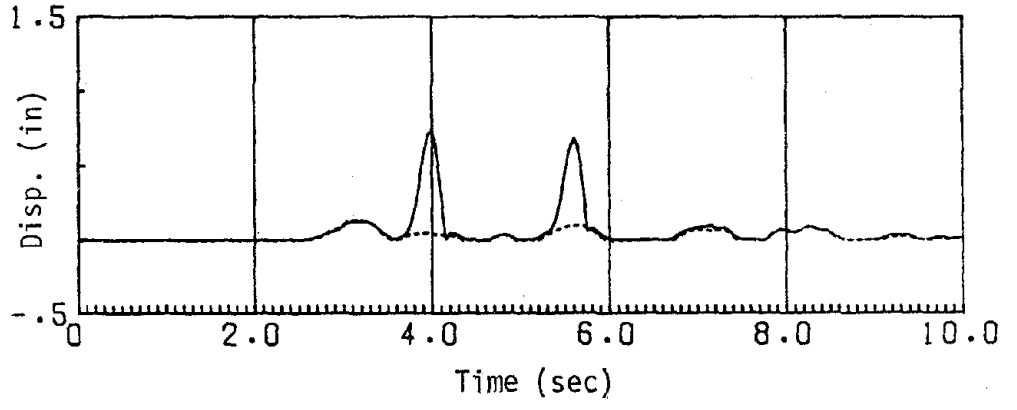

a) Columns 1 (solid) and 2 (dashed)

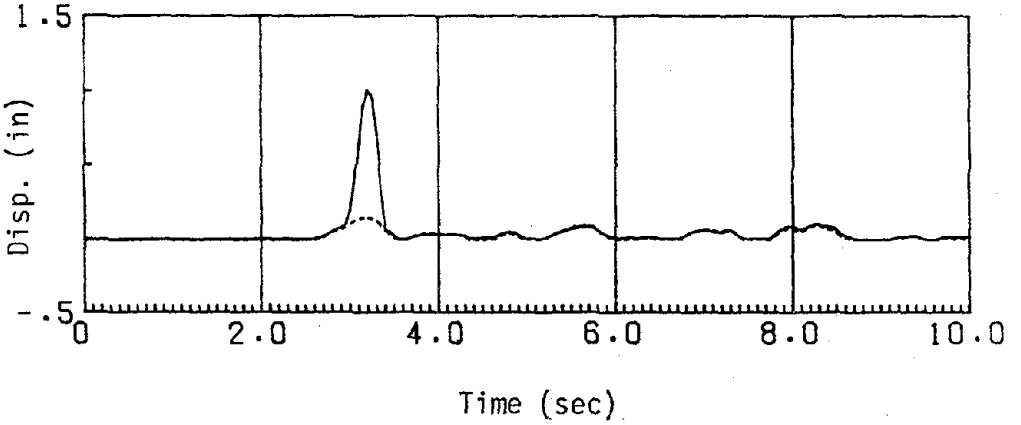

b) Columns 3 (dashed) and 4 (solid)

Figure 5.1.9. Moment Frame Column Uplifts, Pacoima Dam Record

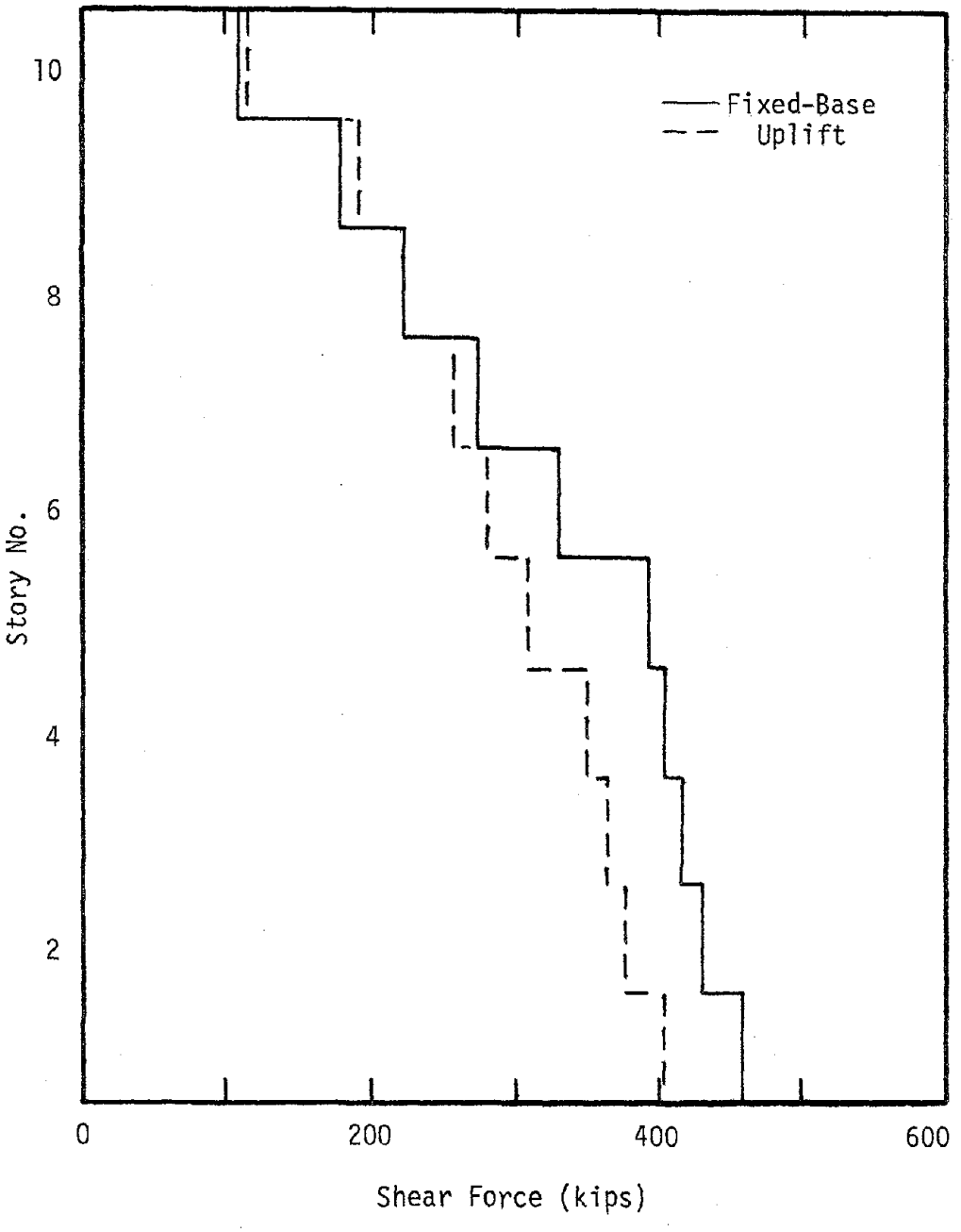

Figure 5.1.10. Moment Frame Peak Story Shears, Pacoima Dam Record

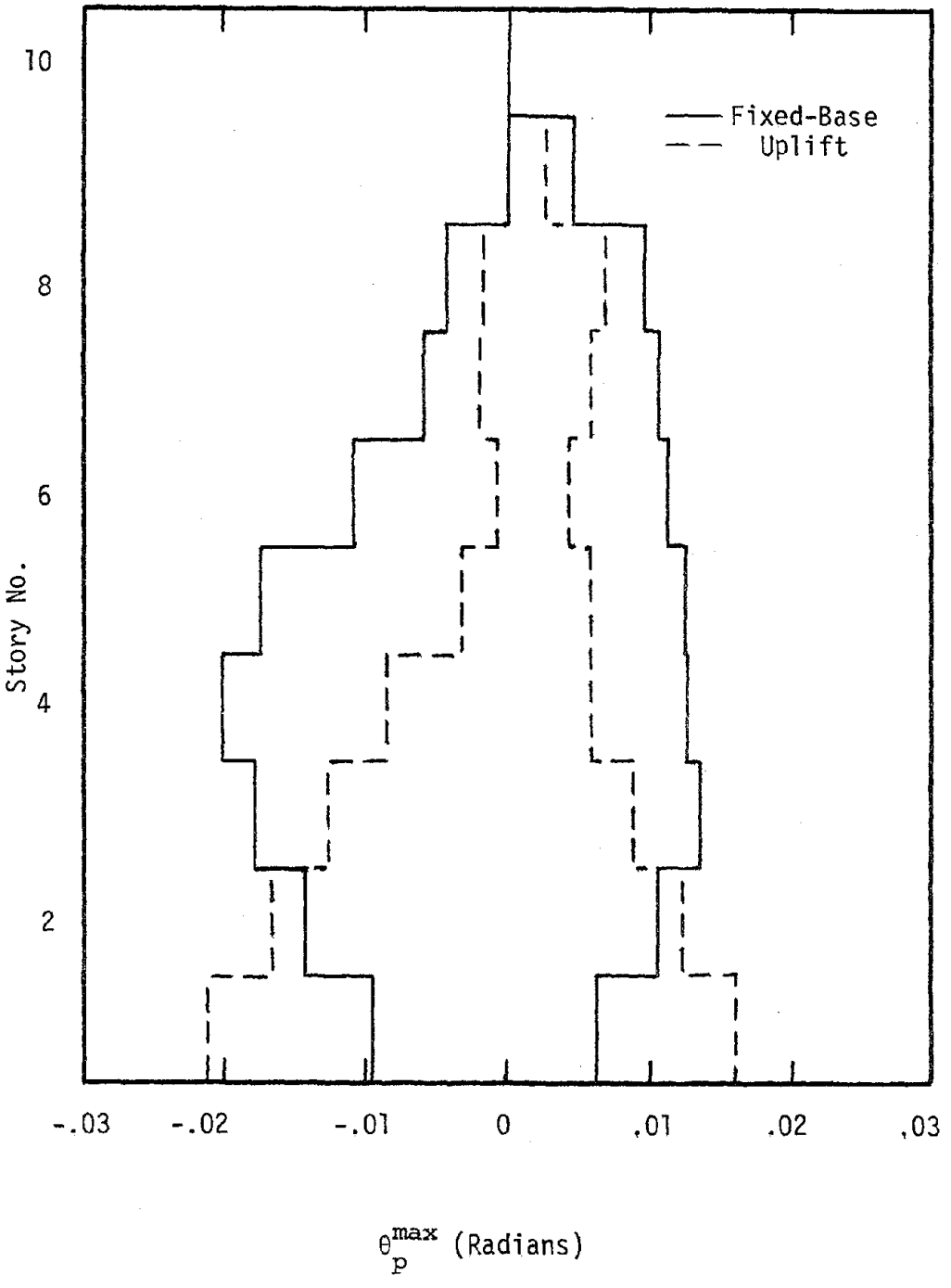

Figure 5.1.11. Maximum Girder Plastic Hinge Rotations, Exterior Bay of Moment Frame, Pacoima Dam Record

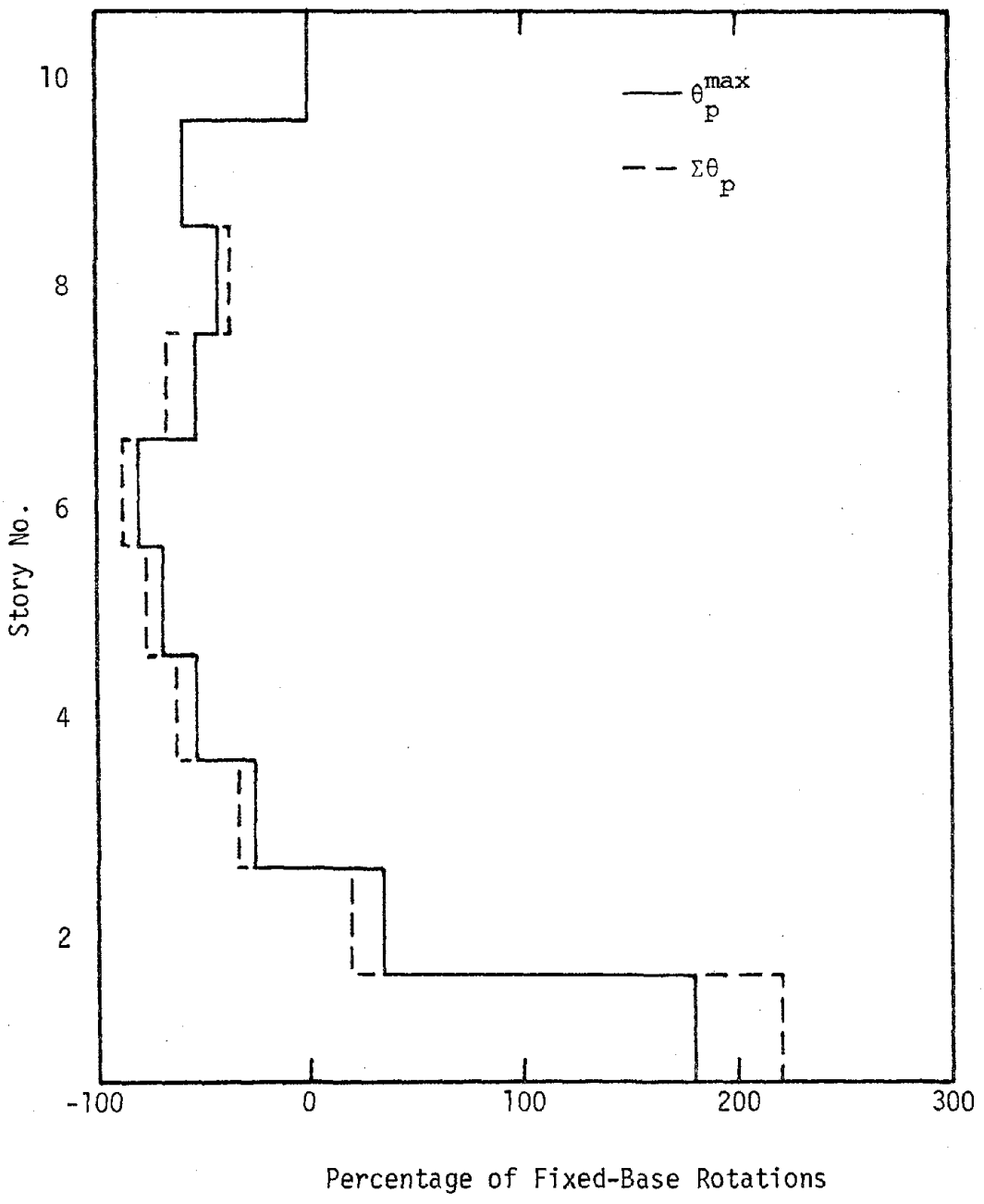

Figure 5.1.12. Average Change due to Uplift in Moment Frame Girder Plastic Hinge Rotations, Pacoima Dam Record

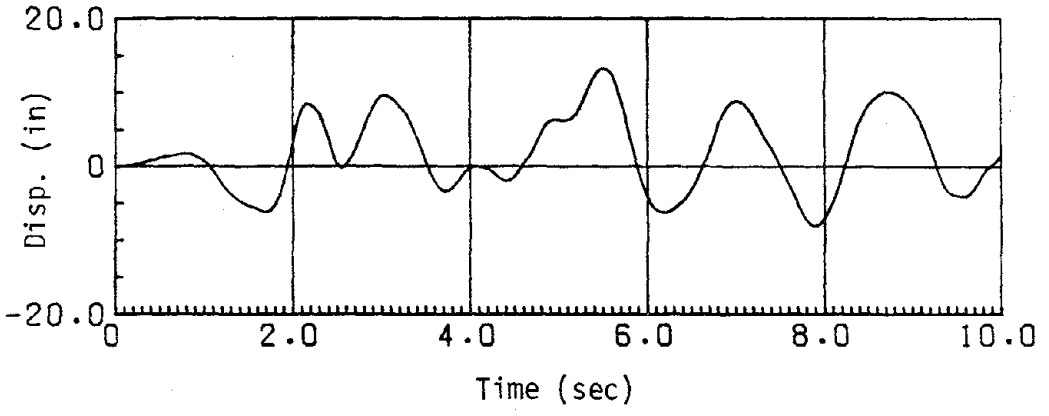

a) Fixed-Base Response

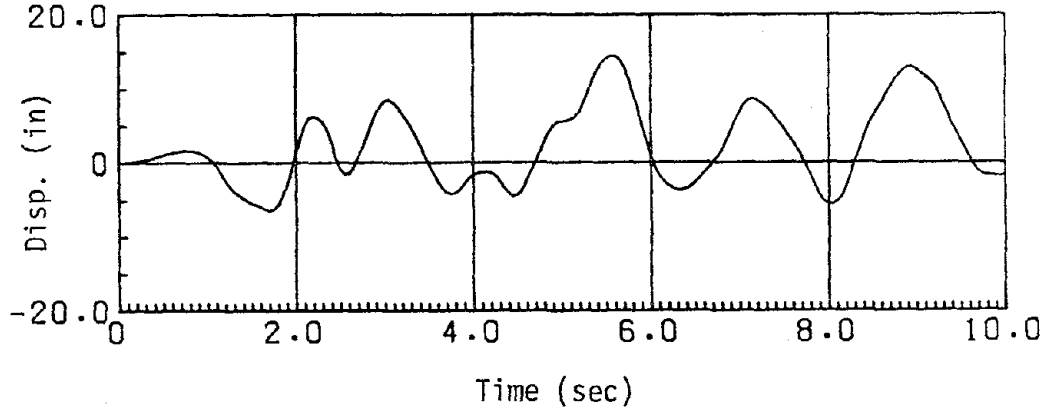

b) Uplift Response

Figure 5.1.13. Moment Frame Lateral Roof Displacements, Magnified El Centro Record

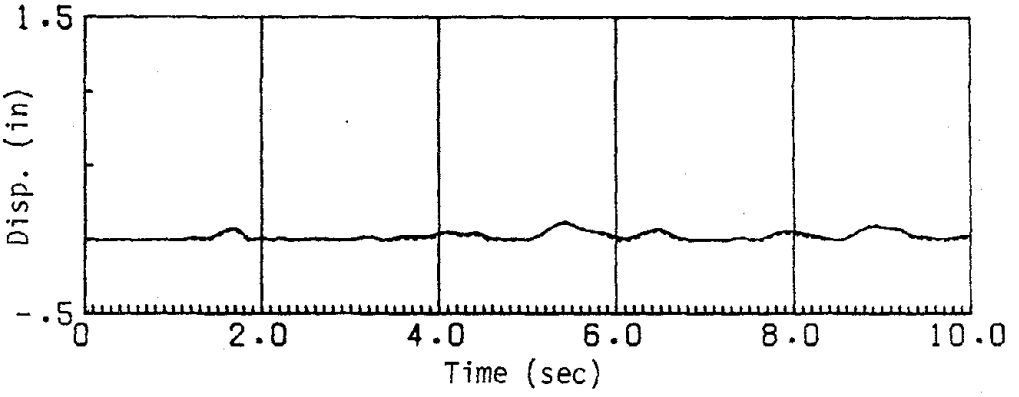

a) Columns 1 (solid) and 2 (dashed)

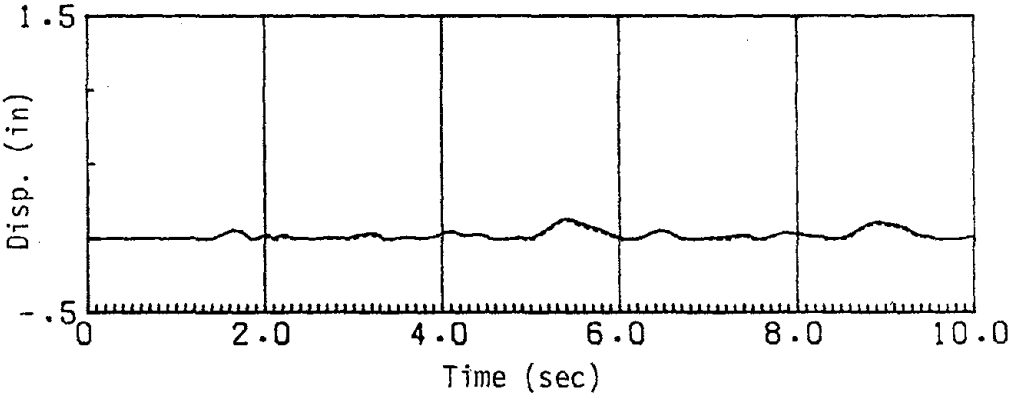

b) Columns 3 (dashed) and 4 (solid)

Figure 5.1.14. Moment Frame Column Uplifts, Magnified El Centro Record

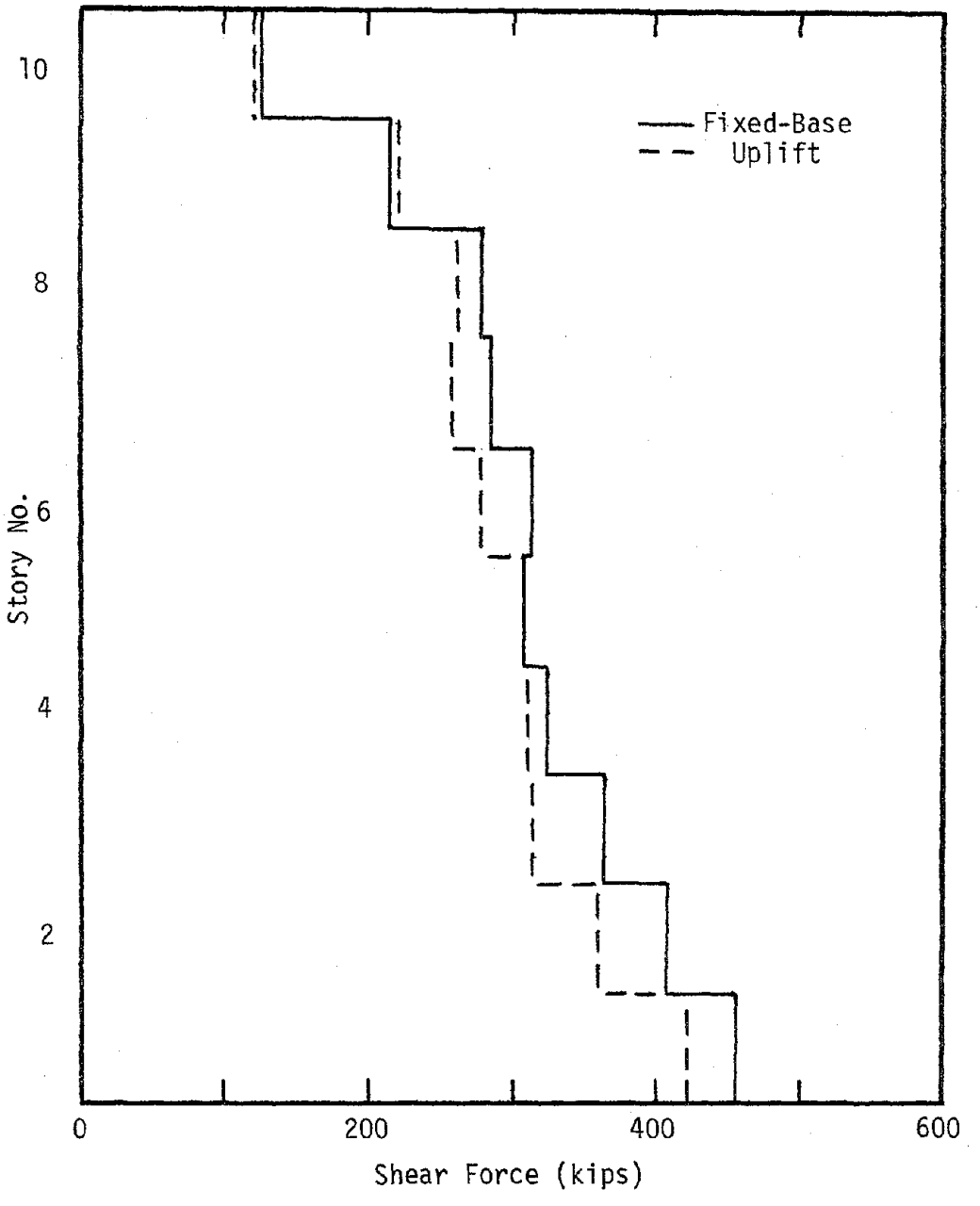

Figure 5.1.15. Moment Frame Peak Story Shears, Magnified El Centro Record

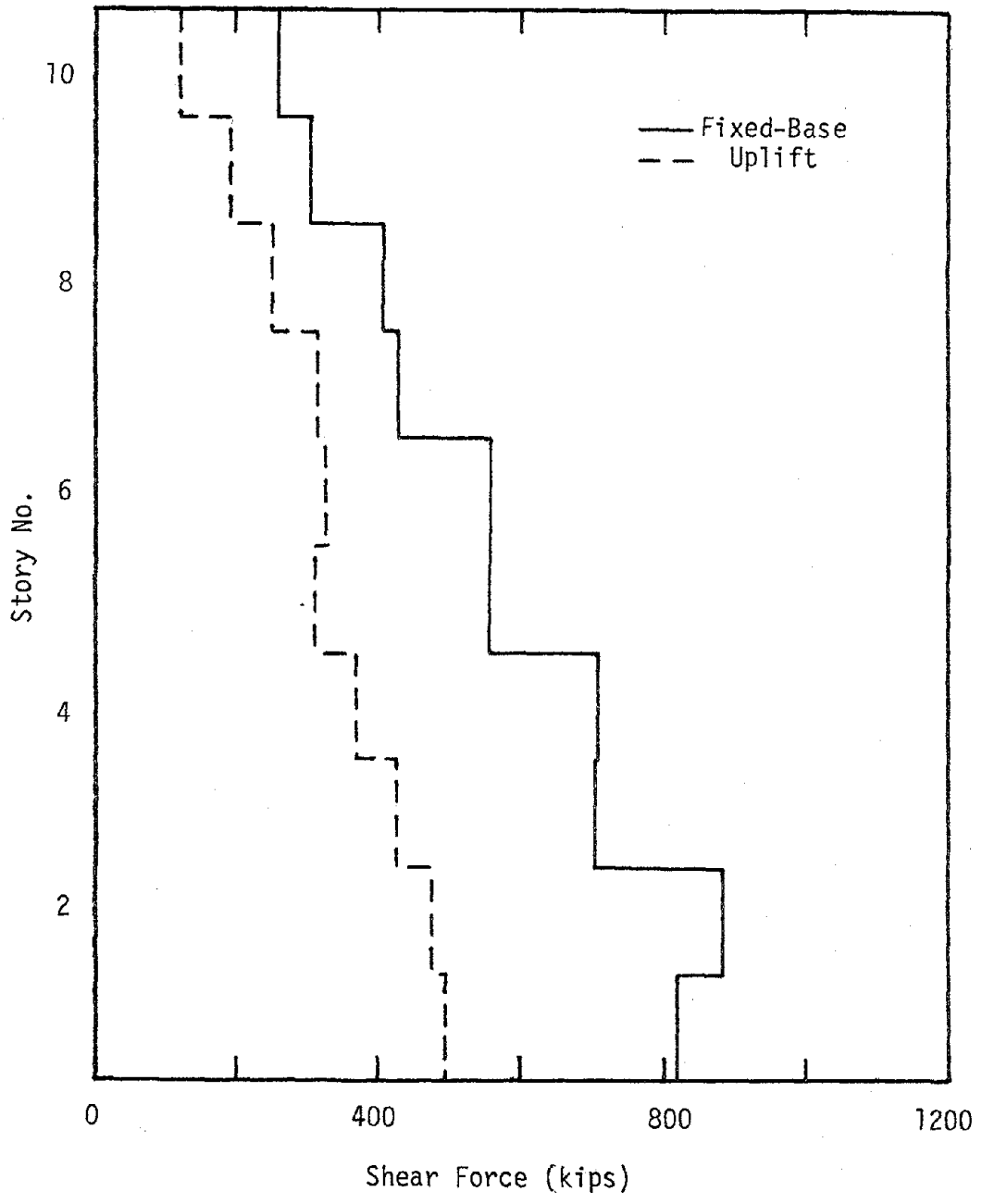

Figure 5.1.16. Modified Moment Frame Peak Story Shears, Pacoima Dam Record

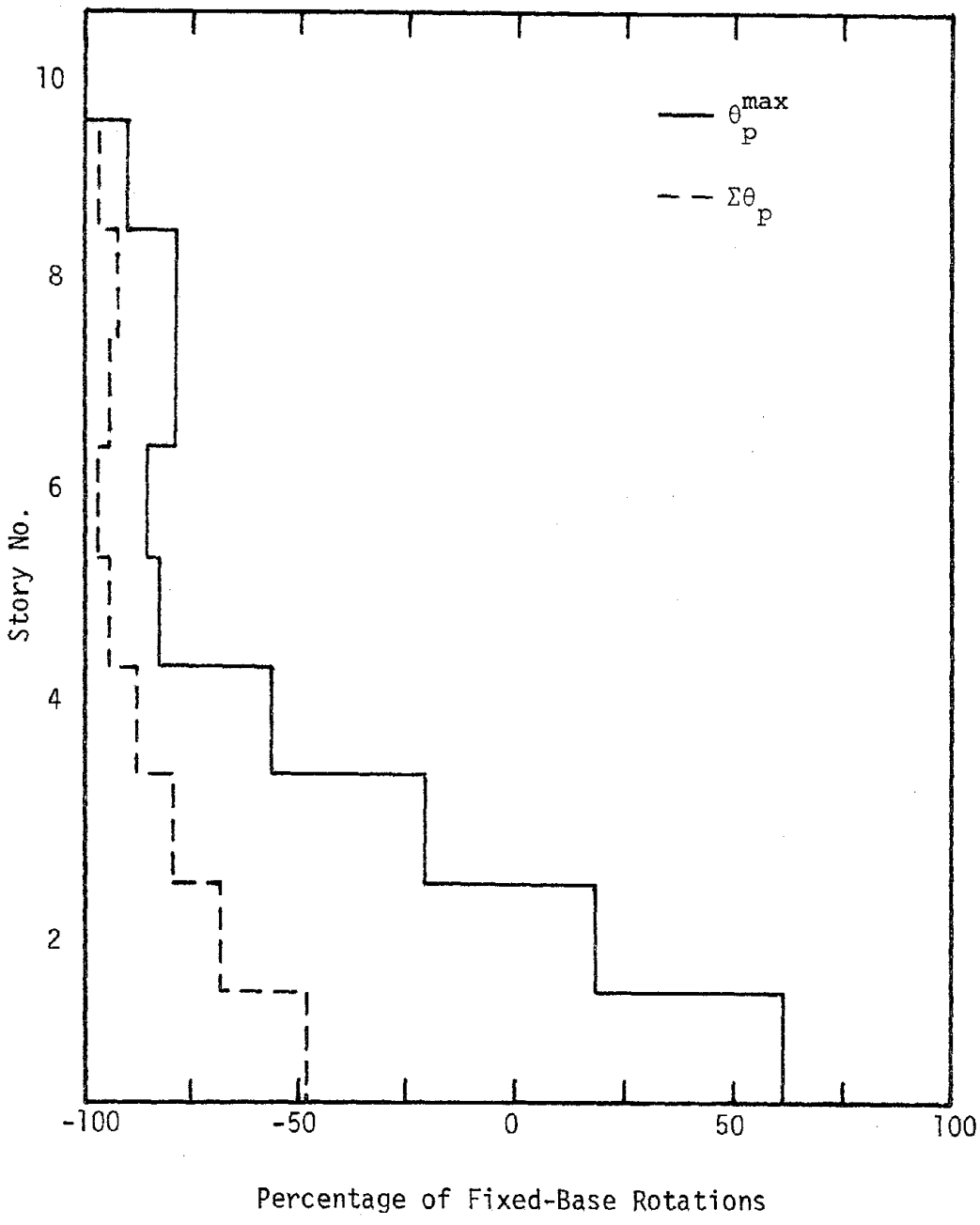

Figure 5.1.17. Average Change due to Uplift in Modified Moment Frame Girder Plastic Hinge Rotations, Pacoima Dam Record

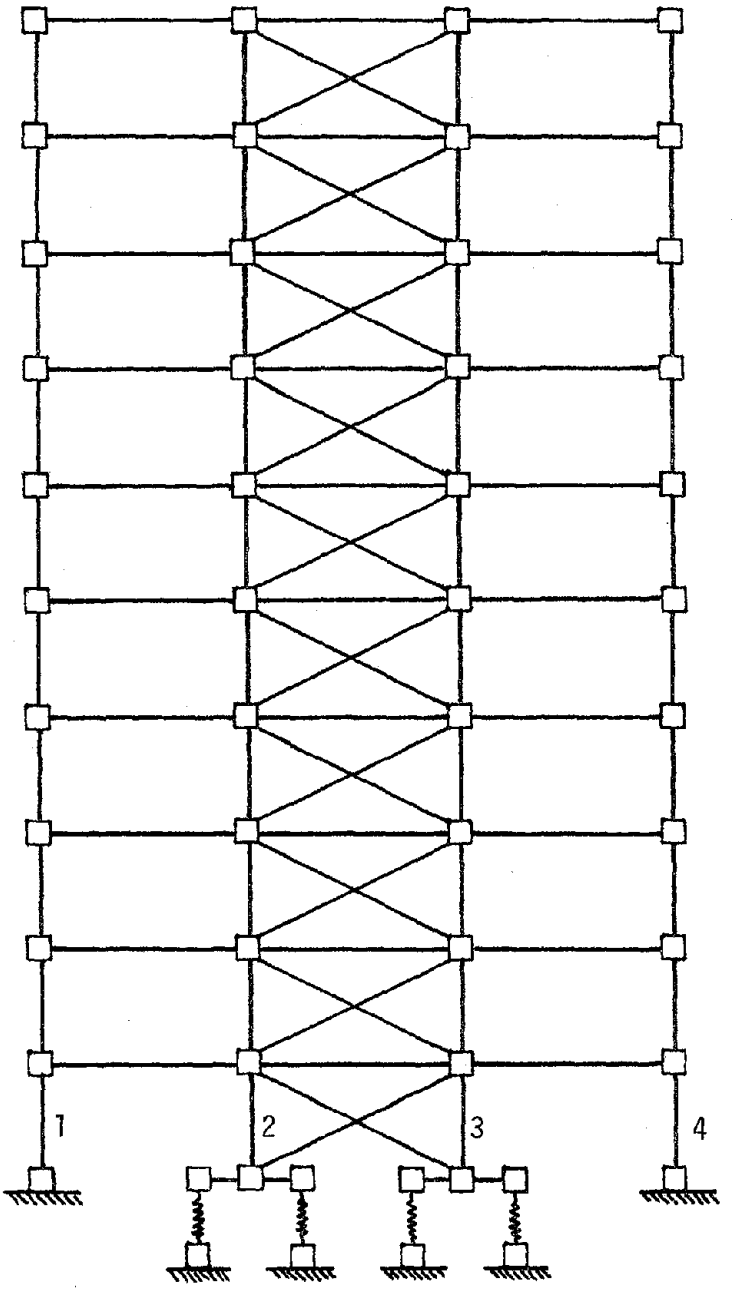

Figure 5.2.1. Braced Frame Analytical Model

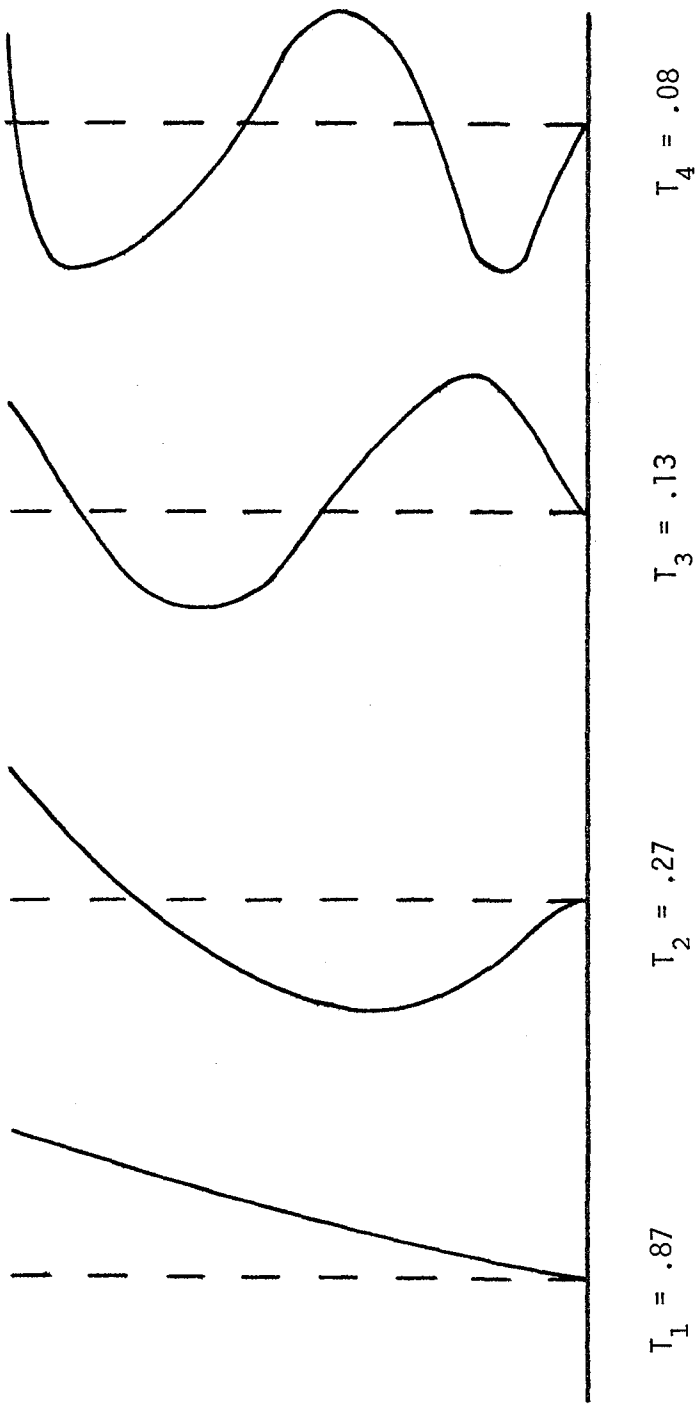

Figure 5.2.2. First Four Periods (sec) and Modes of Vibration, Braced Frame

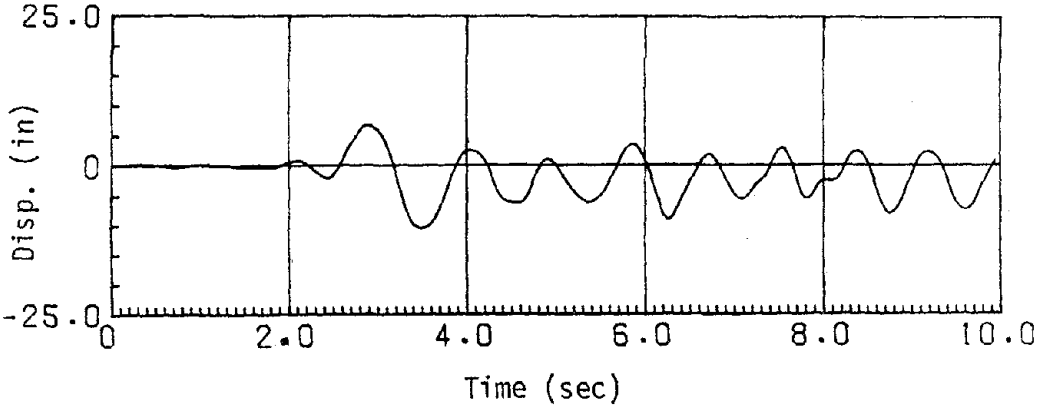

a) Fixed-Base Response

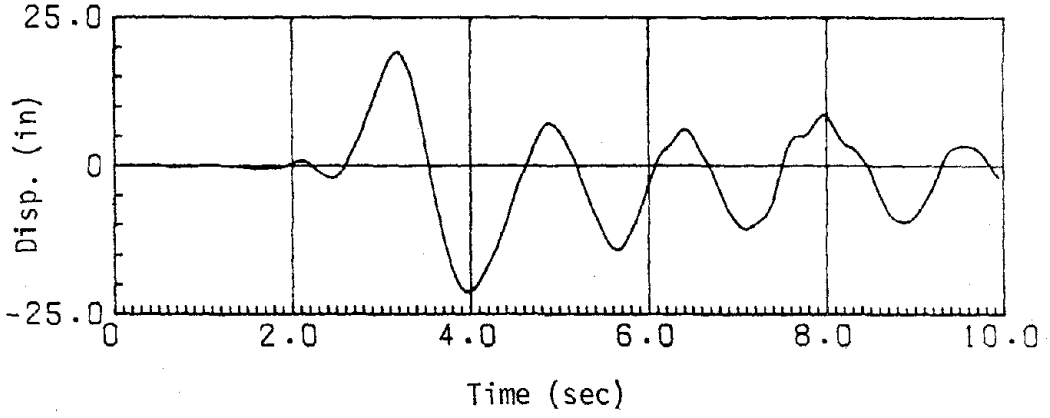

b) Uplift Response

Figure 5.2.3. Braced Frame Lateral Roof Displacements, Pacoima Dam Record

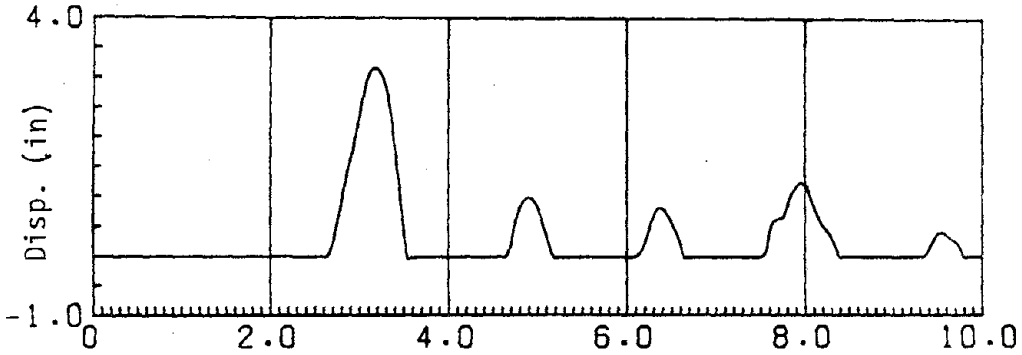

a) Column 2

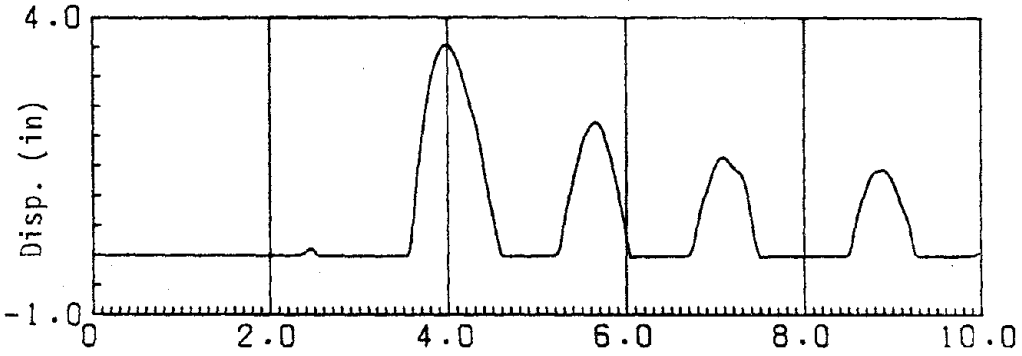

b) Column 3

Figure 5.2.4. Braced Frame Column Uplifts, Pacoima Dam Record

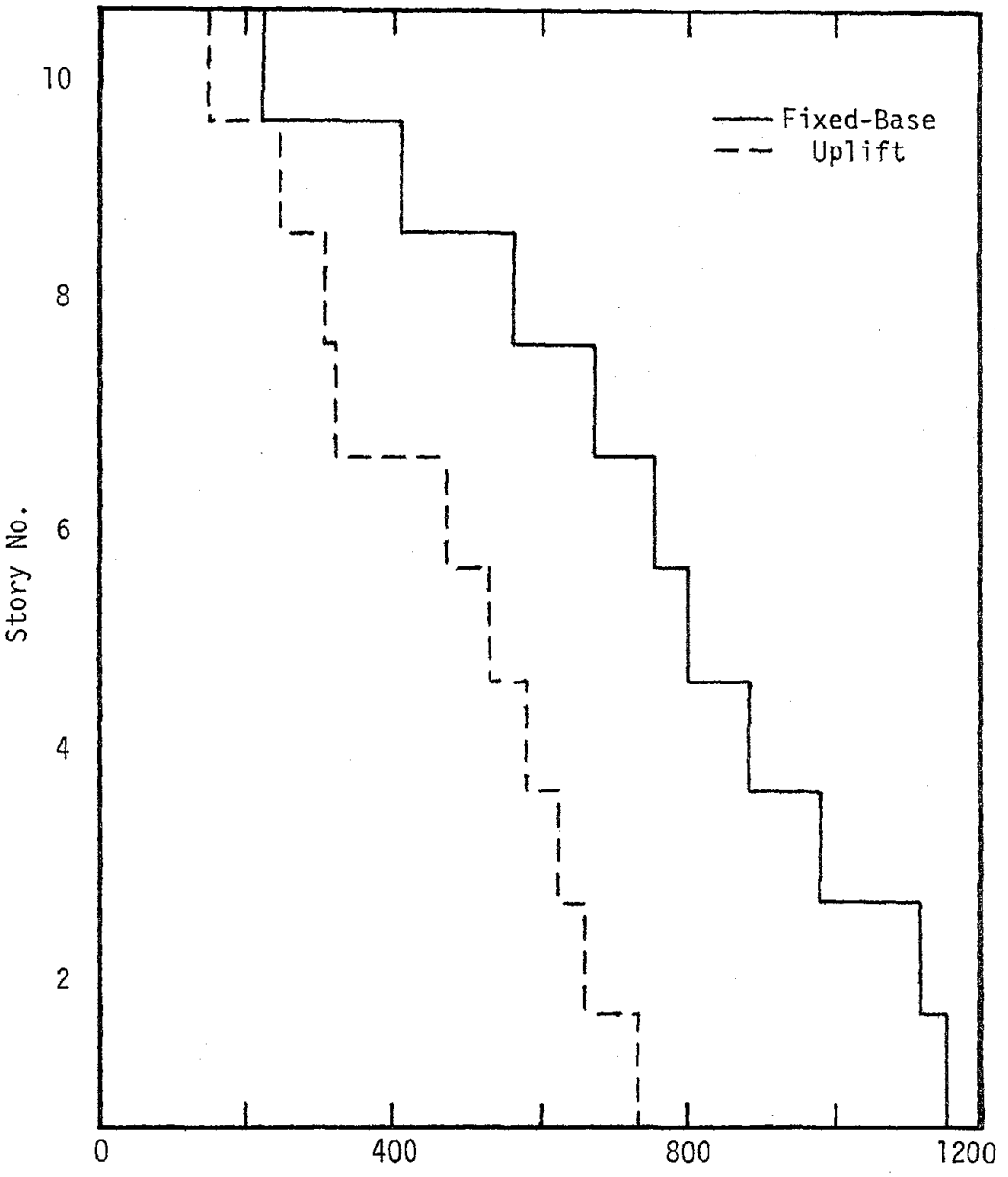

Figure 5.2.5. Braced Frame Peak Story Shears, Pacoima Dam Record

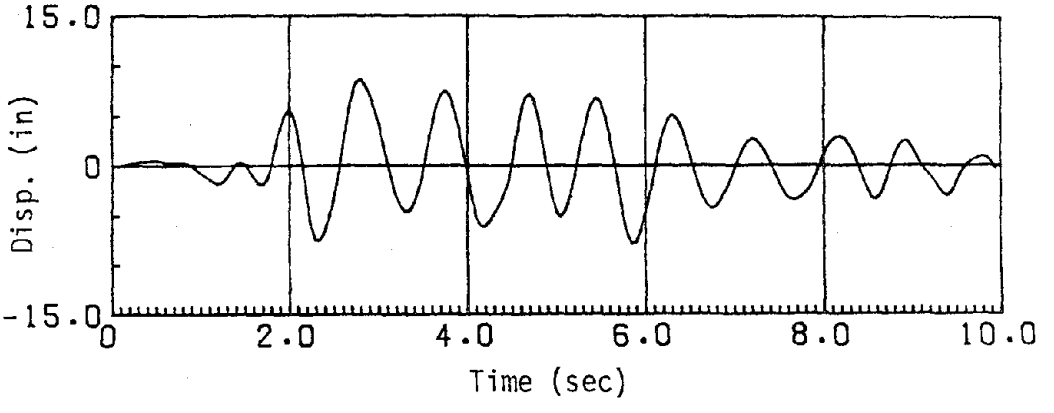

a) Fixed-Base Response

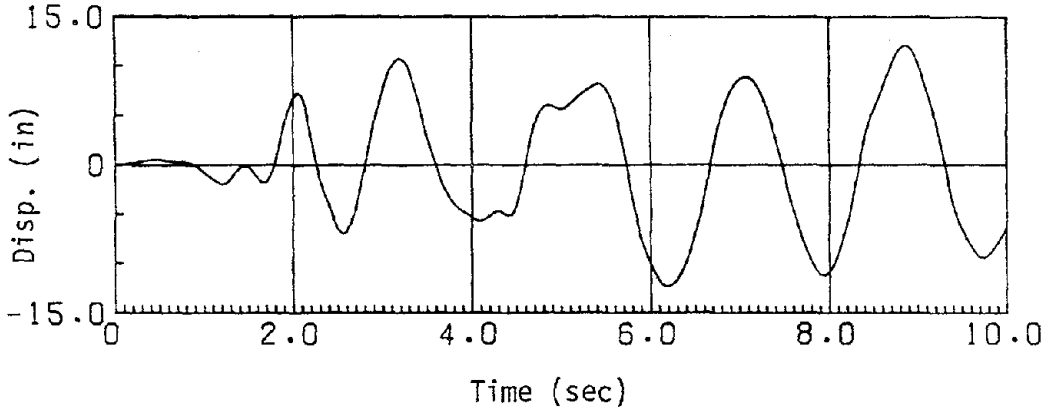

b) Uplift Response

Figure 5.2.6. Braced Frame Lateral Roof Displacement, Magnified El Centro Record

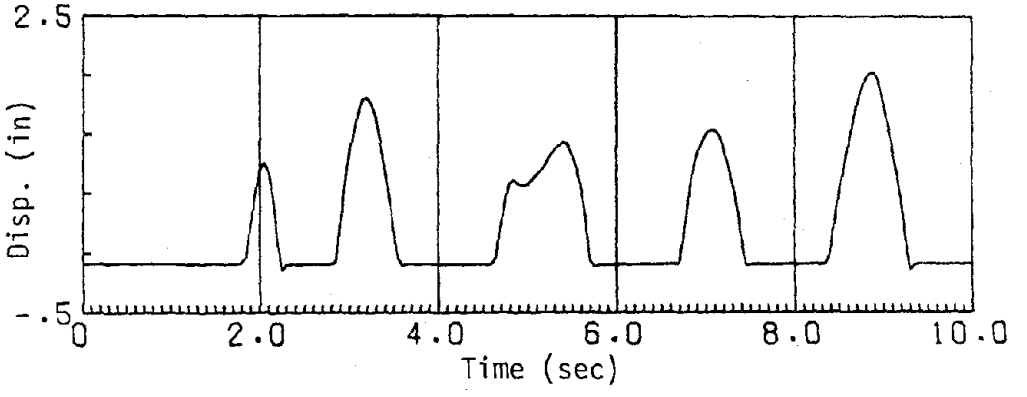

a) Column 2

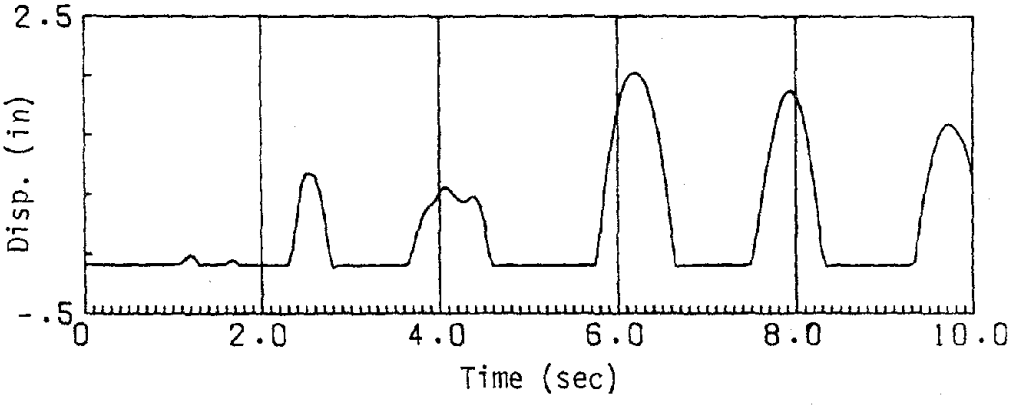

b) Column 3

Figure 5.2.7. Braced Frame Column Uplifts, Magnified El Centro Record

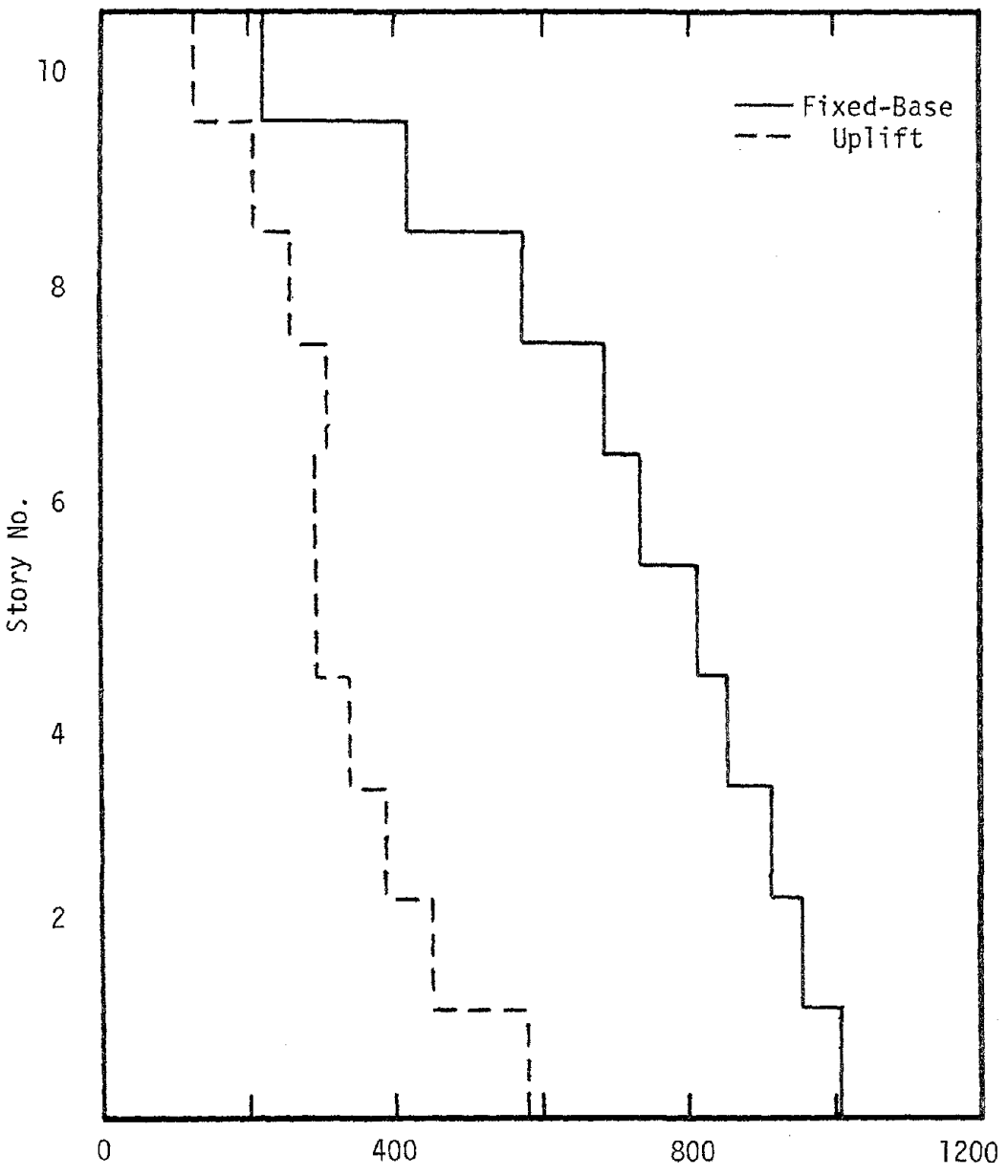

Figure 5.2.8. Braced Frame Peak Story Shears, Magnified El Centro Record

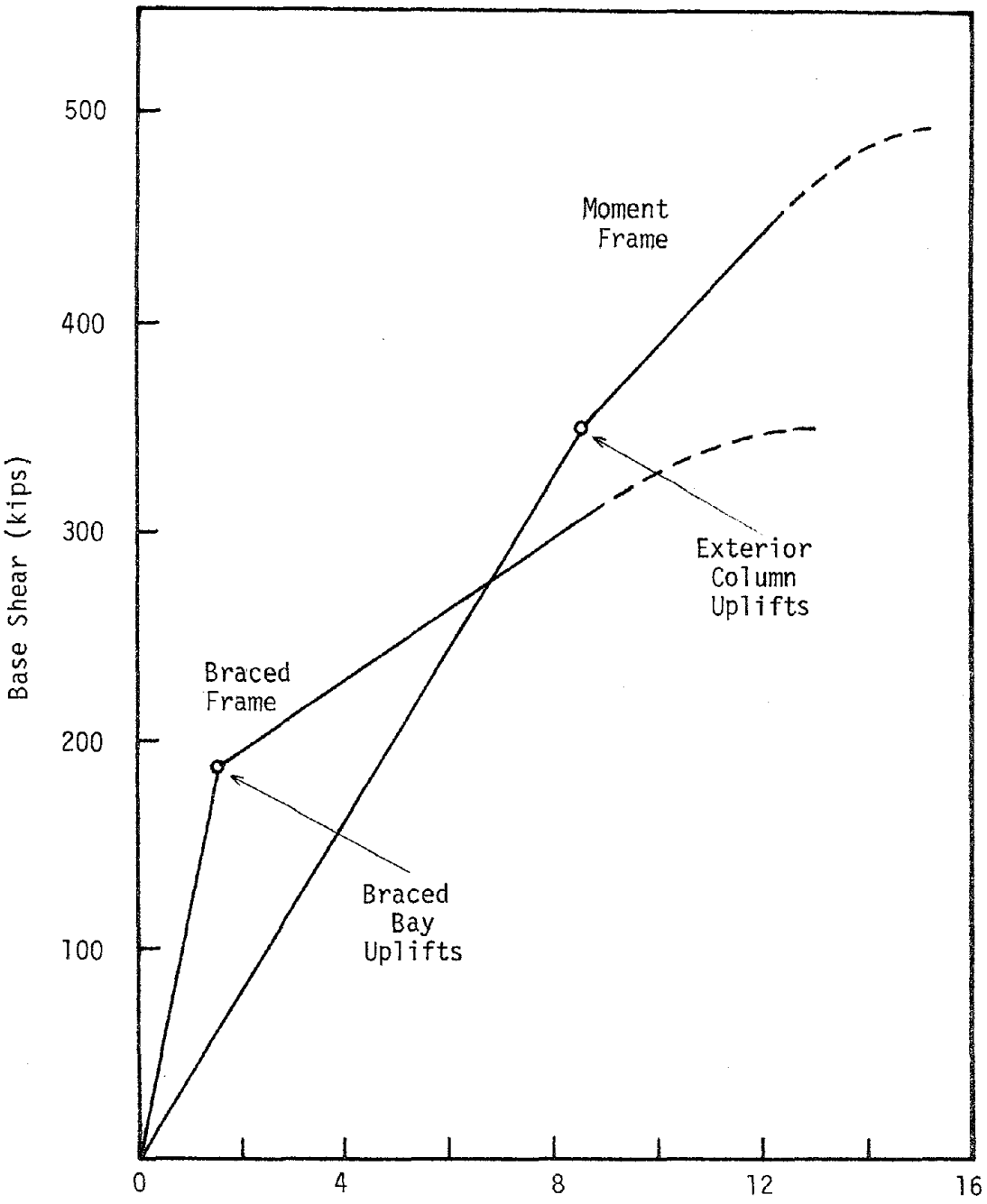

Figure 5.2.9. First Mode Pseudo-Dynamic Load-Deformation Behavior

5.3 Shear Walls

Two conceptually different shear wall systems were examined; a core-stiffened structure and a coupled shear wall system. The core-stiffened structure will be discussed prior to the coupled-wall.

20-STORY CORE-STIFFENED FRAME

The plan and elevation of the 20-story structure studied is shown in Figure 5.3.1. As can be seen, the plan is doubly symmetric with five bays in each direction and a central stiffening core. The elevation consists of 20 equal floors at twelve feet each. The core is intended to provide essentially all the initial lateral resistance, although full continuity is assumed for all connections. Rigid diaphram action is intended to be provided by the floor slab at each level. The structure is designed so as to remain linear and elastic under combined dead, live and seismic loads corresponding to a dead weight base shear coefficient of .06. All provisions of ATC-3 are satisfied for Zone 7 and stiff soil conditions.

The two-dimensional analytical model utilized in the study is shown in Figure 5.3.2. Basically, the structure is assumed to be a collection of line elements connected at the indicated nodes, at which the mass of the structure is also assumed to be lumped.

The core is modeled as a column with rigid links extending laterally from the central node to either edge of the core. The core is supported on springs with zero tensile capacity and stiffness, representing the uplift behavior of this element. The interaction of the core with the moment frames is modeled by the indicated overlapping of beam elements;

(see Figure 2) the stiffness and capacity of each beam element is scaled to represent the actual number of elements of the physical structure modeled. The moment frame columns are assumed rigidly fixed to the foundation, implying no potential for uplift behavior in these elements; this assumption was verified by subsequent analyses. For analyses in which unlimited overturning capacity is assumed, the foundation support springs are assigned equal tensile and compressive capacity. The first two linear mode shapes and corresponding natural periods of this model are shown in Figure 5.3.3. Damping is assumed to be approximately 2% critical for the first mode.

Seismic Response

The roof displacements predicted during the Pacoima Dam earthquake for the two base condition assumptions are shown in Figure 5.3.4. As can be seen there is essentially no difference between the two cases; the maximum roof displacement of approximately 90 cm (3 feet) corresponds to a relative drift index of 1.80.

The shears developed in the core for this ground motion are shown in Figure 5.3.5. The dramatic reduction in seismic loads with uplift allowed is obvious. The core overturning moments, shown in Figure 5.3.6 are reduced to a similar degree. Stress resultants in the core for the Pacoima Dam ground motion are reduced by a factor of nearly one-half by allowing transient base uplift. The maximum amplitude of uplift predicted is 3.5 cm (1.4"). Restraining this uplift would require a net anchorage force of approximately 44,600 kN (10,000^{k}) at each corner of the core wall.

The total shear envelopes for this frame subjected to the Pacoima Dam earthquake are shown in Figure 5.3.7. The total shear reduction is not

as large as that observed for the core alone; the connected moment frames carried more shear with core uplift allowed. A considerable degree of higher mode response is evident as well in these envelopes.

Ductility demand was not significantly affected during the Pacoima Dam earthquake by the base condition assumption. The maximum plastic hinge rotation with uplift allowed was .046 radians. In both cases ductility demand was limited to the beams connecting the core with the remainder of the structure.

The roof displacements predicted during the magnified El Centro earthquake are shown in Figure 5.3.8. Again there is very little difference between the two base condition assumptions; with uplift allowed the maximum displacement is 42 cm (16.7"), compared to 46 cm (18.5") for the fixed base condition.

The shears developed in the core for the El Centro record are shown in Figure 5.3.9. As for the previous ground motion, the reduction in seismic loads on the core is significant. The core overturning moments, shown in Figure 5.3.10, are reduced similarly. The maximum amplitude of uplift predicted for the magnified El Centro earthquake is 2 cm (0.8"); restraining this uplift would require a net anchorage of 31,200 kN (7000^k) at each corner of the core.

The total shear envelopes for the El Centro earthquake are shown in Figure 5.3.11. As for the Pacoima Dam response, the moment frames carried a greater degree of shear once the core had uplifted. There is a lesser degree of higher mode response evident for the El Centro record, which would be expected from an examination of the response spectrum.

The only really surprising result from these analyses is the total lack of any loss in drift control when base uplift is allowed. This maintenance of drift control is at least partially attributable to the energy dissipation mechanism associated with hinging of the link beams. This degree of hinging and of energy dissipation was nearly unaffected by the base condition. Without this mechanism present, some loss of drift control would possibly be evident with uplift allowed.

As demonstrated by the previous two described examples, stiffened building frames would appear to benefit considerably through the action of transient foundation uplift during severe seismic excitation. Seismic loadings in the example structures were reduced by as much as 50%, and ductility demand was limited to connecting elements between stiffened and non-stiffened portions of the structures. There was no marked loss of drift control for the structures examined, and considerable foundation anchorage requirements were eliminated.

In such stiffened building frames as those examined, the transition in behavior at the initiation of uplift is quite abrupt; the stiffness is immediately reduced to that associated with a mechanism or near mechanism, depending on the stiffness of the coupled moment frame. An unstiffened multi-bay moment frame by comparison has a more gradual transition; uplift progresses from the outer column lines inward, and a mechanism forms only after all column lines but the most "leeward" have uplifted.

The addition of additional bays for either a braced or unbraced frame would therefore tend to make the transition to uplift behavior less abrupt, for a braced frame the assumption being made that additional bays would

increase the stiffness of the coupled frame. With such a less abrupt transition one would in general expect less dramatic load reductions and a greater retention of drift control. This trend was observed for the 3 and 5 bay stiffened frames examined in this study, as well as for 3 and single bay moment frames examined in earlier work. [3,7]

In light and moderate earthquakes, for which very little or no uplift would be anticipated, the additional drift control offered by stiffened building frames is extremely helpful in limiting or eliminating nonstructural damage. A potential disadvantage of conventional stiffened frames, a lack of available ductility under severe excitations, has been mitigated in the examples offered through allowing transient uplift of the stiffening element. Ductility demand has thus been limited to non-gravity load resisting bending elements, where it is more easily and more safely accommodated.

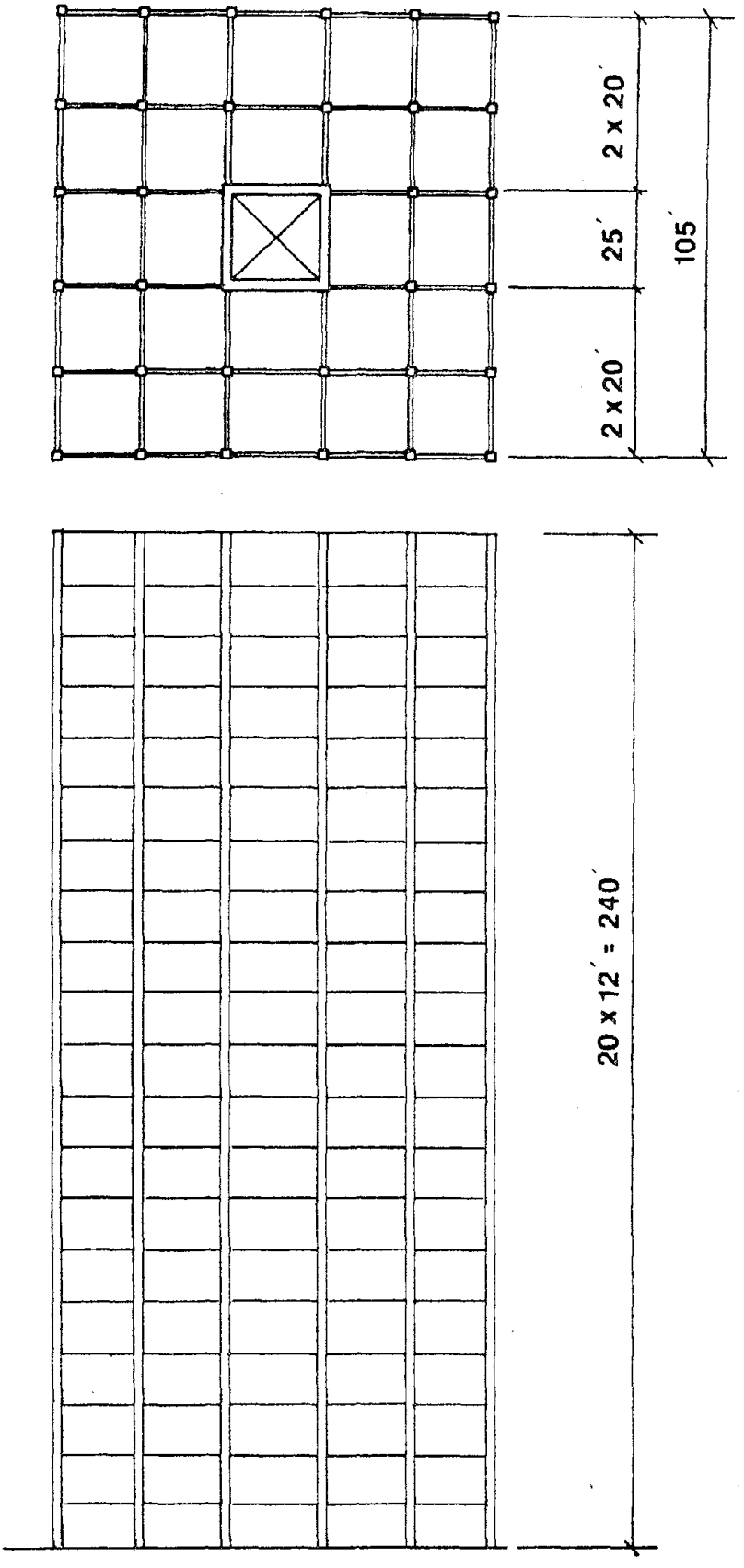

Figure 5.3.1. Twenty story core wall structure

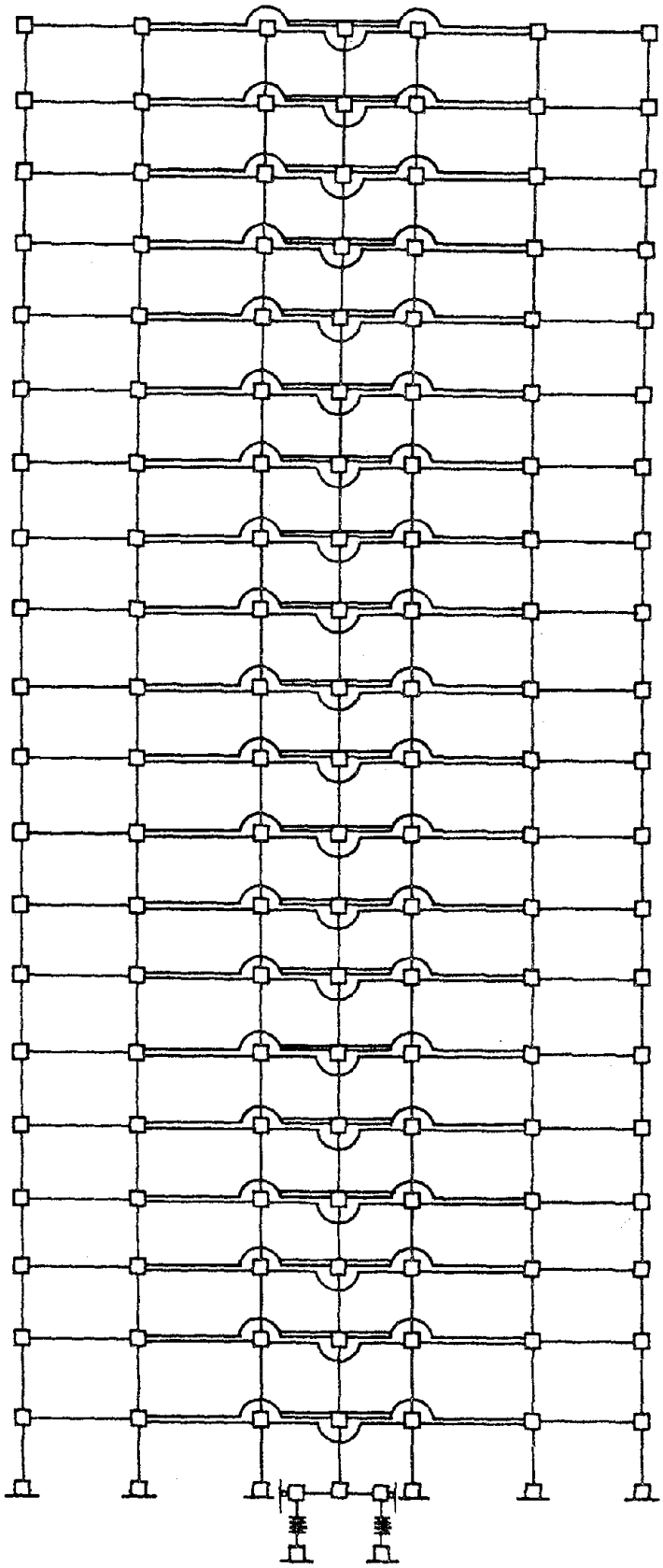

Figure 5.3.2. Analytical model of core wall structure

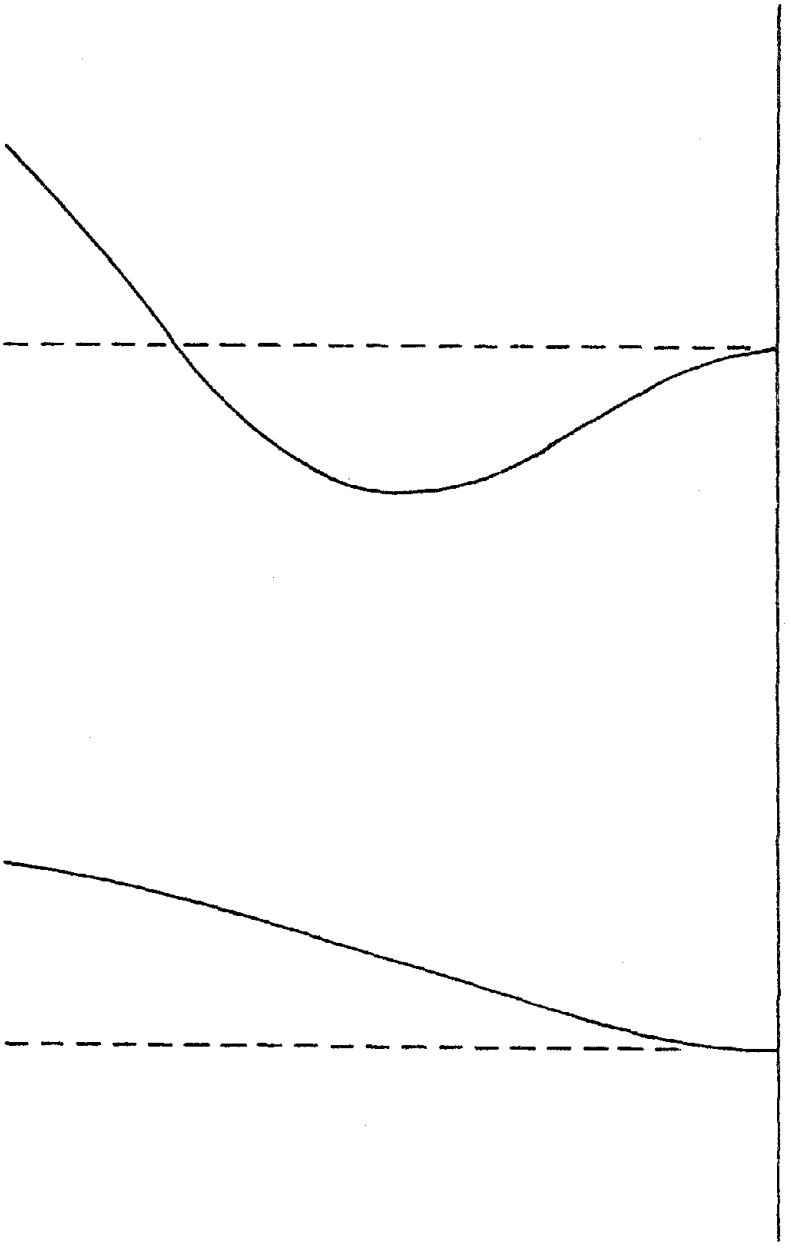

Figure 5.3.3. Periods and mode shapes; core wall structure

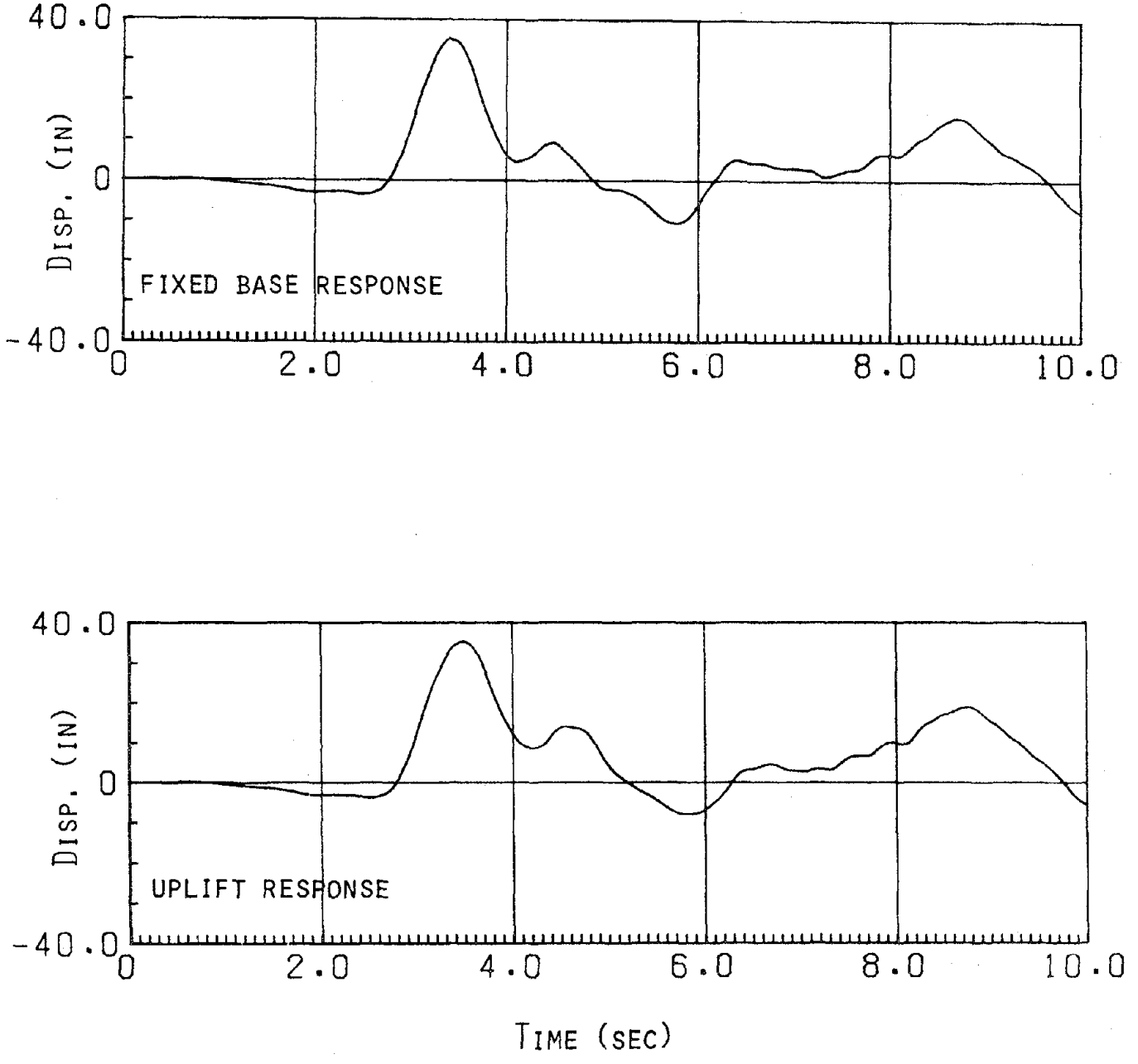

Figure 5.3.4. Roof Displacements; Pacoima Dam EQ

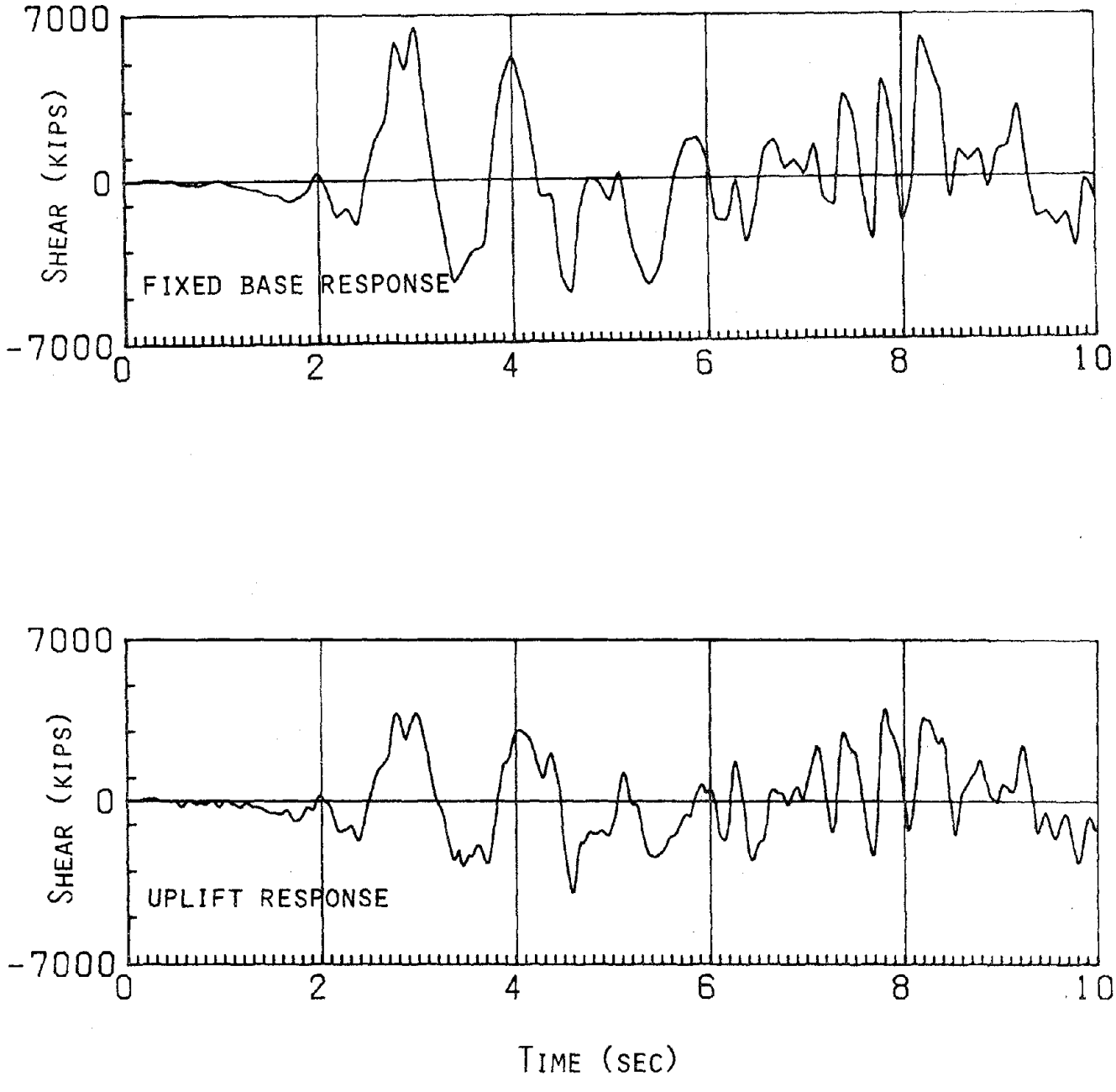

Figure 5.3.5. Core shears; Pacoima Dam EQ

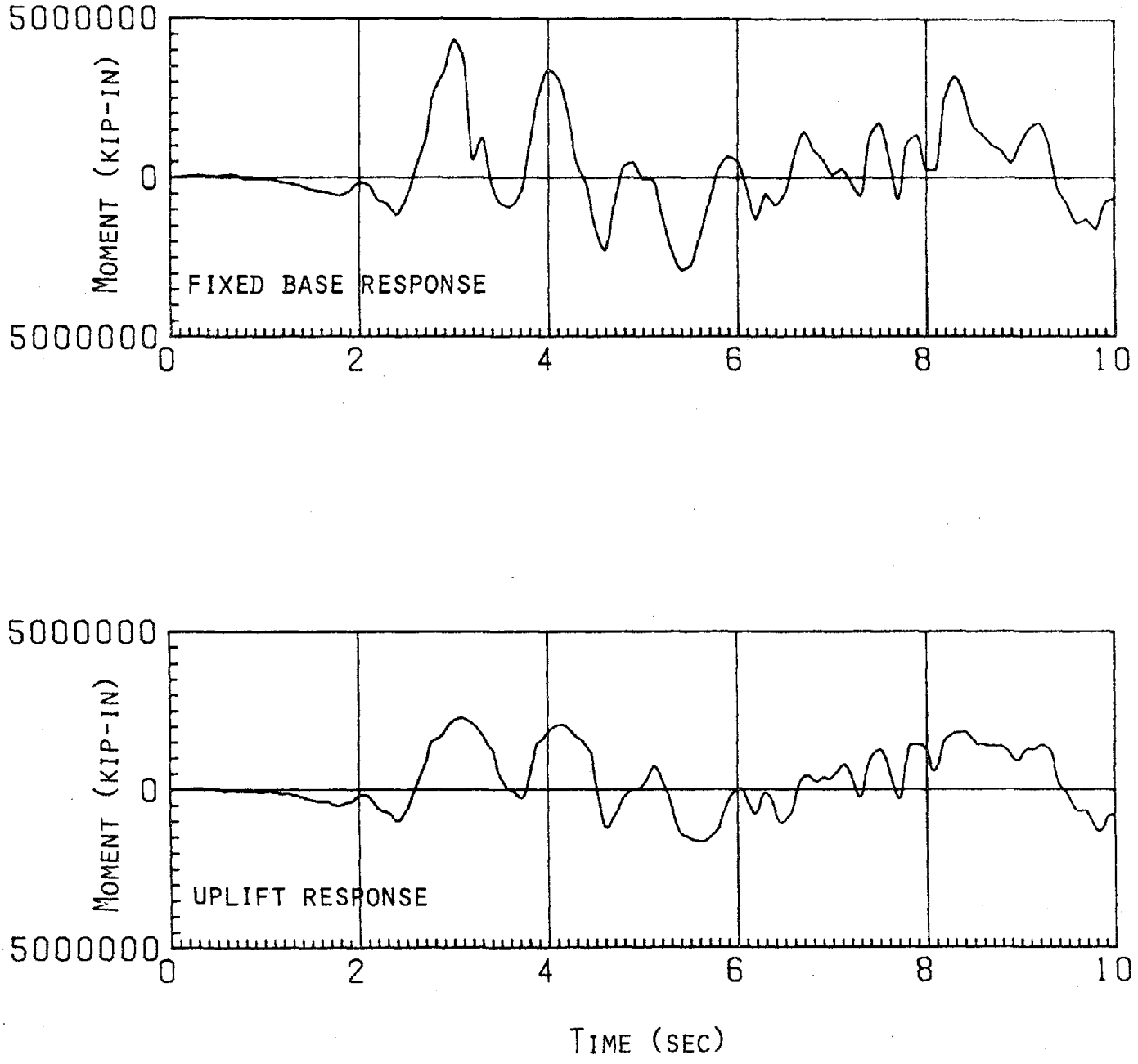

Figure 5.3.6. Core overturning ements; Pacoima Dam EQ

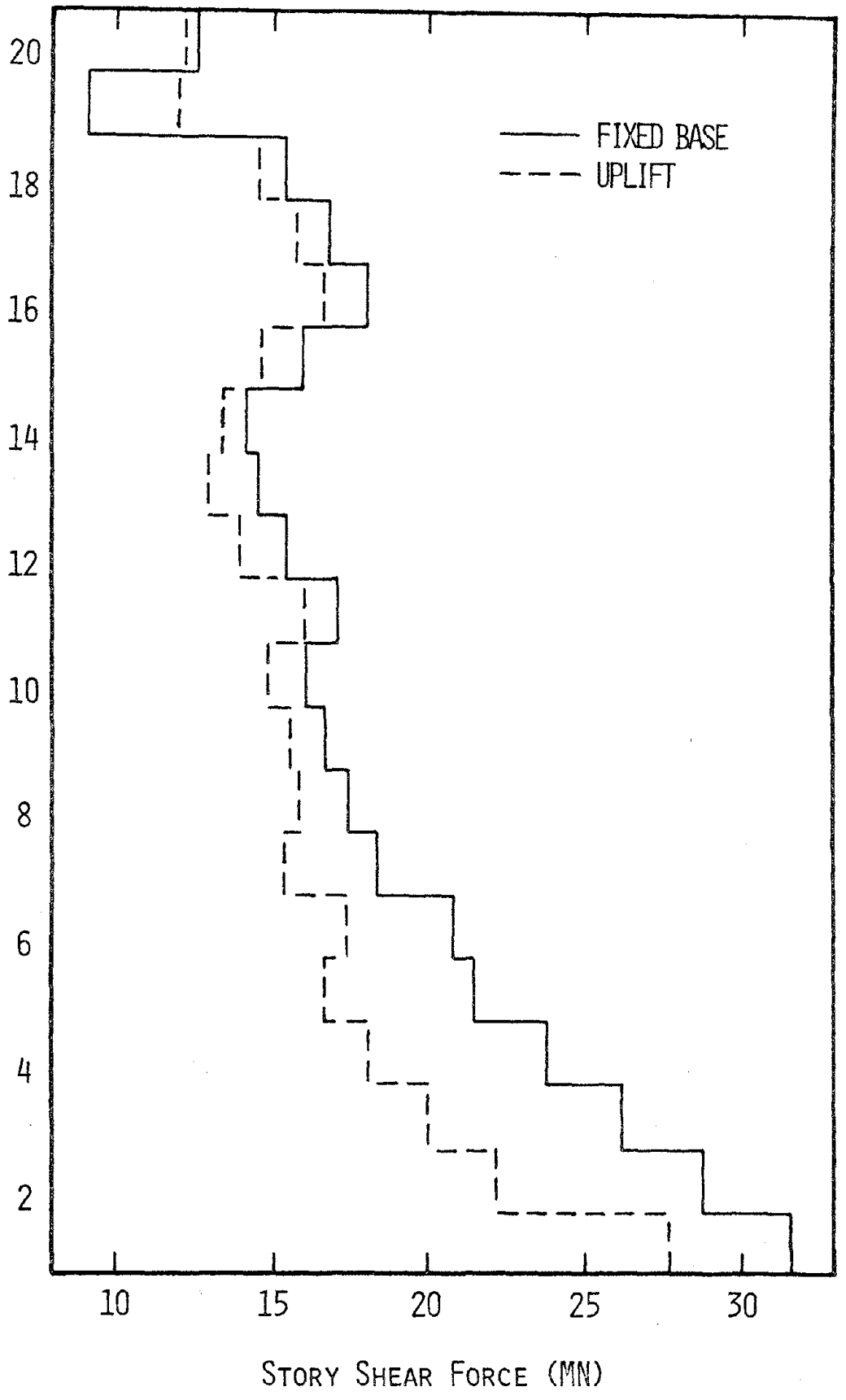

Figure 5.3.7. Total Shear Envelopes; Pacoima Dam EQ

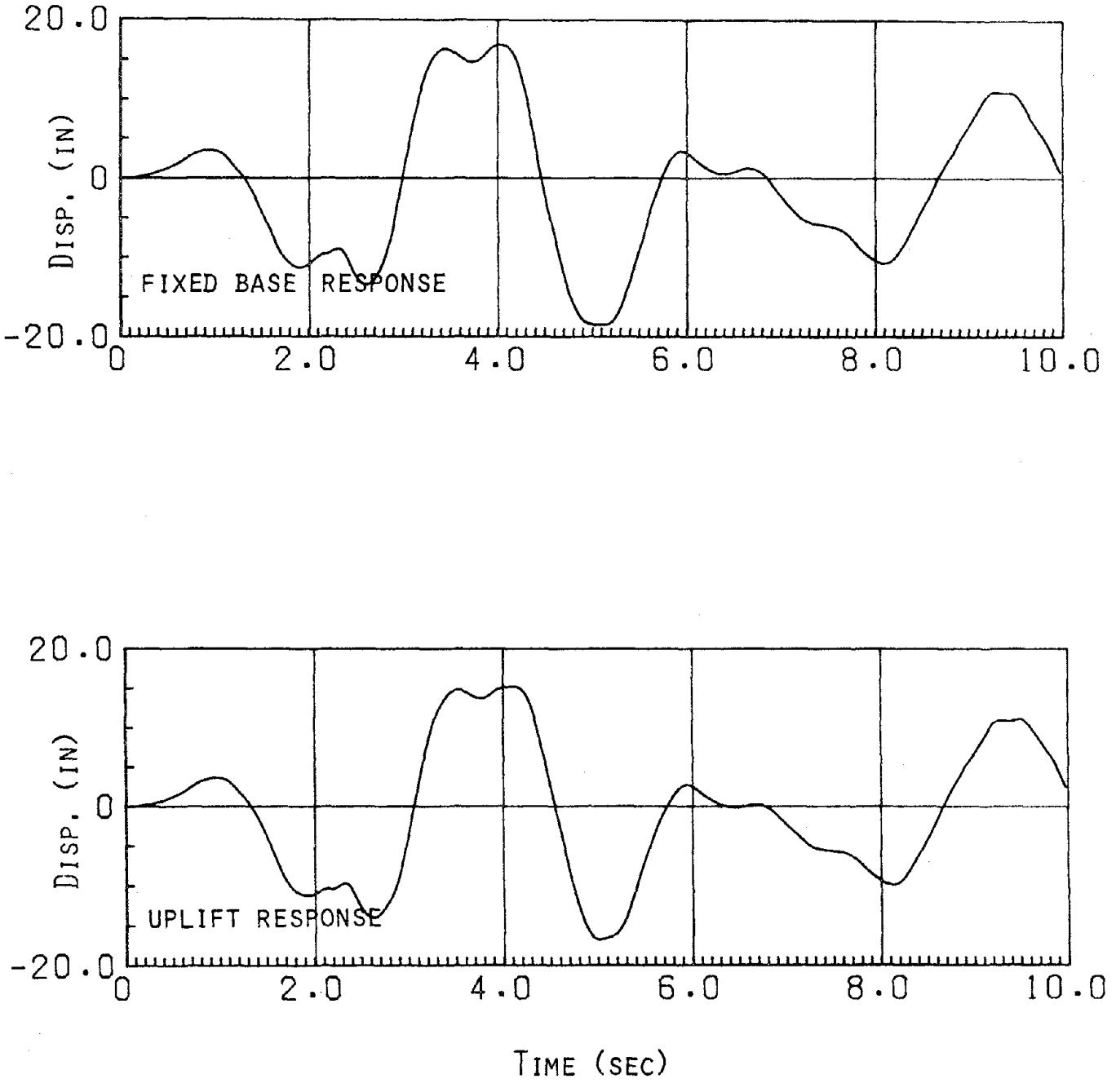

Figure 5.3.8. Roof displacements; El Centro EQ

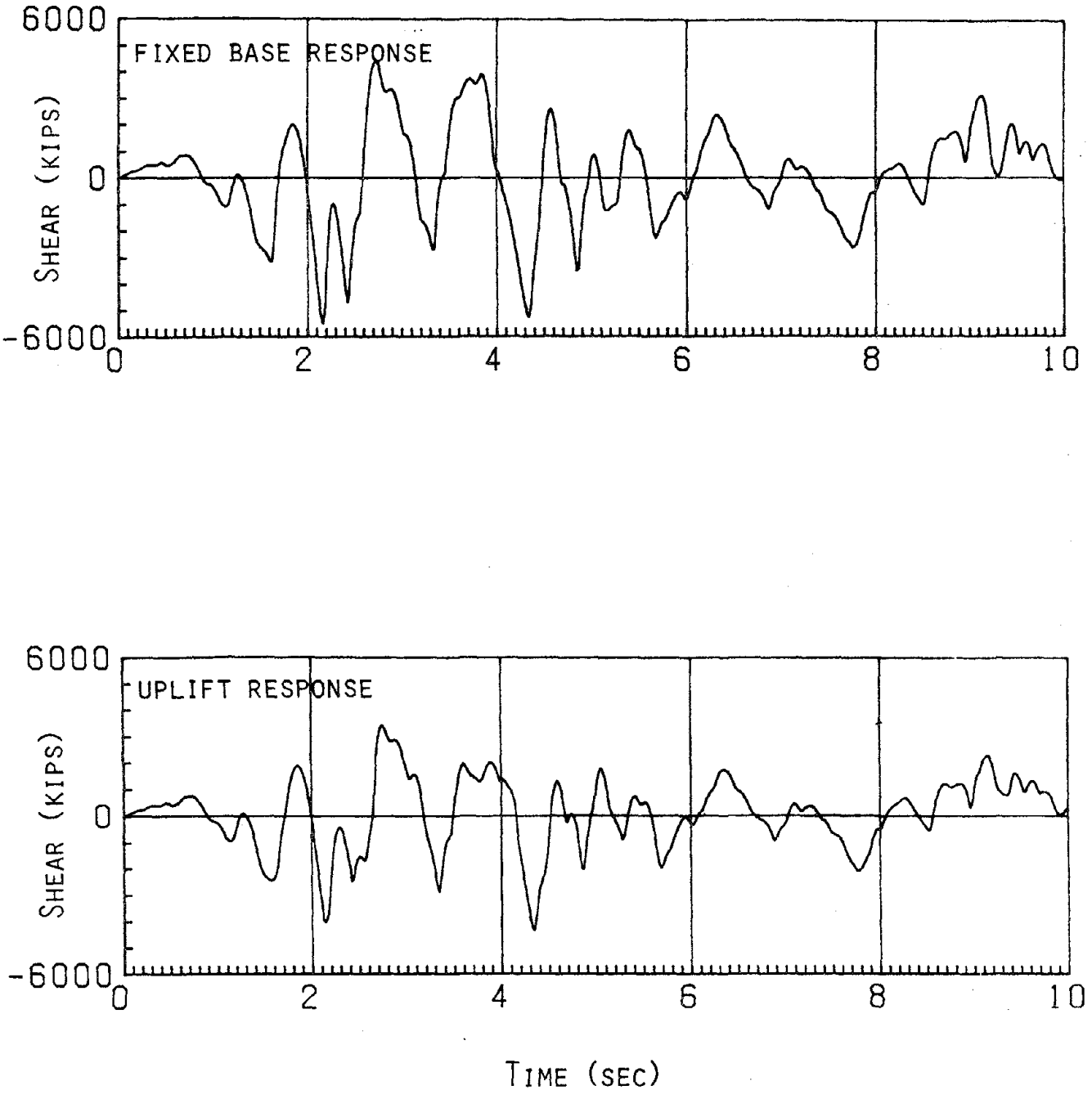

Figure 5.3.9. Core shears; El Centro EQ

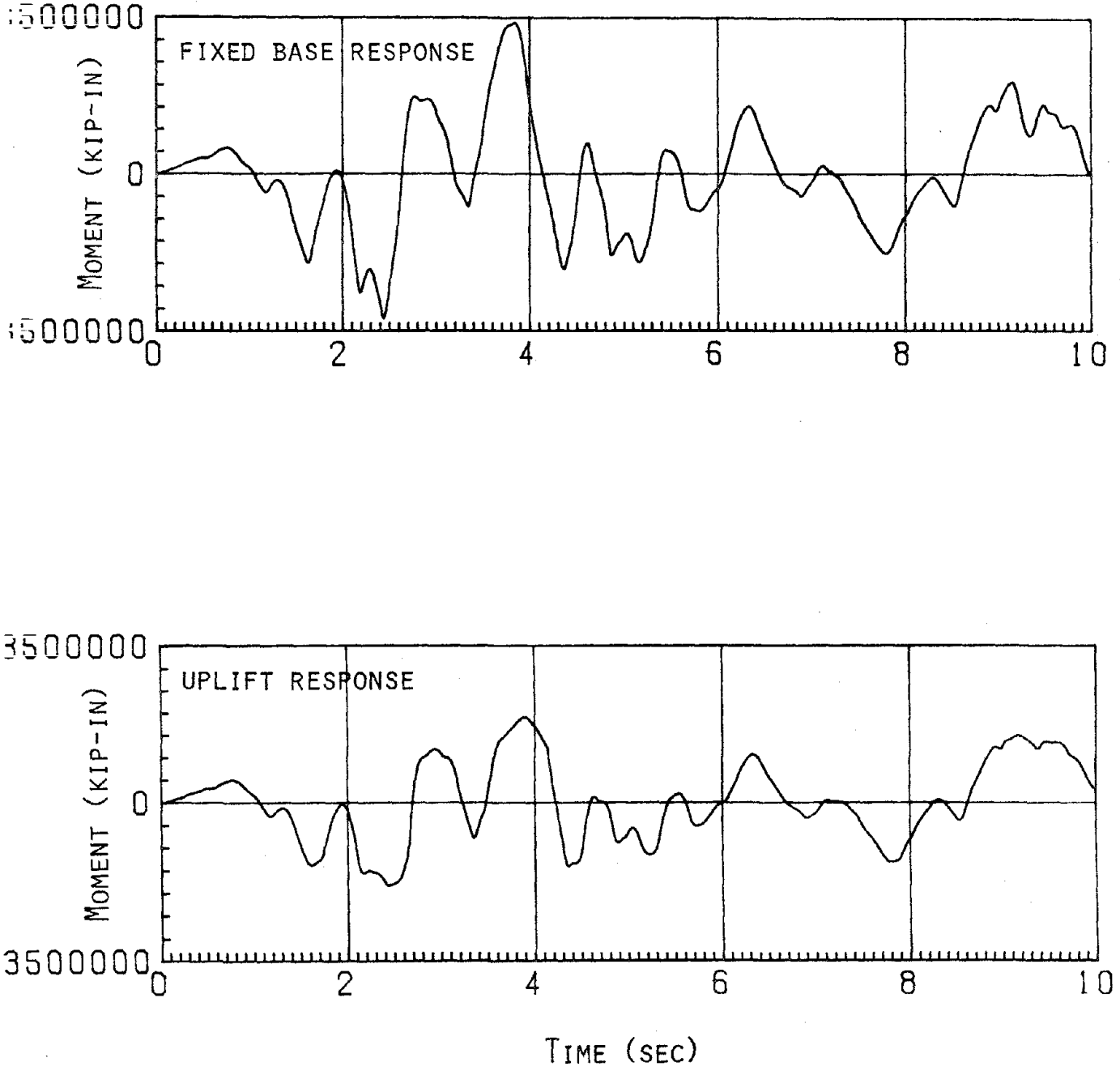

Figure 5.3.10. Core overturning moments; El Centro EQ

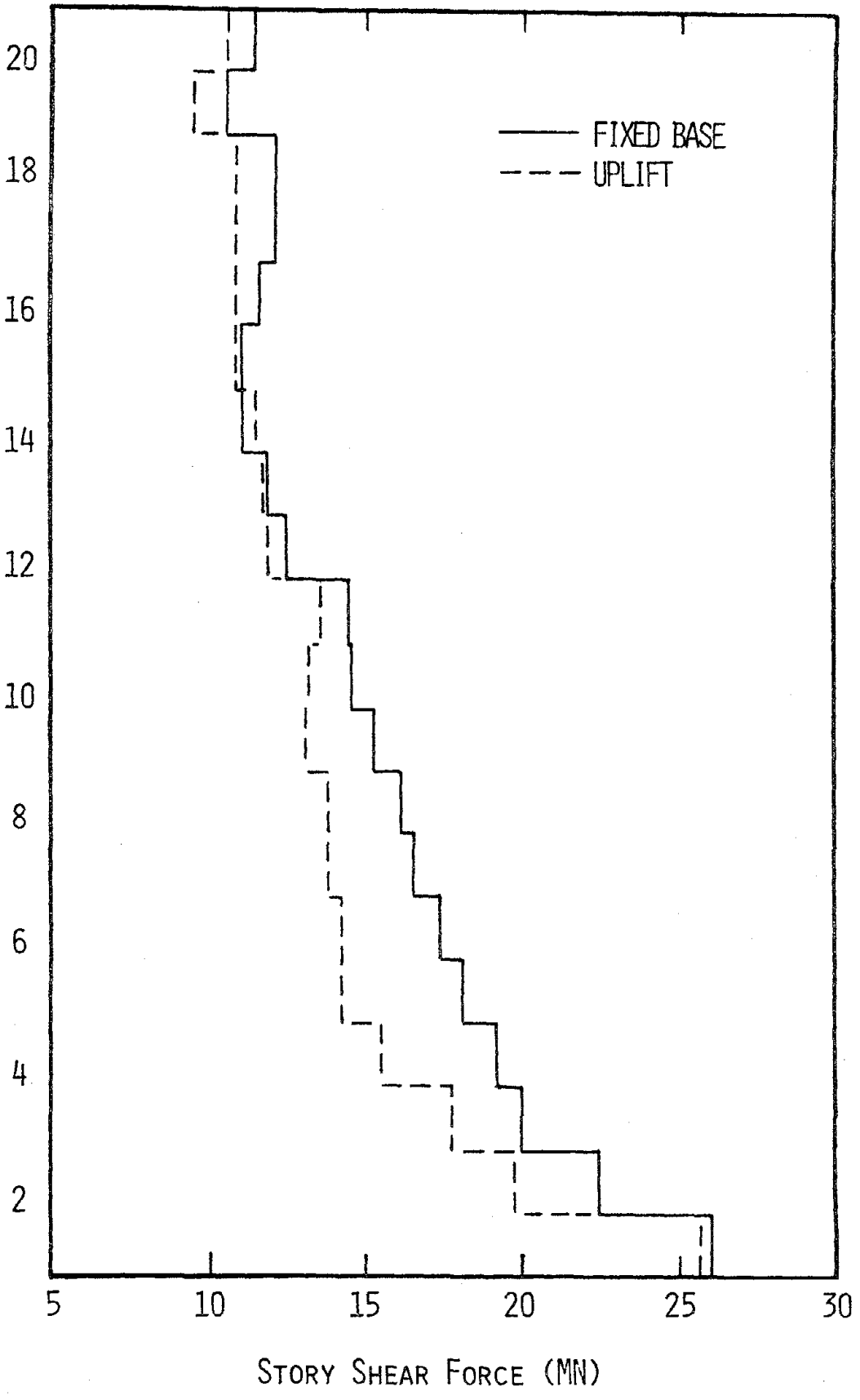

Figure 5.3.11. Total shear envelopes; El Centro EQ

15 STORY COUPLED SHEAR WALL

The elevation of this perforated shear wall structure is shown in Fig. 5.3.12; the two-dimensional coupled wall analytical model is shown in Fig. 5.3.13. Shear deformations are included in the coupling girders. The periods of the first three modes of this model are 1.49 sec., .704 sec. and .300 sec., respectively. The example structure was designed to be within basic ATC 3-06 seismic requirements for zone 7, with the coupled shear wall assumed to carry 100% of the lateral loading but only approximately 25% of the gravity loading. Analyses indicate that the coupled walls will begin to uplift at a base shear level of approximately 8% of the dead weight of the structure.

Seismic Response; Pacoima Dam EQ

The lateral displacements of the roof level in response to the 1971 Pacoima Dam S166 ground motion are indicated in Fig. 5.3.14. Although the character of the time histories with and without uplift differ greatly, the envelope drift levels are essentially identical, i.e. there is very little sacrifice in drift control associated with uplift of the shear wall. The actual drift index of approximately 1:80, although high, is not unreasonable for such severe ground shaking.

The uplift displacements at the four foundation support points are shown in Figure 5.3.15. As seen from the time histories presented, only the most "leeward" support point remained in contact during the large amplitude response cycles. The maximum base separation was on the order of four inches (100 mm) during sidesway to the right and only slightly over 0.1 inch (2.5 mm) during sidesway to the left. The extreme one-sidedness

of the response is not too surprising, due to the often mentioned long acceleration pulses present in the Pacoima ground motion.

The base moment, shear and normal force in the left wall element are plotted in Figures 5.3.16 through 5.3.18. As seen in the upper time history of Figure 5.3.16, the base moment at first reverses as the outer edge of the wall uplifts, but then returns to a nearly zero value as the inner edge uplifts, resulting in a moment free boundary condition. This process repeats itself during each cycle of uplift response. The base shear continues to oscillate during the uplift cycles, however, as the shear boundary condition is not released, i.e. a positive shear transfer is assumed to exist even during uplift. The base normal force is, similarly to base moment, released during uplift, as reflected in the upper time history of Figure 5.3.18. The corresponding fixed base response quantities are much more conventional in nature. Significant 2nd mode effects are noticeable in the time histories, and response amplitudes are approximately 600%, 300% and 1250% higher for moment, shear and axial force, respectively, than for the case with uplift allowed.

Time histories for the right wall base stress resultants during the Pacoima ground motion are shown in Figures 5.3.19 through 5.3.21. The right wall remains in contact with the ground except during two very brief intervals, as seen in the time histories of Figure 5.3.15. Consequently, the stress resultants with uplift allowed are somewhat higher for the right wall than for the left wall. Nevertheless, there are still drastic reductions in comparison to the fixed base response.

The normal force time histories of Figures 5.3.18 and 5.3.21 are of particular significance, as they indicate tensile forces of approximately

10000^{k} for both walls during the fixed base response, as compared to no tensile force during uplift response. Maintaining shear capacity in the presence of such large tensile forces would be extremely troublesome, not to mention the difficulty in developing such a large anchorage capacity in the foundation.

Shear envelopes for both walls over the height of the structure are indicated in Figure 5.3.22. From the shear envelopes it is obvious that the large reduction in lateral loading extends over the full height of the structure, and that reductions are equally significant for both walls.

Envelopes for shear and plastic hinge rotations in the coupling girders are shown in Figure 5.3.23. These members show large reductions in both shears and plastic hinge rotations with uplift allowed. Indeed, the coupling girders in the top 13 floors remain within the elastic range of behavior for the response case including uplift. Particularly significant when considering the implications of the reductions in shear levels of the coupling girders are the associated nominal shear stresses. The maximum nominal shear stress in the coupling girders during the fixed base response was nearly 800 psi, while for the uplift response the corresponding maximum was slightly over 400 psi. Assuming a value of f'_c of 4000 psi, the fixed base shear stress is well over $12\sqrt{f'_c}$, while the uplift response shear stress is somewhat over $6\sqrt{f'_c}$. The former value is probably not achievable, i.e. a structural failure is implied for the fixed base response. With proper detailing, the latter stress level, although high, is attainable. For this structure, therefore, allowing transient uplift could well make the difference between survival or failure under the prescribed ground motion.

Seismic Response; Amplified El Centro EQ

The lateral roof displacement time histories for the amplified 1940 El Centro N-S ground motion are shown in Figure 5.3.24. It is readily apparent that allowing uplift during this ground motion did result in some loss in drift control. Drift levels with uplift allowed are still less than that associated with the previous ground motion, however, and they can still probably be considered acceptable for such an extreme event. (The ductility demand is relatively modest for both response cases during this ground motion.

The uplift response time histories for the four foundation support points are shown in Figure 5.3.25. The amplitudes of uplift motion are comparable to those associated with the Pacoima record, thus explaining the comparable drift levels. Again it is evident that both individual walls separate completely from the foundation during large amplitude response.

The left wall base overturning moment time histories for the El Centro ground motion are shown in Figure 5.3.26. The considerable reductions associated with allowing uplift are again readily apparent; the fixed base overturning moments are approximately twice as great as the corresponding uplift response values.

The left wall base shear time histories for this ground motion are shown in Figure 5.3.27. There is no really significant reduction in base shears for this ground motion, indicating that response modes other than the fundamental mode are significant. (As mentioned previously, shear transfer capability is assumed to be maintained during uplift.)

The left wall axial force time histories are shown in Figure 5.3.28.

Again apparent, from this time history, is the elimination of significant tensile forces from the shear walls. This effect has a two-fold benefit, as described previously; wall integrity in shear is enhanced as well as elimination of tensile requirements in the foundation.

Response Summary

Allowing transient uplift was seen to have a very significant effect upon the seismic response of the example coupled shear shear wall. Substantial benefits from transient uplift were evident both in the walls and the coupling girders. Indeed, for the Pacoima Dam record, allowing transient uplift seemed to make the difference between survival and failure.

The girders experienced very considerable reductions in both shear levels and ductility requirements. The walls experiences drastic reductions in overturning effects, both in bending moments and in axial forces resulting from overturning. The elimination in axial tension is particularly significant in elements subjected to substantial shears.

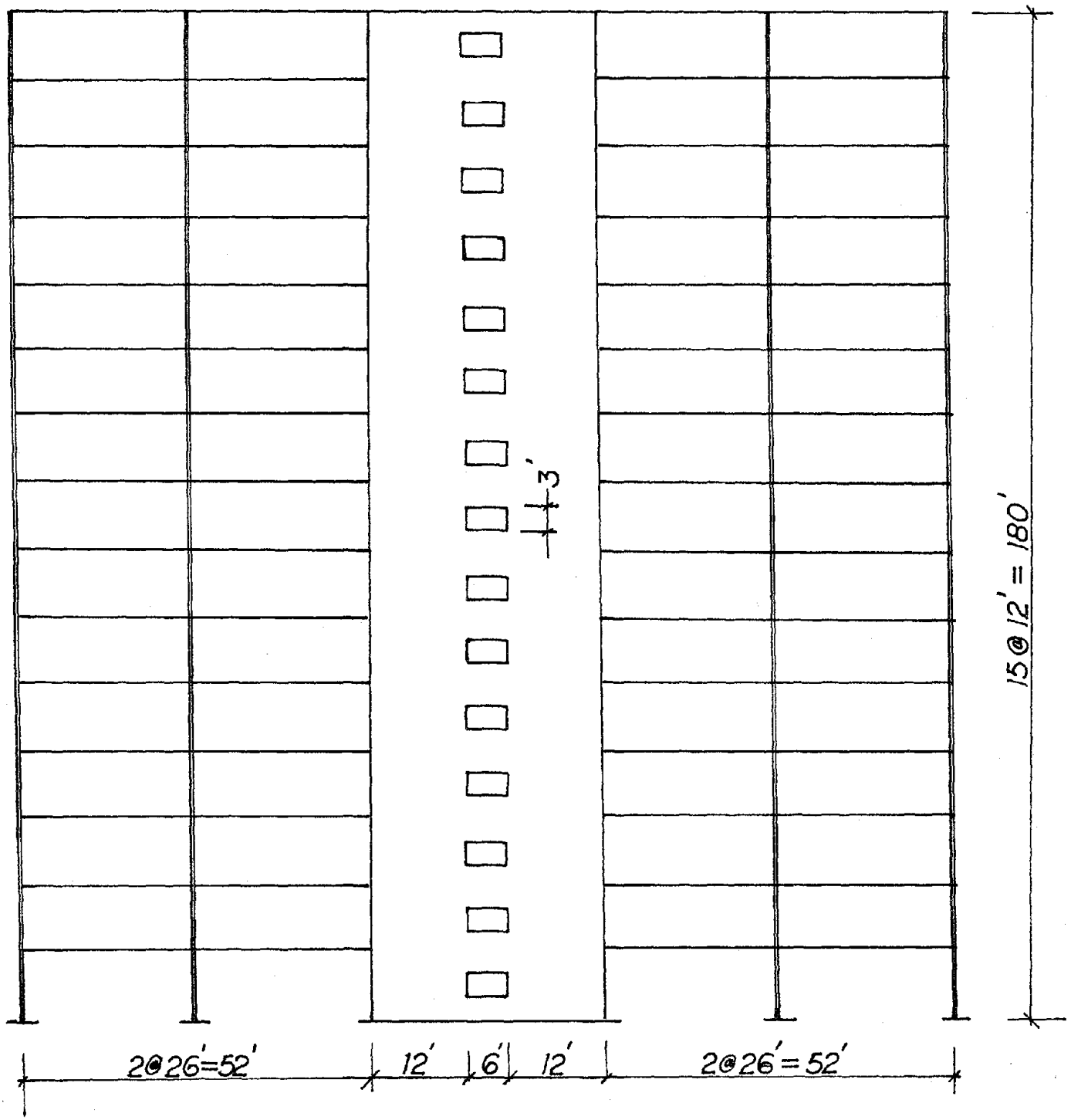

Figure 5.3.12: 15 Story Coupled Shear Wall

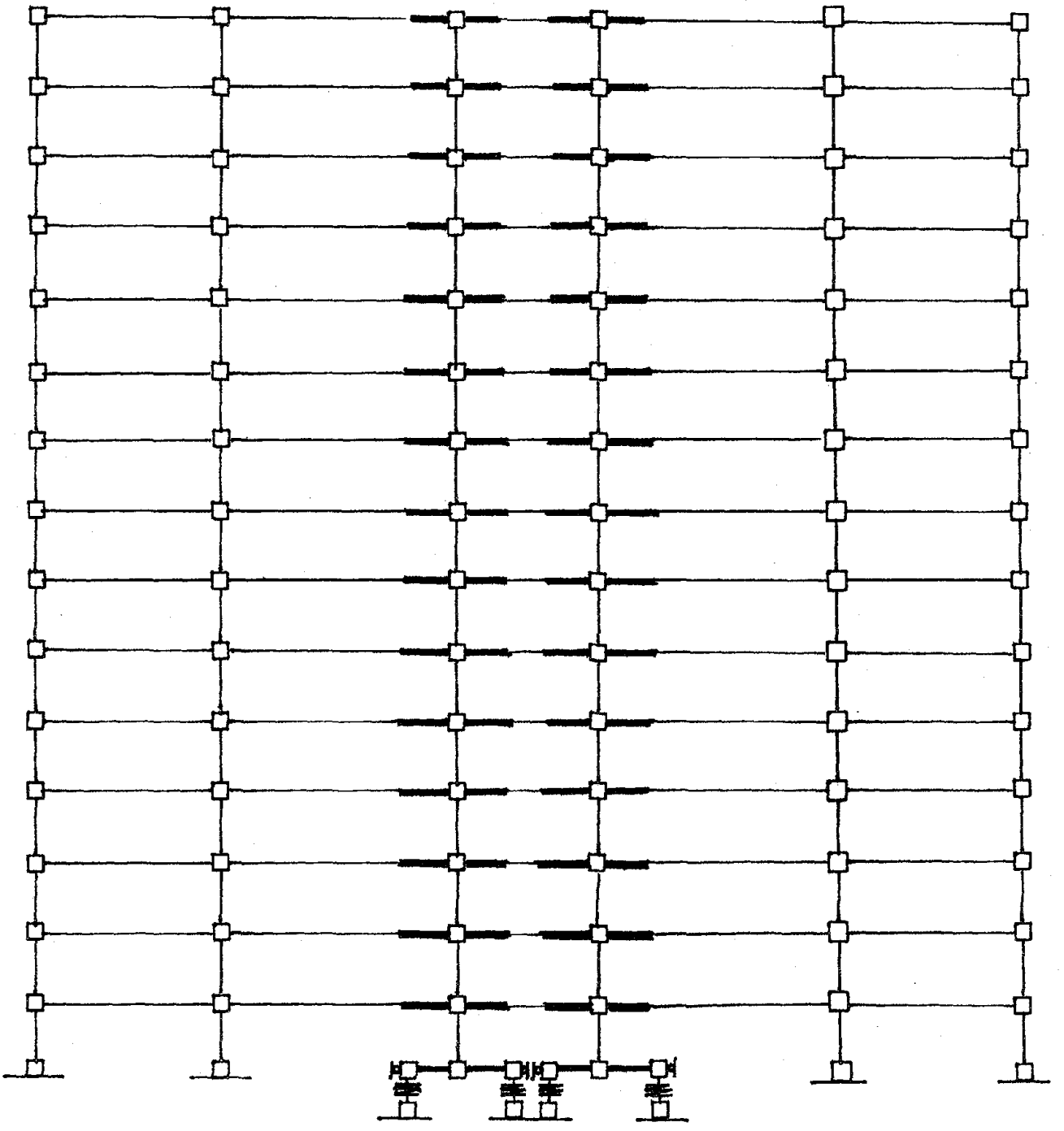

Figure 5.3.13 Analytical Model

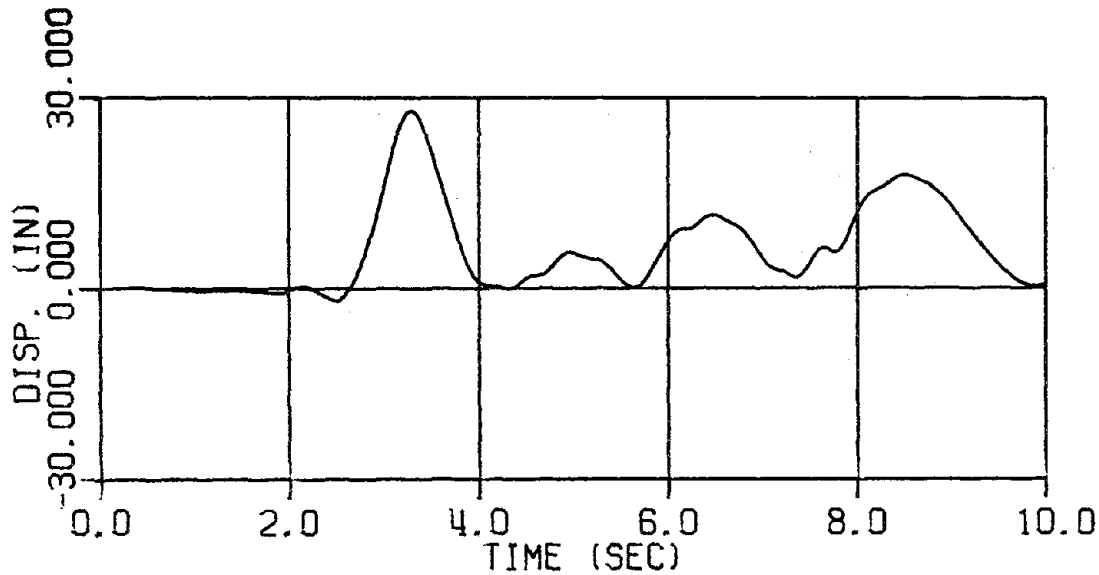

Uplift Allowed

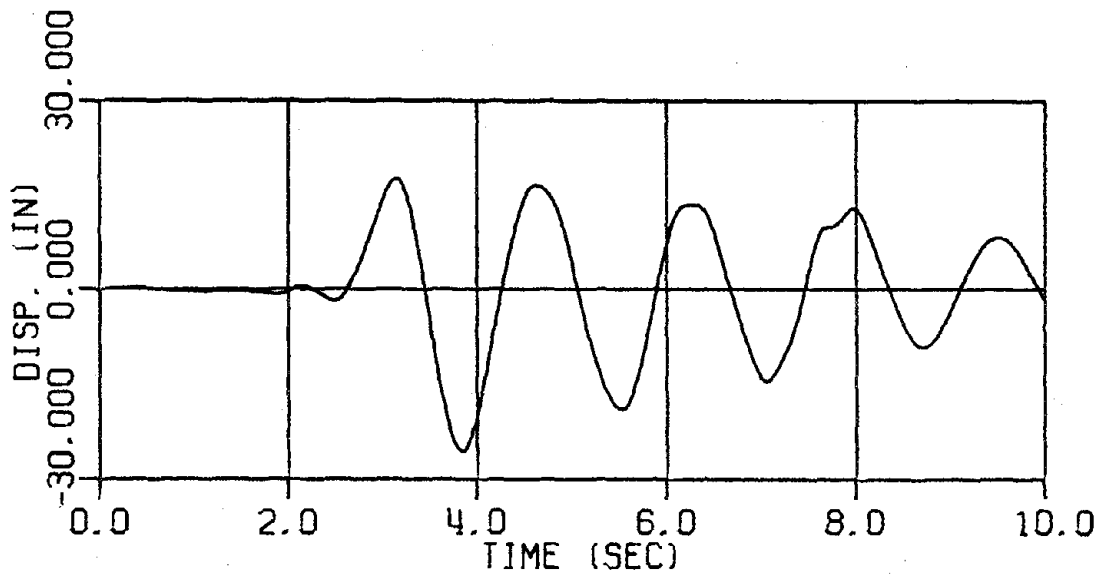

Fixed Base

Figure 5.3.14: Roof Displacements, 1971 Pacoima S16E

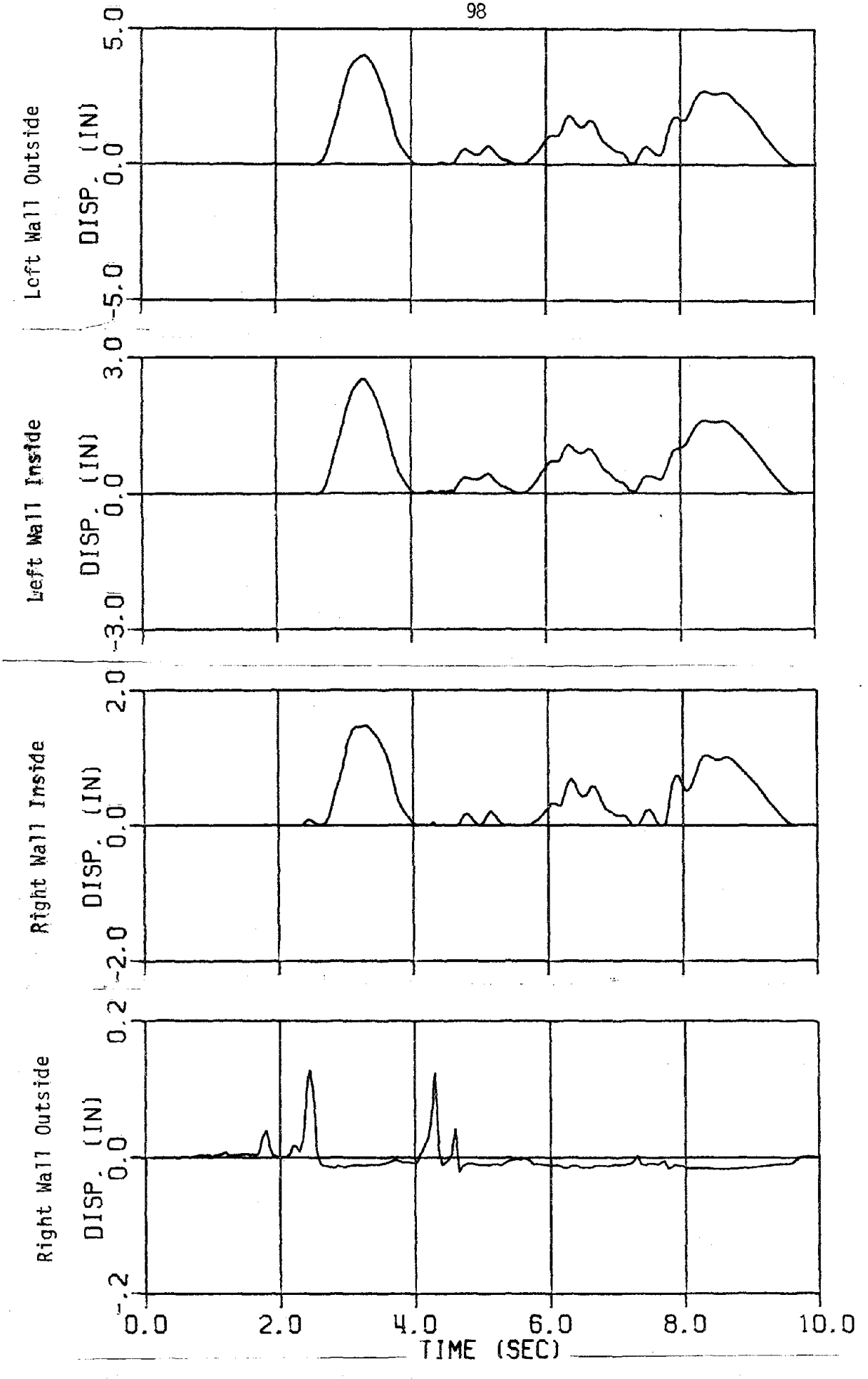

Figure 5.3.15: Uplift Displacements; Pacoima S16E

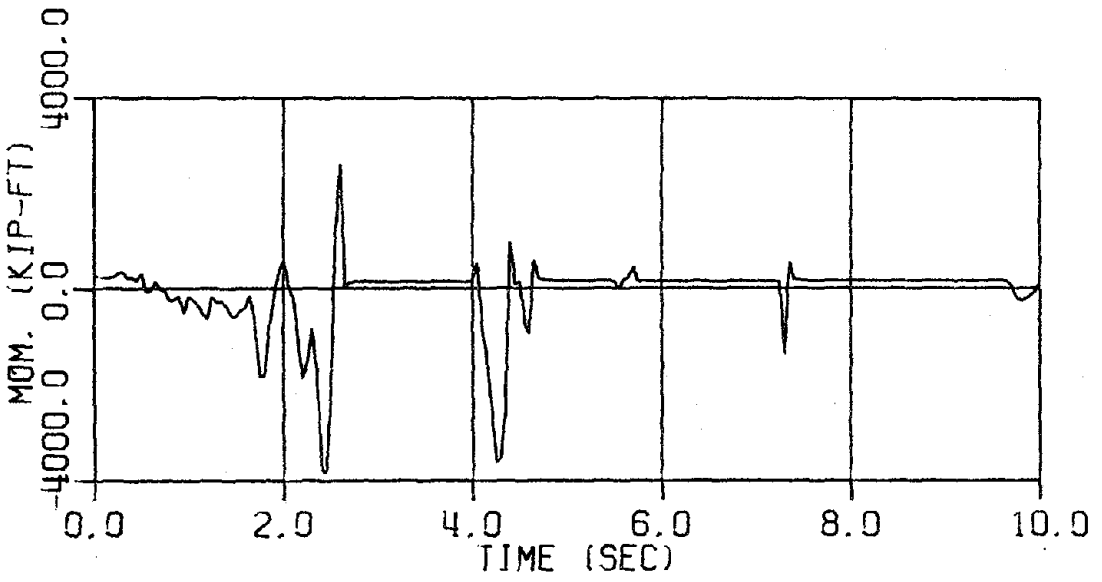

Uplift Allowed

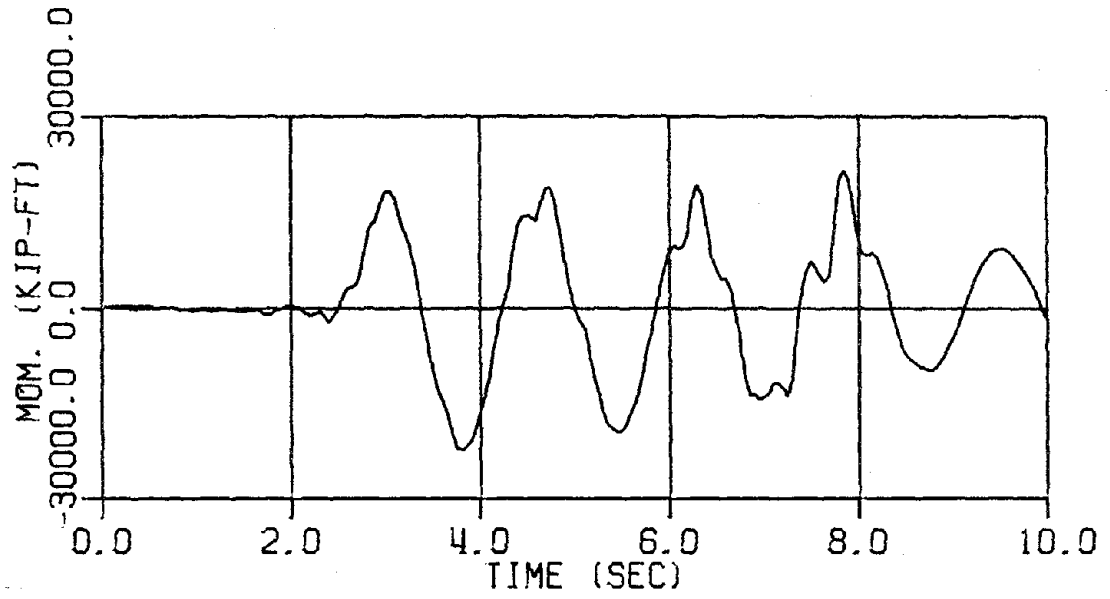

Fixed Base

Figure 5.3.16: Left Wall Base Overturning Moment; Pacoima S16E

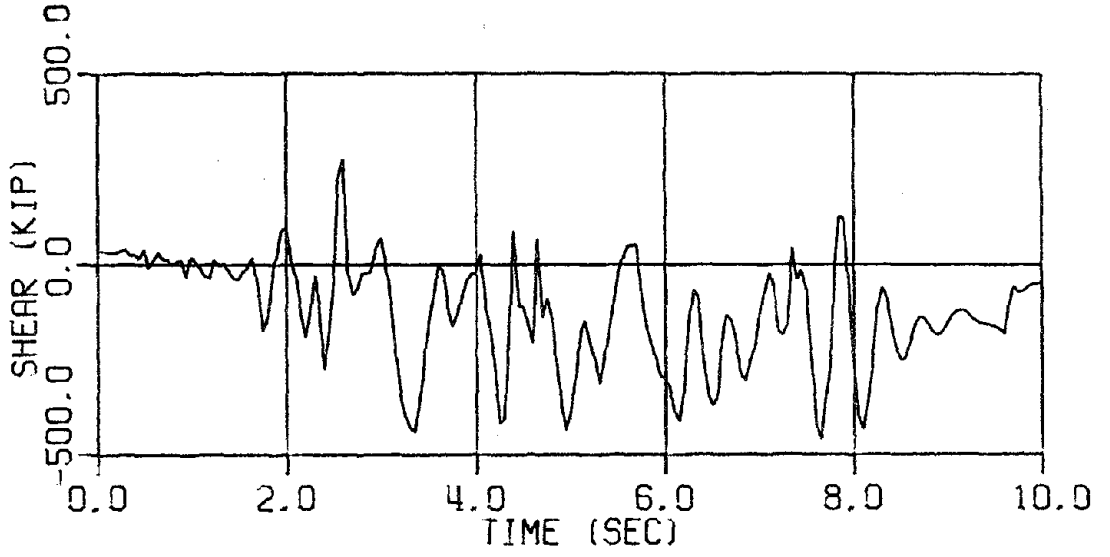

Uplift Allowed

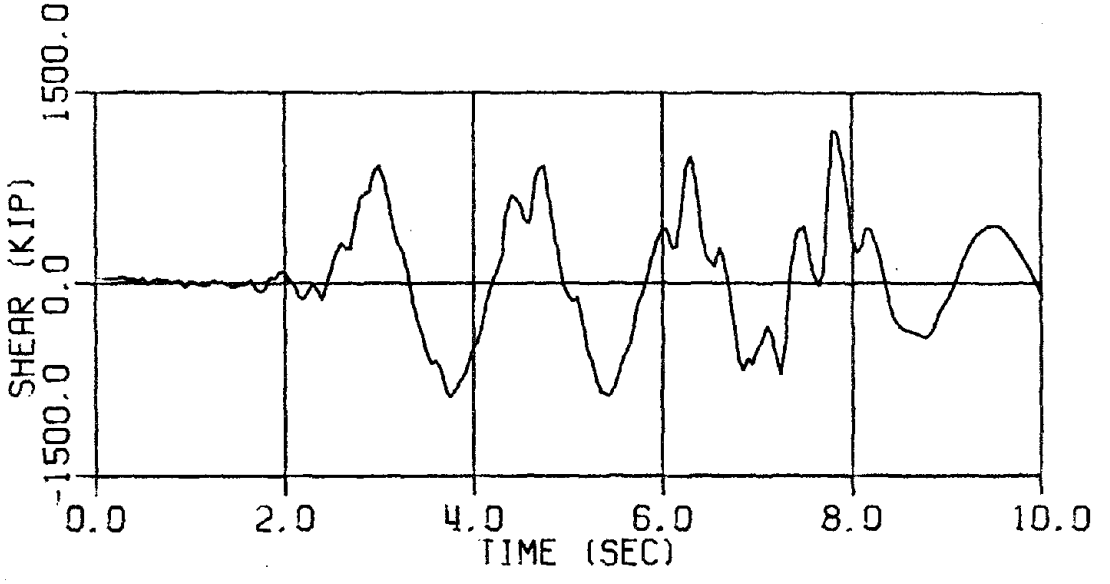

Fixed Base

Figure 5.3.17: Left Wall Base Shear; Pacoima S16E

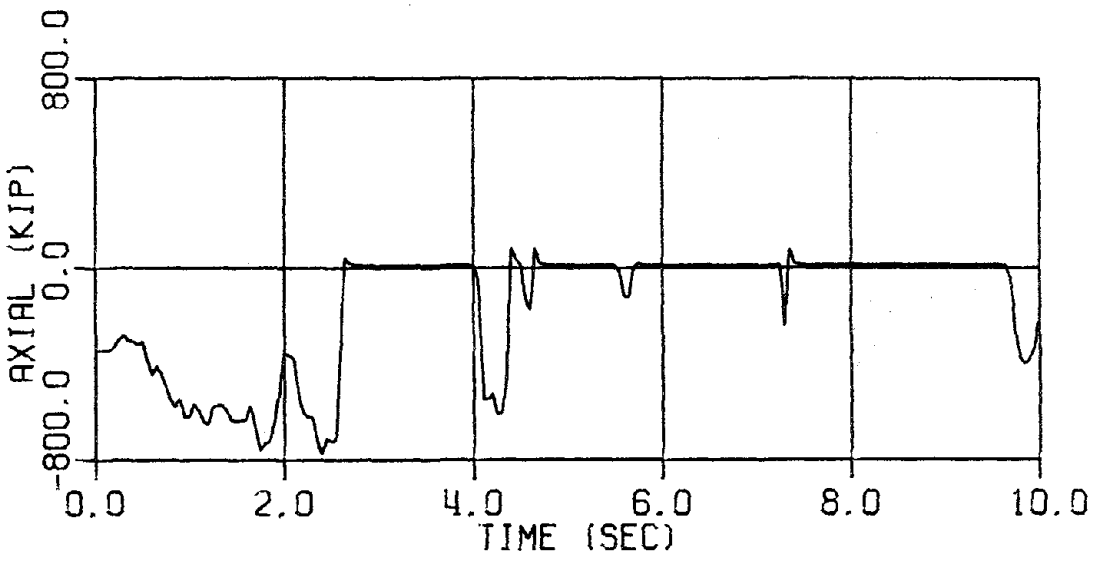

Uplift Allowed

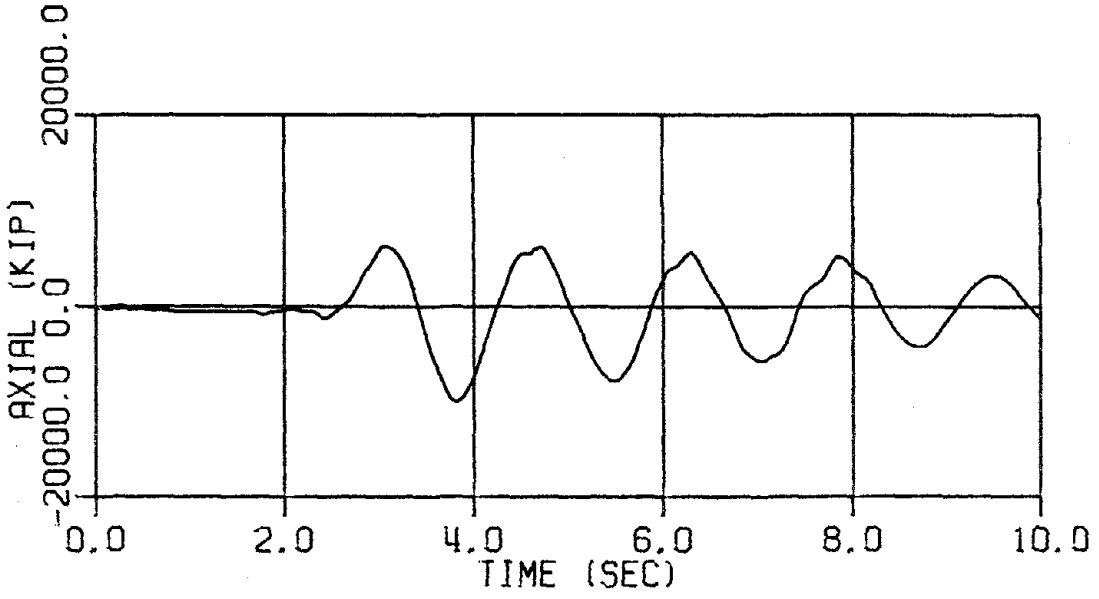

Fixed Base

Figure 5.3.18 Left Wall Base Normal Force; Pacoima S16E

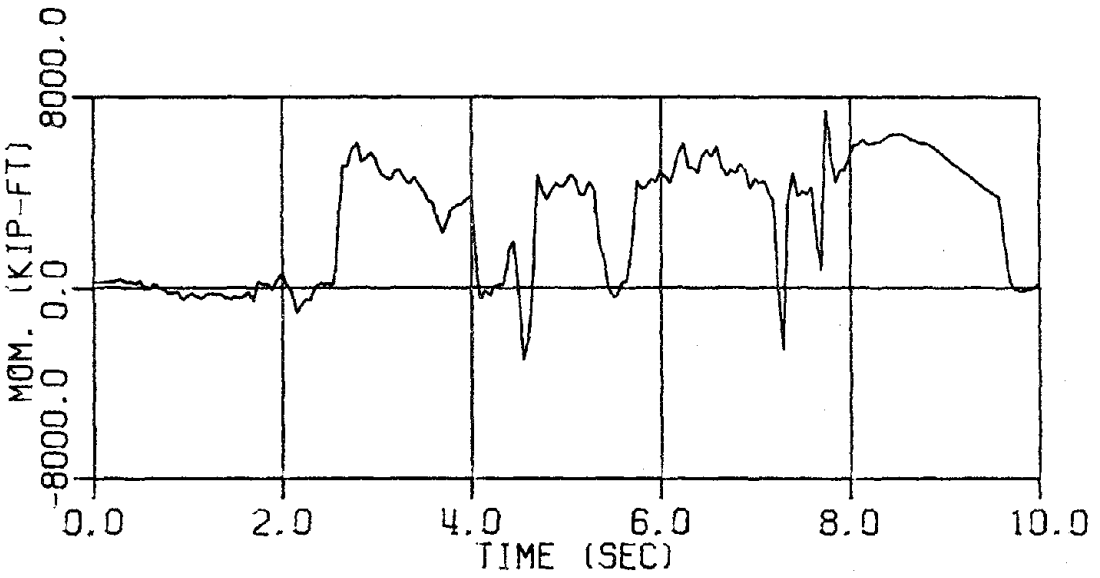

Uplift Allowed

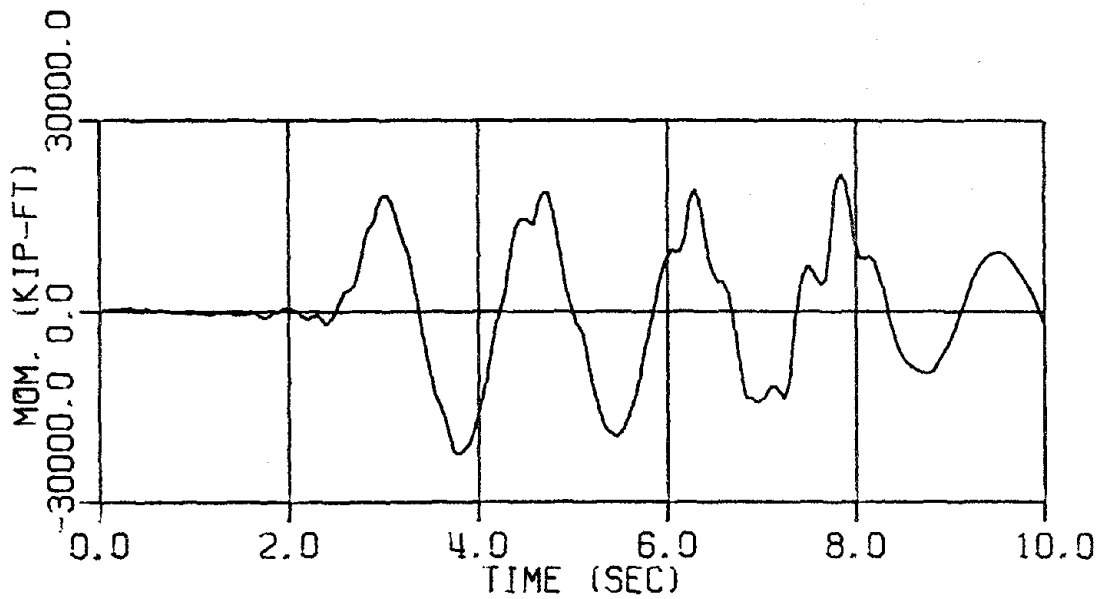

Fixed Base

Figure 5.3.19: Right Wall Base Overturning Moment; Pacoima S16E

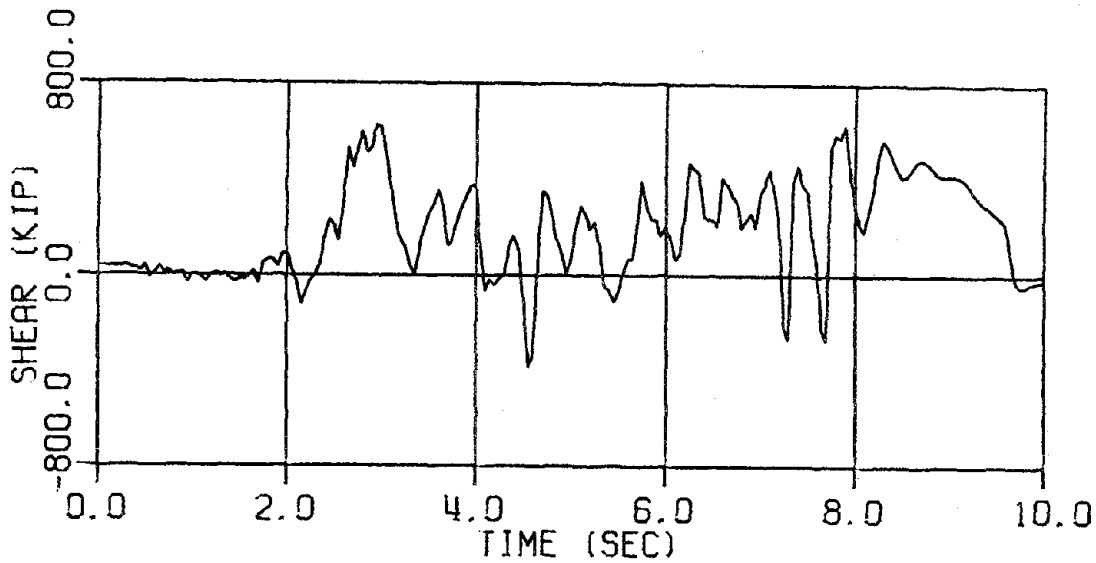

Uplift Allowed

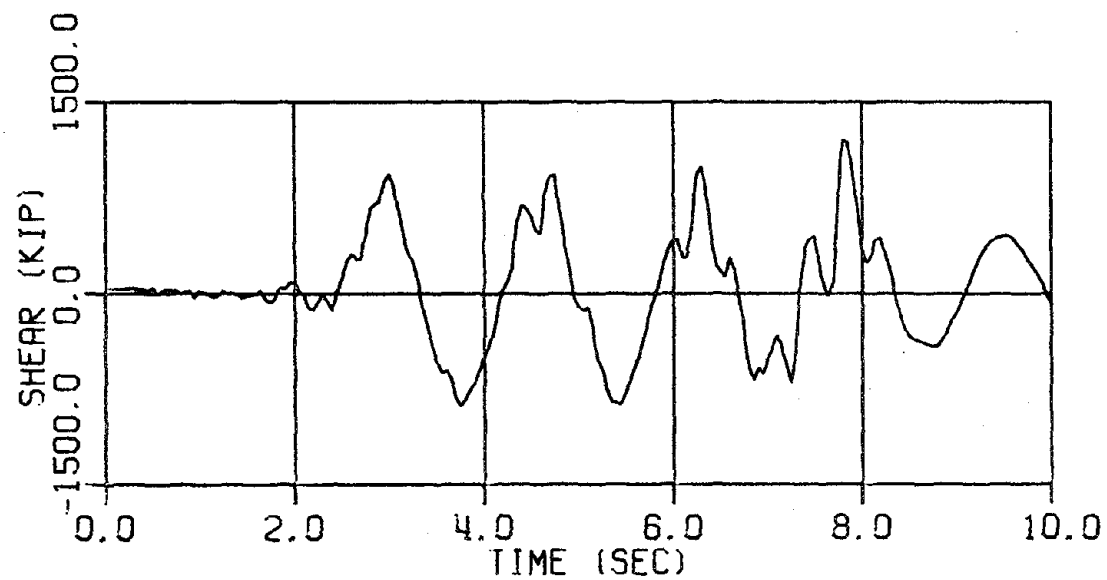

Fixed Base

Figure 5.3.20: Right Wall Base Shear; Pacoima S16E

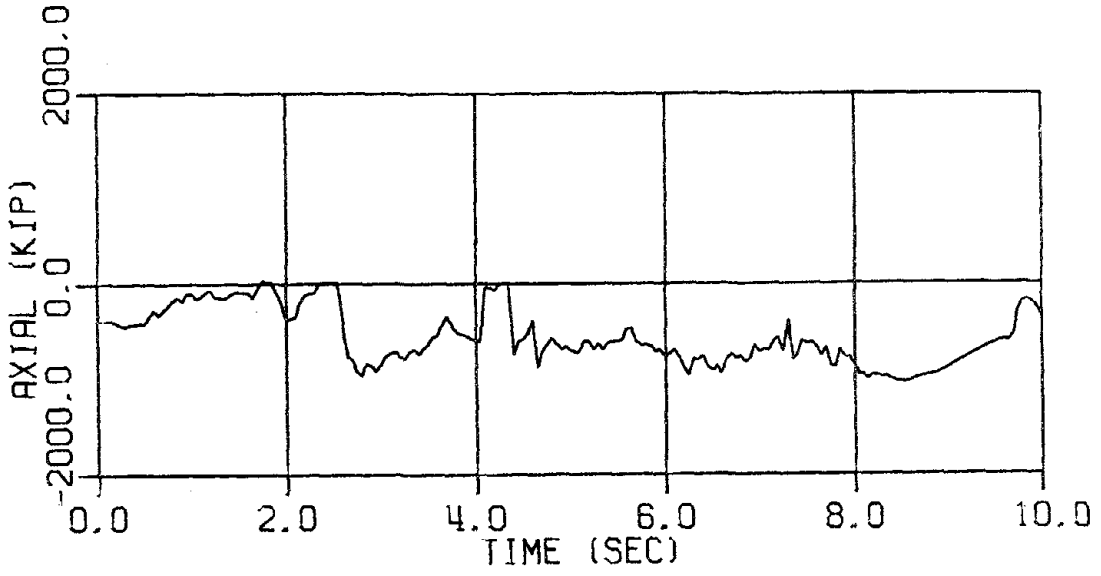

Uplift Allowed

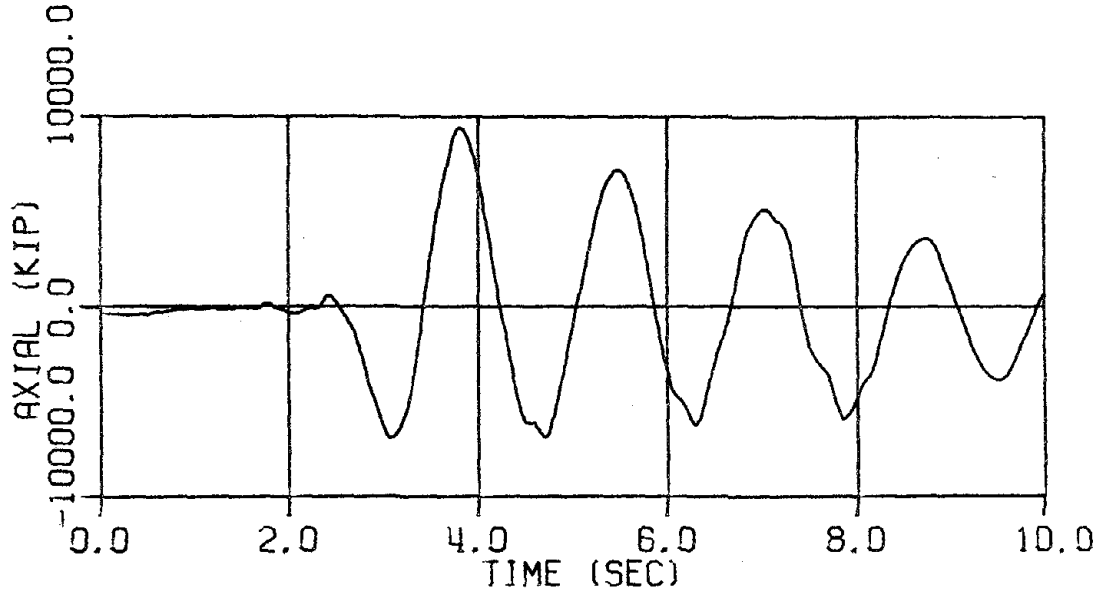

Fixed Base

Figure 5.3.21: Right Wall Base Normal Force; Pacoima S16E

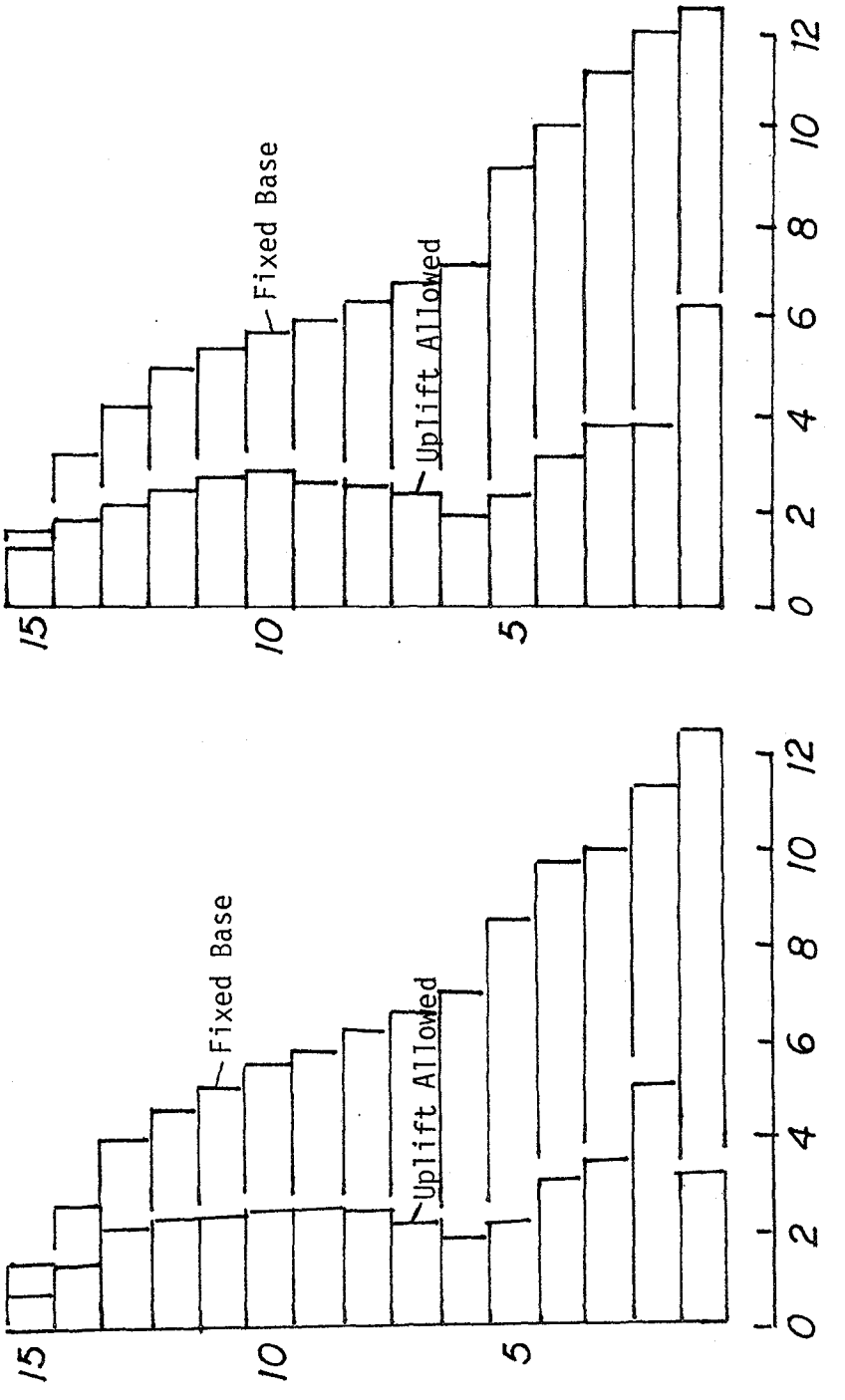

Figure 5.3.22: Shear Wall Response Envelopes; Pacoima S16E

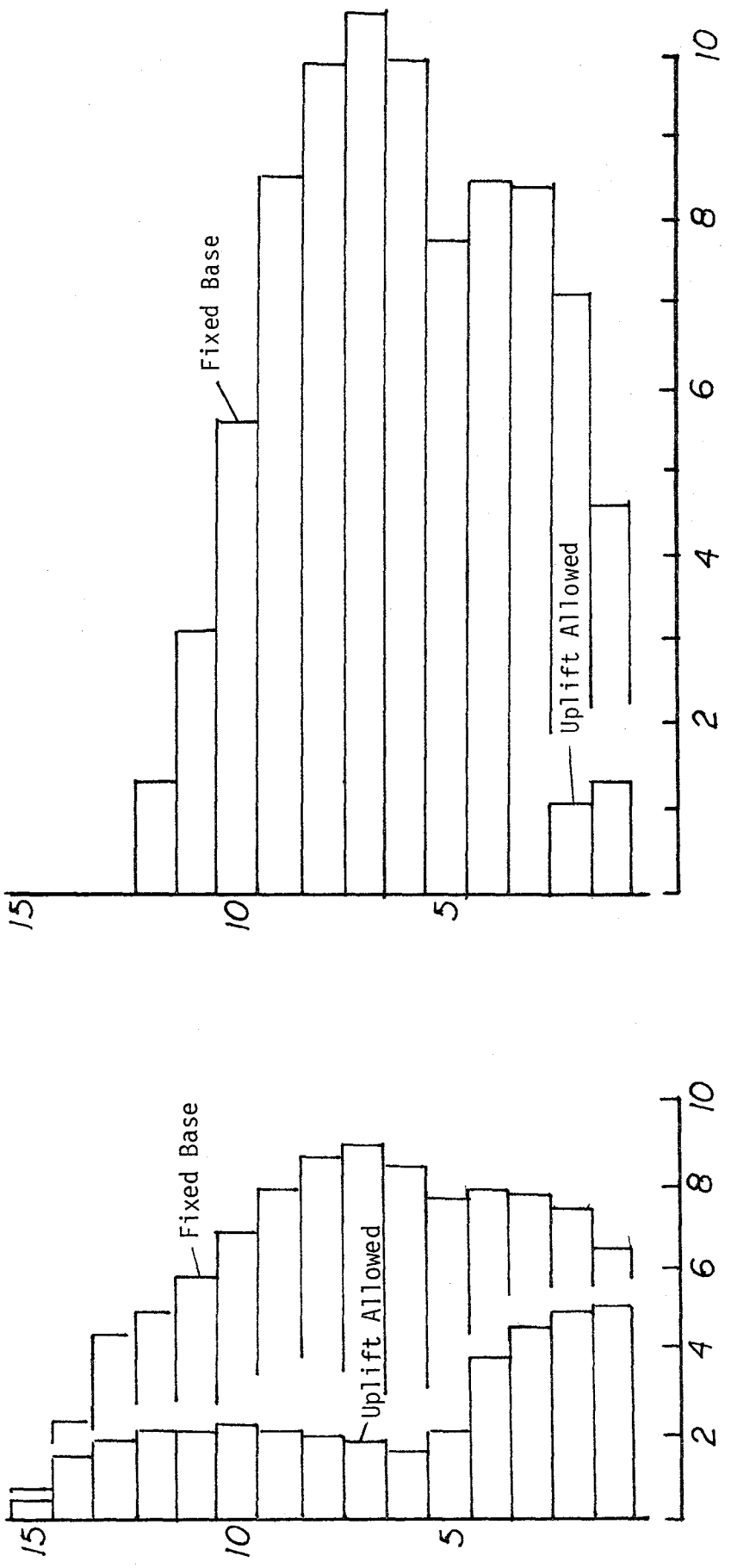

Figure 5.3.23: Response Envelopes for Coupling Girders: Pacoima S16E

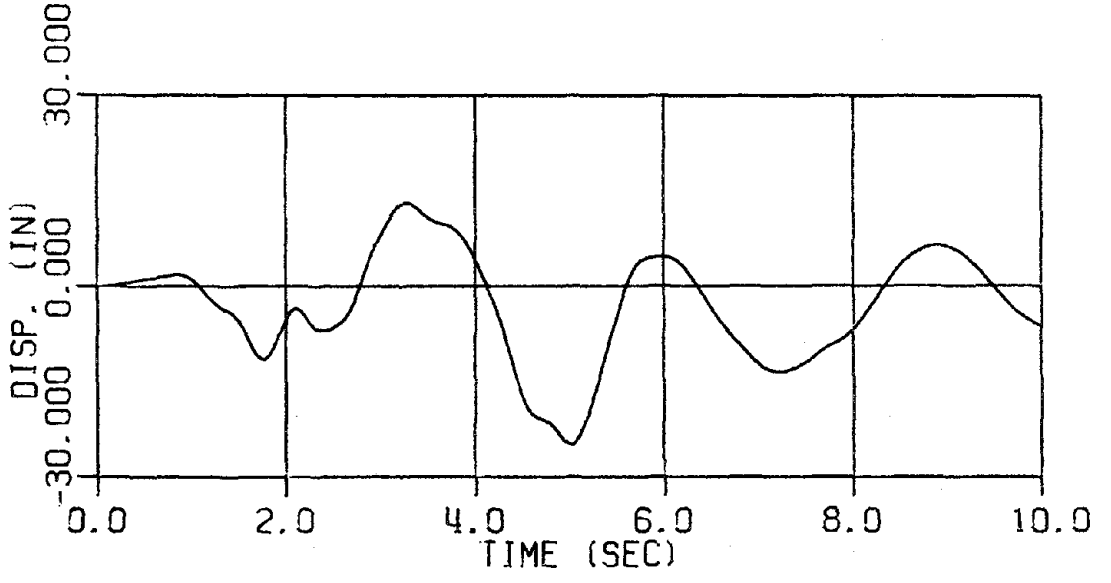

Uplift Allowed

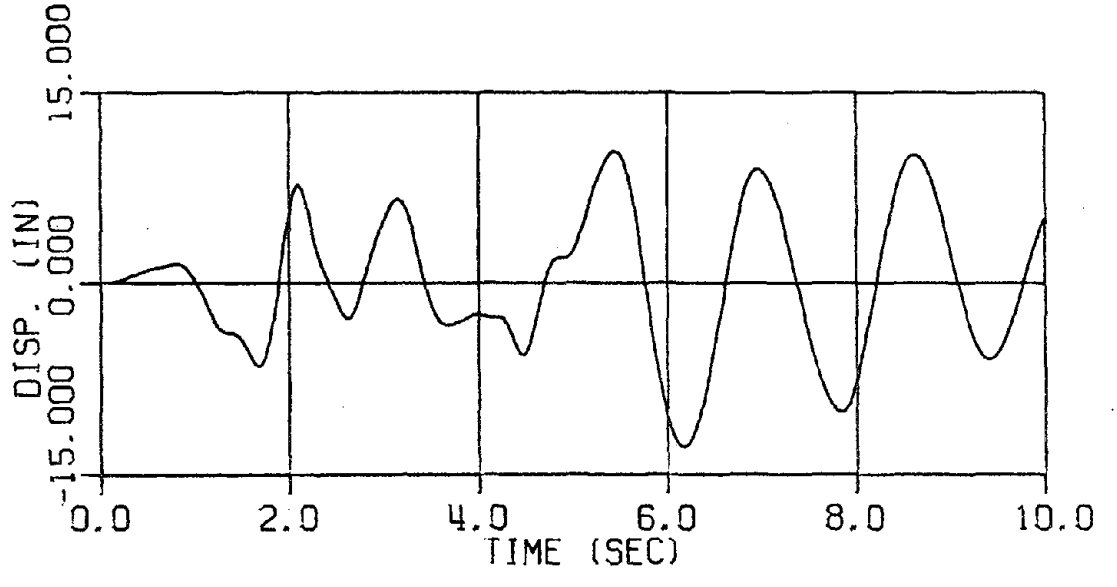

Fixed Base

Figure 5.3.24: Roof Displacements; 2x1940 El Centro N-S

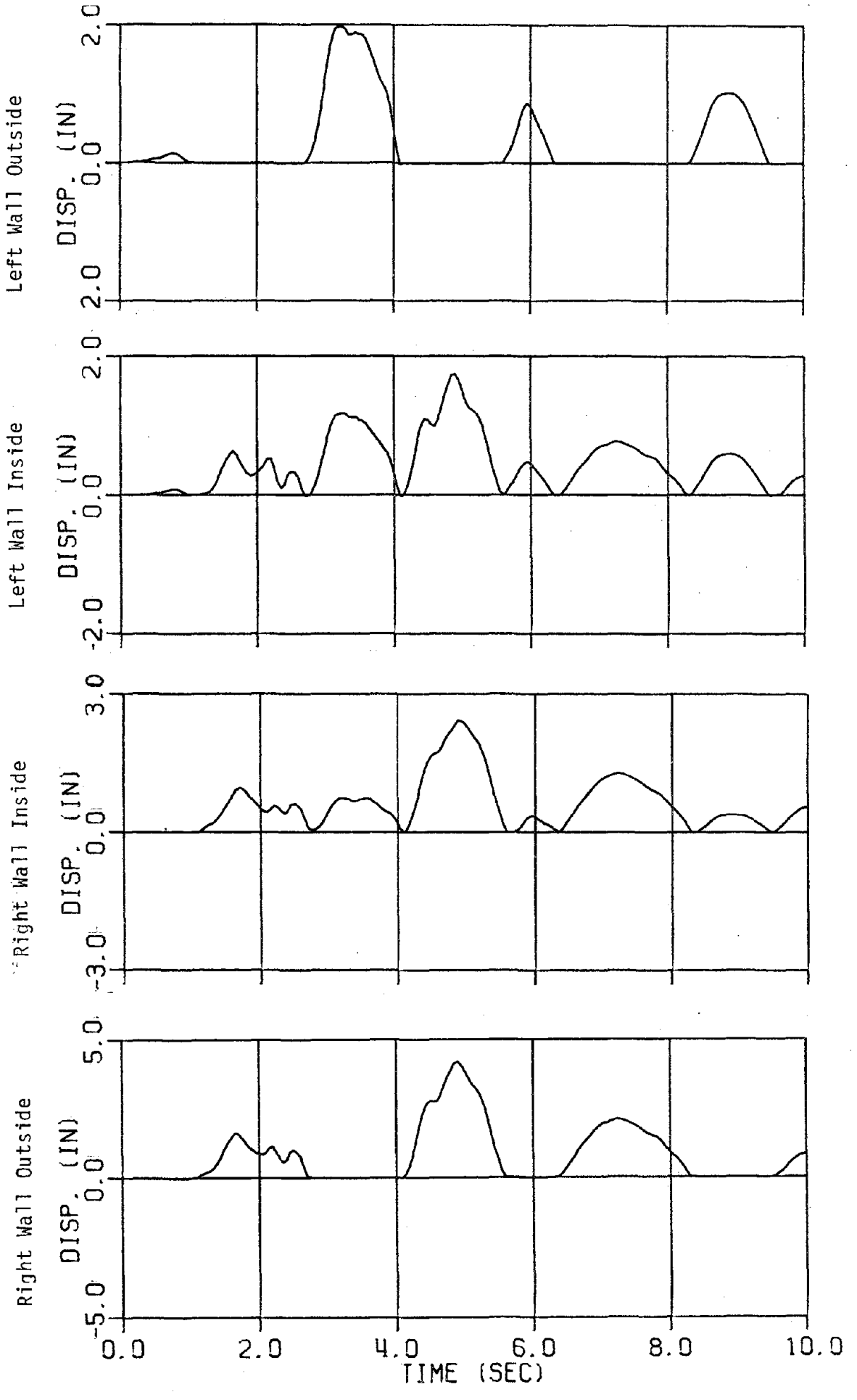

Figure 5.3.25: Uplift Displacements; 2x1940 El Centro N-S

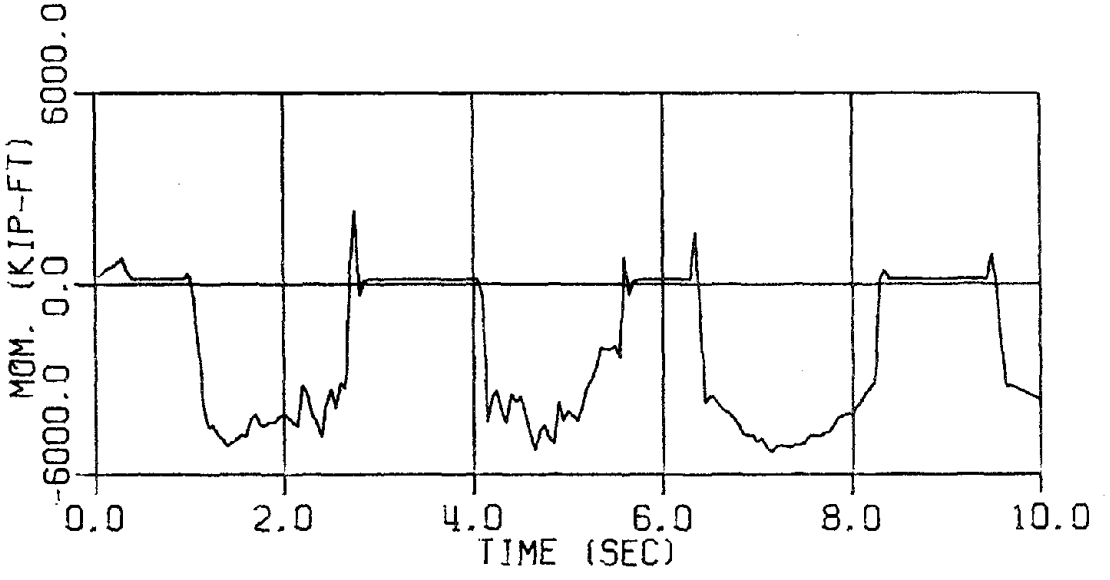

Uplift Allowed

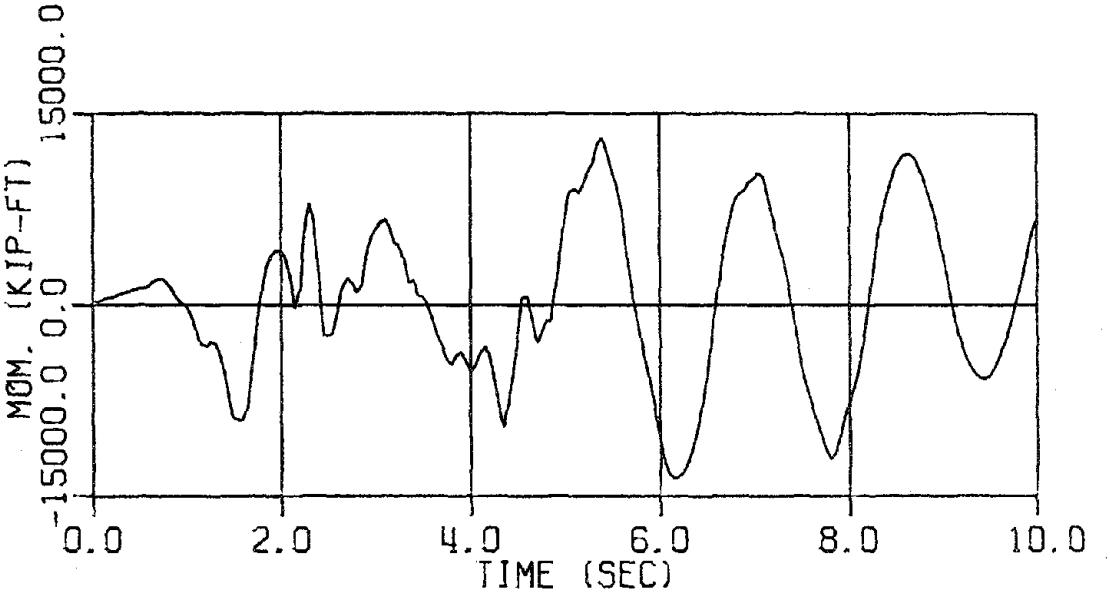

Fixed Base

Figure 5.3.26: Left Wall Base Overturning; 2x1980 El Centro N-S

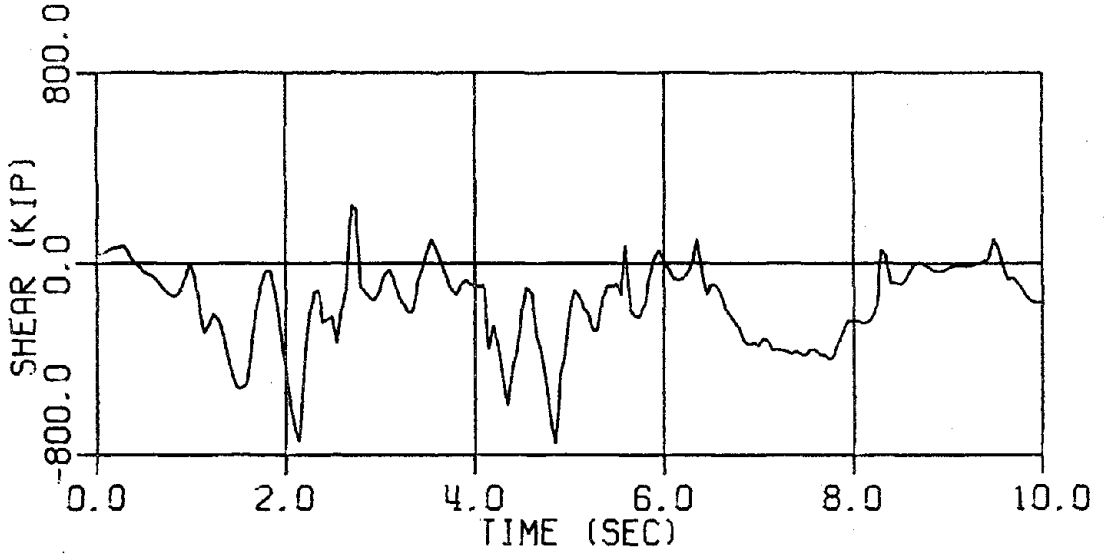

Uplift Allowed

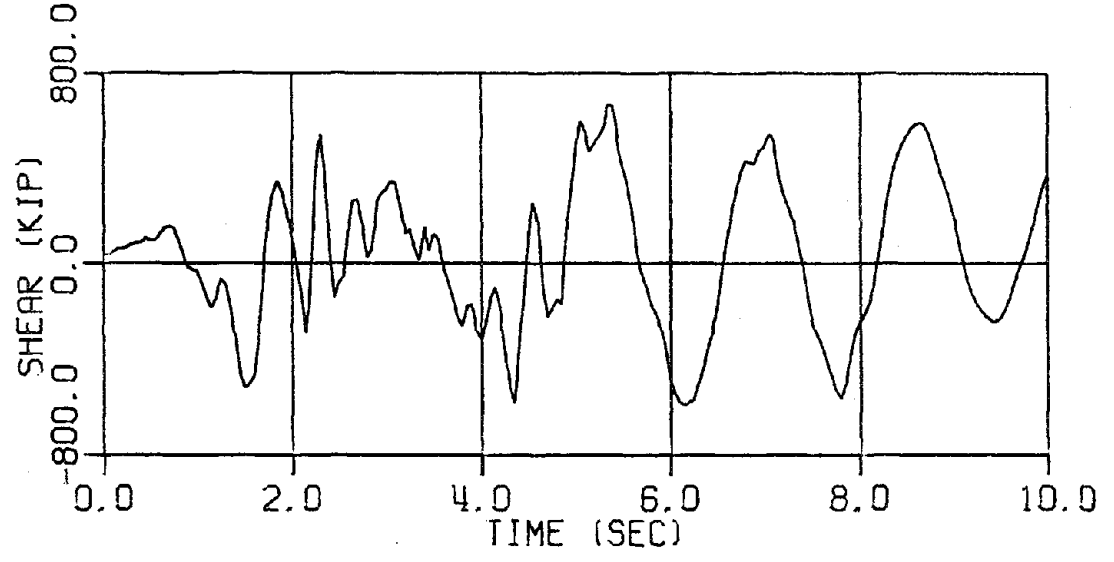

Fixed Base

Figure 5.3.27: Left Wall Base Shear; 2x1980 El Centro N-S

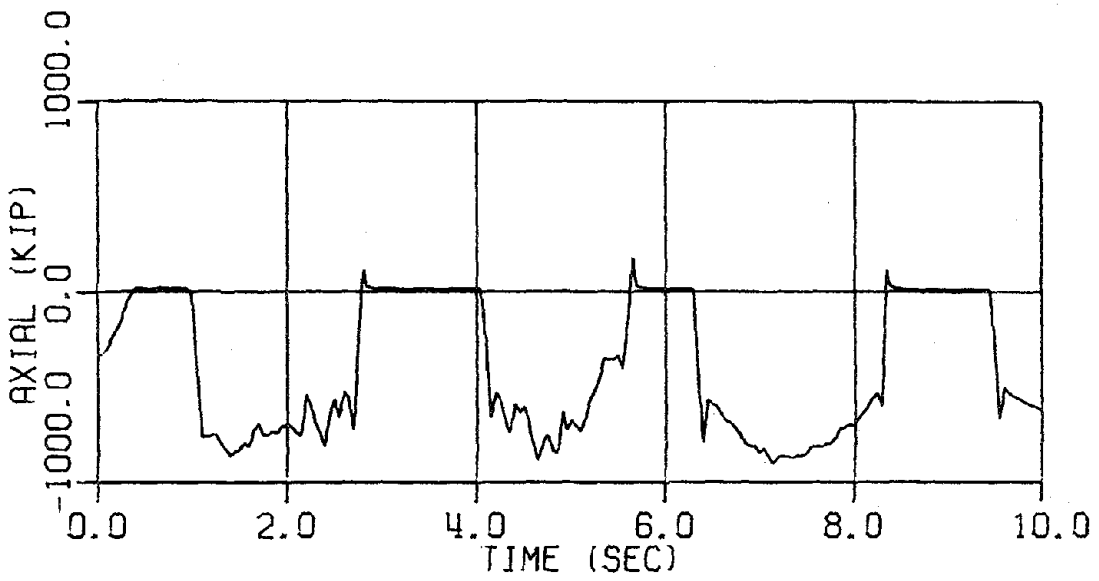

Uplift Allowed

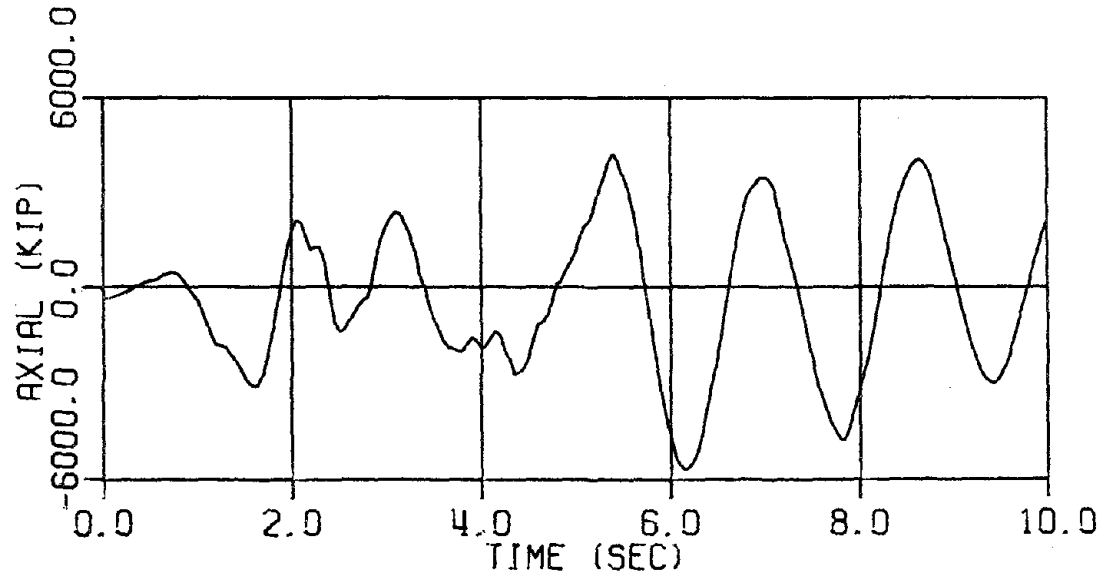

Fixed Base

Figure 5.3.28: Left Wall Base Normal Force; 2x1940 El Centro N-S

5.4 Framed Tube

This structure,which was also utilized to demonstrate and evaluate the substructuring process,is a 30 story framed tube, shown in Figure 5.4.1. The structure was designed for a base shear coefficient equal to 6% of the superstructure dead weight. Although a three-dimensional system, a rectangular tube can be analyzed as a two-dimensional system if out of plane deformations of the flanges are ignored. The structure can then be unfolded as shown in Figure 5.4.1; all horizontal displacements of the unfolded flanges are prevented while the vertical displacements of the flange corner nodes are constrained to match those of the corresponding web edge nodes. All of the horizontal mass is attributed to the web while vertical mass is attributed to both web and flange. Normal symmetry boundary conditions are enforced at the flange centerlines.

The uplift behavior of the structure is modeled by bilinear foundation springs which have only compressive capacity and stiffness, i.e. no tensile connection exists between superstructure and foundation. Only dead weight plus partition loads were assumed to contribute to horizontal mass while a fraction of the live load was assumed to contribute to the vertical mass; the vertical mass was, as a result, 20% greater than the horizontal mass.

With the assumption of axially rigid web beams, the total number of dynamic degrees of freedom for this analytical model is 836. The resulting first four mode shapes and natural periods are shown in Figure 5.4.2. The effective horizontal mass for the first mode is 71% of the total, while the effective mass for the 2nd mode is 19% of the total; the first two modes thus represent 90% of the total horizontal mass of the superstructure.

Examining the 1st mode overturning effect, for the given ratio of vertical/horizontal mass, one would anticipate the initiation of a rigid body type of uplift response at a base shear coefficient of 14% of the horizontal mass. With a design base shear slightly less then one-half of this value, one would therefore anticipate some degree of nonlinearity in the superstructure prior to such rigid, body uplift response. It should be noted, however, that due to shear deformations in the tube walls, the transition from "fixed base" to "rigid body" response will not be instantaneous, but instead a gradual transition as base separation progresses across the superstructure-foundation interface.

The second mode will also undoubtedly make a very significant contribution to the seismic response of this structure. The 2nd mode natural period of 0.92 sec., for many historical earthquakes, is associated with considerably higher acceleration levels than is the 1st mode natural period of 2.4 sec. For this reason, the base shear contribution of the 2nd mode may well be comparable in magnitude to that of the 1st mode; the 2nd mode response will not be mitigated by uplift, either, as it contributes a negligible base overturning effect.

Substructured (Locally Nonlinear) Response

Partially for reasons of computational economy, it was decided to utilize a brief but intense ground motion as input for these analyses, namely the 1971 Pacoima Dam S16E record. As the 1st four modes were all in a frequency range of considerable seismic energy content for this ground motion, all four were included in the linear substructure comprising the entire

superstructure. Including 26 boundary and nonlinear degrees of freedom, the number of active degrees of freedom in the substructured analysis is 30. Tangent stiffness proportional damping of 2% critical in the 1st mode was assumed.

Figure 5.4.3 illustrates the lateral displacement time histories of the 30th, 20th and 10th floors to the initial 5 seconds of the ground motion, as predicted by the substructured analysis. Figure 5.4.4 illustrates the vertical displacement time histories of mid-flange, corner and mid-web nodes during the same 5 seconds of response. Although very large, the displacements indicated are perhaps not unreasonable for such a high intensity excitation.

Figure 5.4.5 indicates the computed story shear envelope and illustrates its comparison to the design shear envelope. The very significant effect of the 2nd mode is immediately obvious from the shear envelope. Also quite obvious is the large difference between the design story shears and those predicted by the locally nonlinear analysis. The base shear indicated by Figure 5.4.5 is equivalent to a base shear coefficient of 26%, considerably higher than that required to initiate fully rigid body uplift response. As mentioned previously, uplift response can limit only the 1st mode contribution to base shear; the larger portion of this base shear is actually attributable to the 2nd mode.

Figure 5.4.6 illustrates the 1st floor column shear and axial force envelopes. As can be seen, allowing uplift for a linear superstructure of this sort shifts considerable shearing forces to the "leeward" web columns, but at the same time eliminates potentially large tensile forces in the flange and outermost web columns.

In order to assess the accuracy of the substructured analysis, a nonsubstructured analysis of the same structure subjected to the same ground motion was performed. The superstructure was still restricted to behave in a linear manner, although the entire coupled set of equations was integrated. The results of this nonsubstructured analysis indicated a high degree of accuracy in the substructured analysis. The horizontal displacements agreed consistently within 1%, uplift displacements within 2% and force envelopes agreed generally within 5%. As an indication of the limited discrepancies between the two analyses, the percentage error in the story shear envelopes is plotted Figure 5.4.7.

For this short duration time history (500 time steps), the nonsubstructured analysis required approximately 30% more CPU time than the substructured analysis, not considering the eigenvalue extraction. Since the assumption of superstructure linearity was made for both analyses, and the nonlinear degrees of freedom were restricted to the last few in each case, the forward reduction effort for the stiffness matrices due to nonlinearity in each case was essentially equivalent. Considerable economies were achieved through substructuring, however, in the load term reduction and back substitution operations. (An extremely large difference in forward reduction effort would be apparent if nonlinear terms appears "higher" in the complete stiffness matrix than in the substructured stiffness matrix).

Response with Generalized Nonlinearity

Since the assumption of superstructure linearity for this ground motion led to story shears considerably in excess of design levels, it was decided to investigate the effect of general superstructure nonlinearity in addition to the uplift phenomenon. As mentioned previously, the 2nd mode contributes

very significantly to the seismic response of this structure, particularly in the situation where foundation uplift is acting to limit the 1st mode response. For the analyses described in this section of the paper, therefore, inelastic superstructure behavior, i.e. plastic hinges at the ends of beams and columns, is provided for as well as foundation uplift. Due to a strong column/weak girder design strategy, however, it was anticipated that major inelastic behavior would be limited to the beam members. Obviously, substructuring is not utilized for these analyses.

Displacement time histories for the 30th, 20th and 10th floors are indicated in Figure 5.4.8. Superstructure nonlinearity obviously has a strong influence on the response of this structure; there is some indication of permanent set resulting from the large acceleration impulse in the Pacoima S16E accelerogram at approximately 3.2 seconds into the response.

Figure 5.4.9 illustrates story shear envelopes for the case of generalized superstructure nonlinearity. A considerable reduction in story shears is evidenced, as well as a considerable mitigation of the 2nd mode response. This reduction in 2nd mode response is attributable to superstructure ductility; foundation uplift had a negligible effect upon higher modes.

Figure 5.4.10 illustrates 1st floor column shear and axial force envelopes for the case of generalized superstructure nonlinearity. Comparison with Figure 5.4.6 indicates the obvious effect of placing a limit upon 2nd mode response; base shear is reduced by 38% and is uniformly distributed across the web of the tube. The column axial forces are also reduced by superstructure nonlinearity, indicating that ductility-related reduction in response are also present in the 1st mode as well as the 2nd.

Figure 5.4.11 indicates the maximum girder plastic hinge rotations over the height of the structure; this ductility demand was limited to web girders. As can be seen, the maximum hinge rotations were on the order of .01 radians, generally considered a readily achievable value if not too many cycles of response at this level are indicated. It can also be seen that ductility demand is quite sensitive to section changes, as one might well expect.

SUMMARY AND CONCLUSIONS

A limited substructuring capability has been implemented in the nonlinear seismic response program DRAIN-2D. Sample analyses have shown that accurate approximations with significant reduction of computational effort can be realized when substructuring is used to model structures which exhibit nonlinear behavior in limited, predefinable regions, such as is often the case with transient foundation uplift. While the designation of these regions requires a firm understanding of the expected structural behavior, such engineering judgment has always been a part of dynamic analysis, particularly for extreme seismic response.

Although extremely effective at limiting fundamental mode response, the phenomenon of transient foundation uplift is seen to be of little use in controlling higher mode response. Particularly for the seismic resistant design of slender high-rise structures to intense ground motions originating nearby, these higher mode responses can be important and even critical.

The assumption of linear behavior should be examined closely as well, since the presence of nonlinearity can and often does have a very significant effect upon seismic response. Depending upon design lateral load

levels, aspect ratio and degree of design conservatism, the assumption of superstructure linearity may or may not be a reasonable assumption in the presence of transient foundation uplift. Transient foundation uplift, acting in conjunction with or independent of superstructure ductility is, however, generally an asset rather than a liability in seismic resistant design.

The framed tube structure examined in this paper was shown to be an effective seismic resistant system. With moderate levels of ductility demand an extreme overload was safely accommodated. Adequate drift control was maintained, even in the presence of transient foundation uplift. The second mode response, for the ground motion utilized, was shown to be of considerable importance.

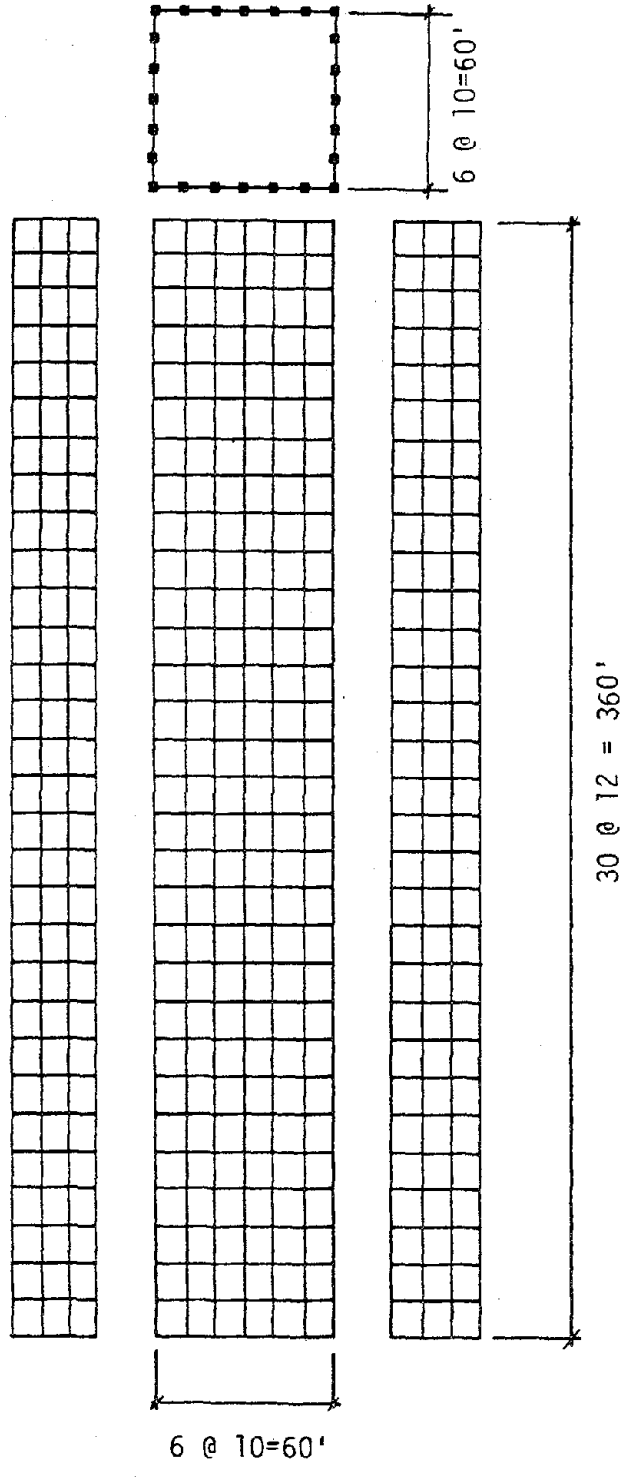

5.4.1. 30 Story Framed Tube Plan and Elevation (unfolded)

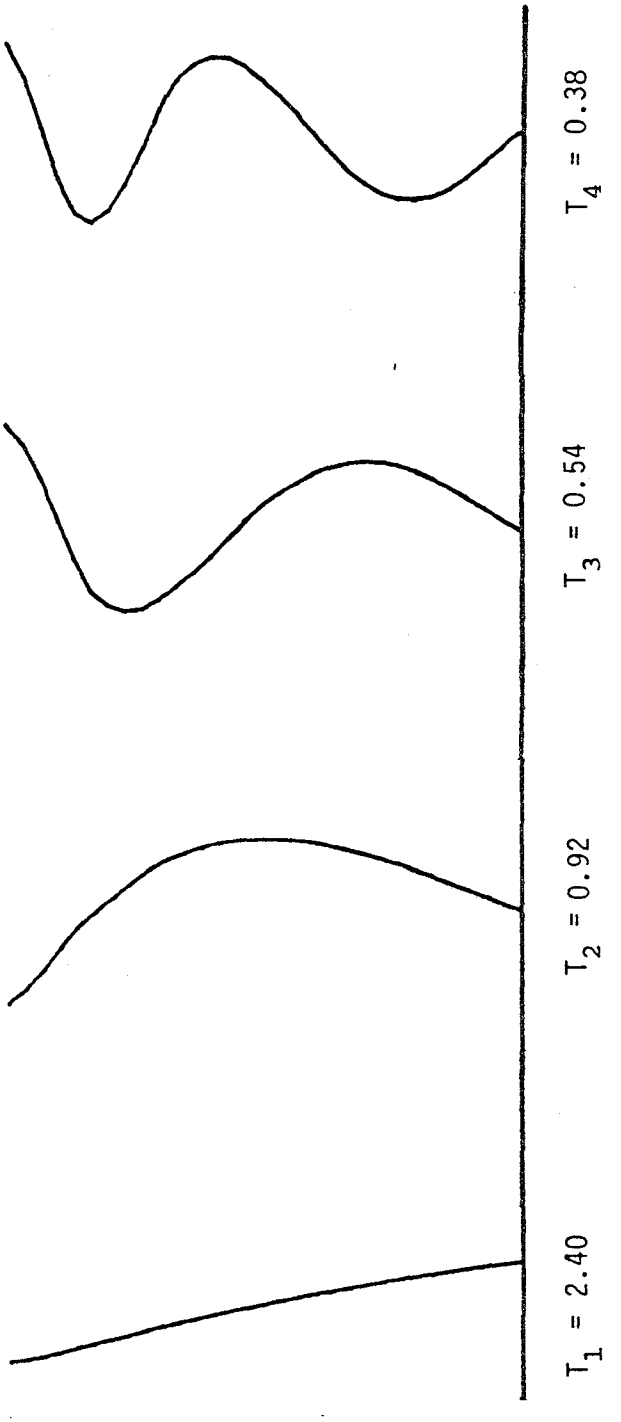

5.4.2. 30 Story Framed Tube; Periods and Mode Shapes

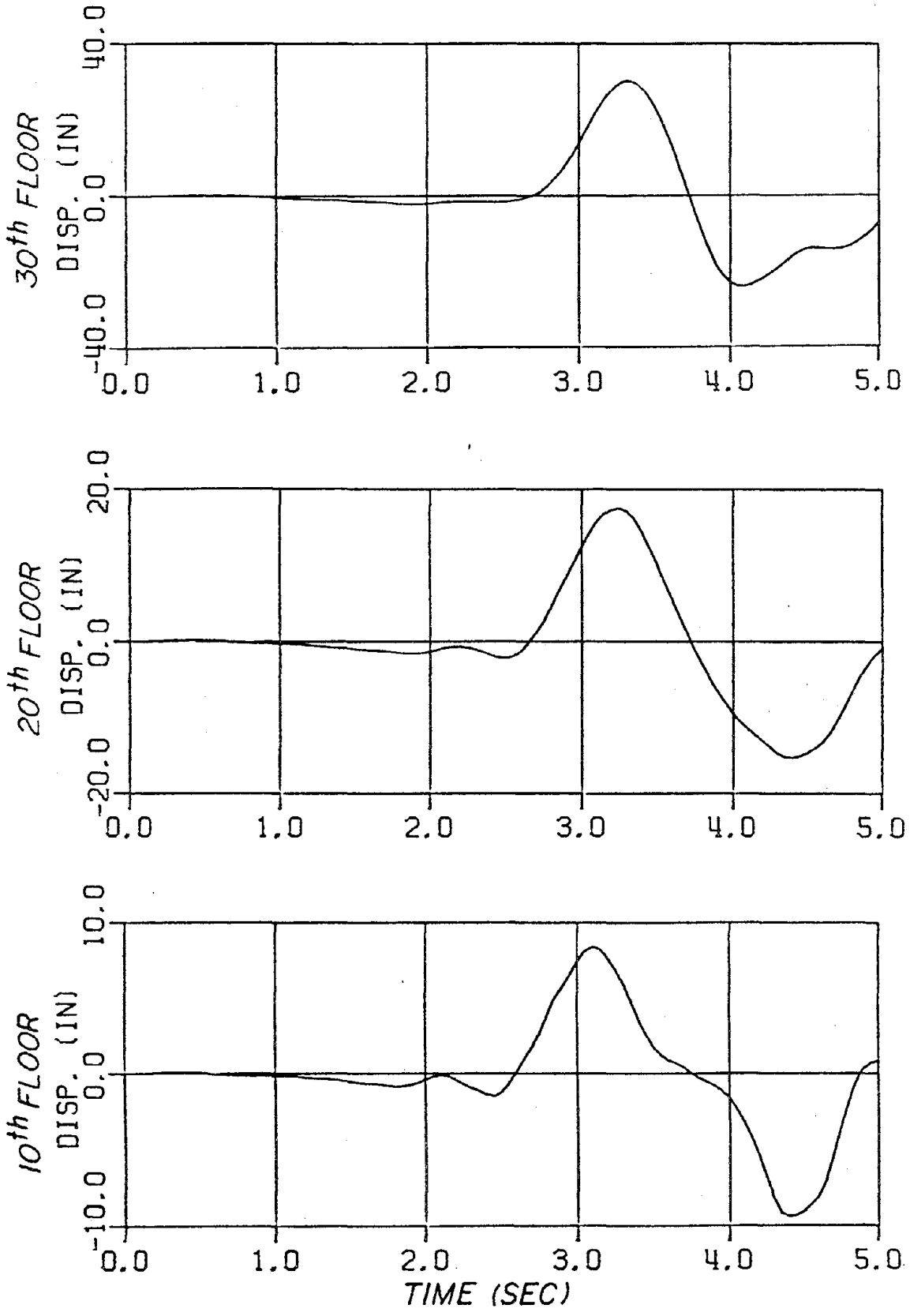

5.4.3. Selected Lateral Floor Displacements; Pacoima S16E (Linear Superstructure)

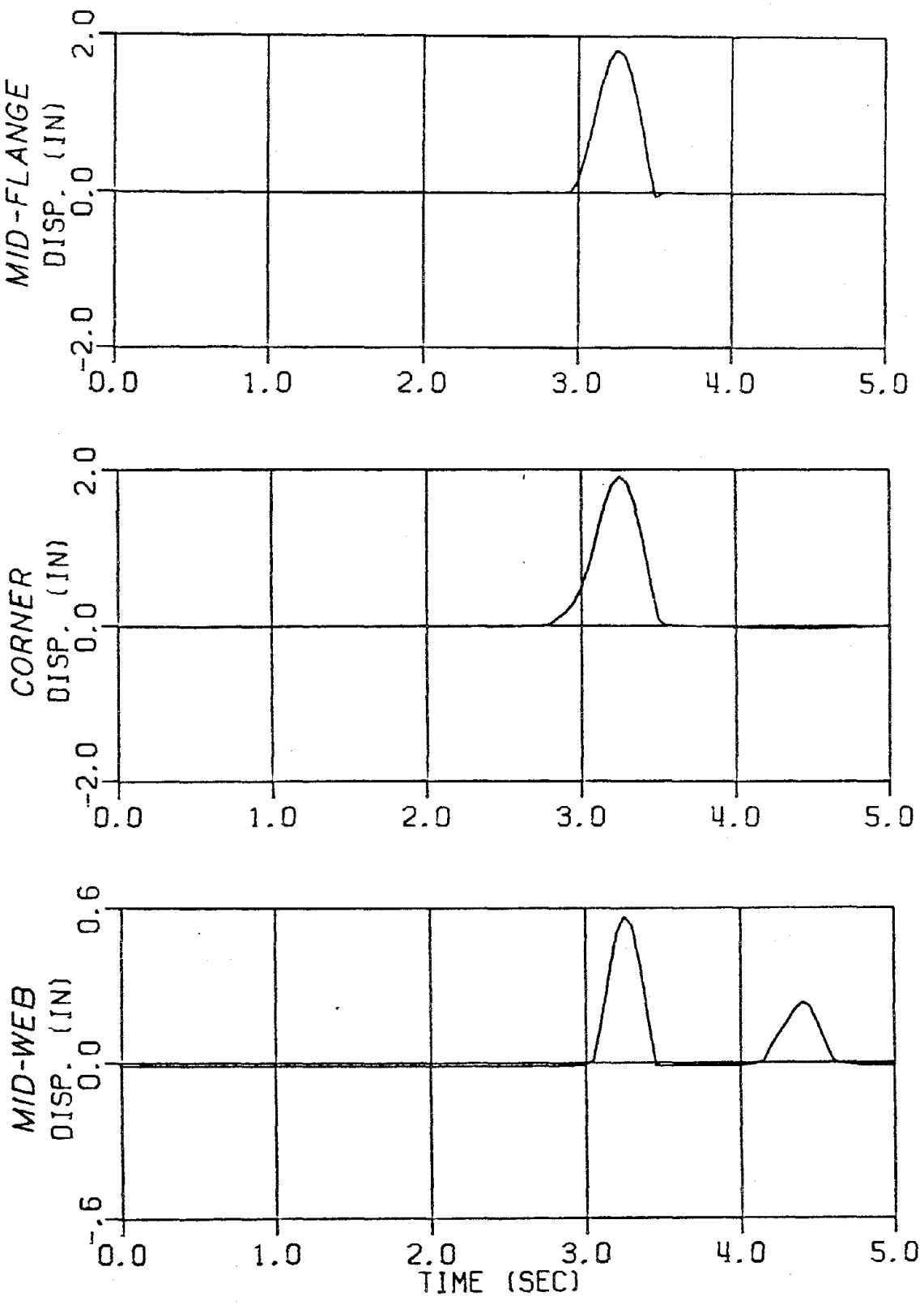

5.4.4. Selected Uplift Displacements; Pacoima S16E (Linear Superstructure)

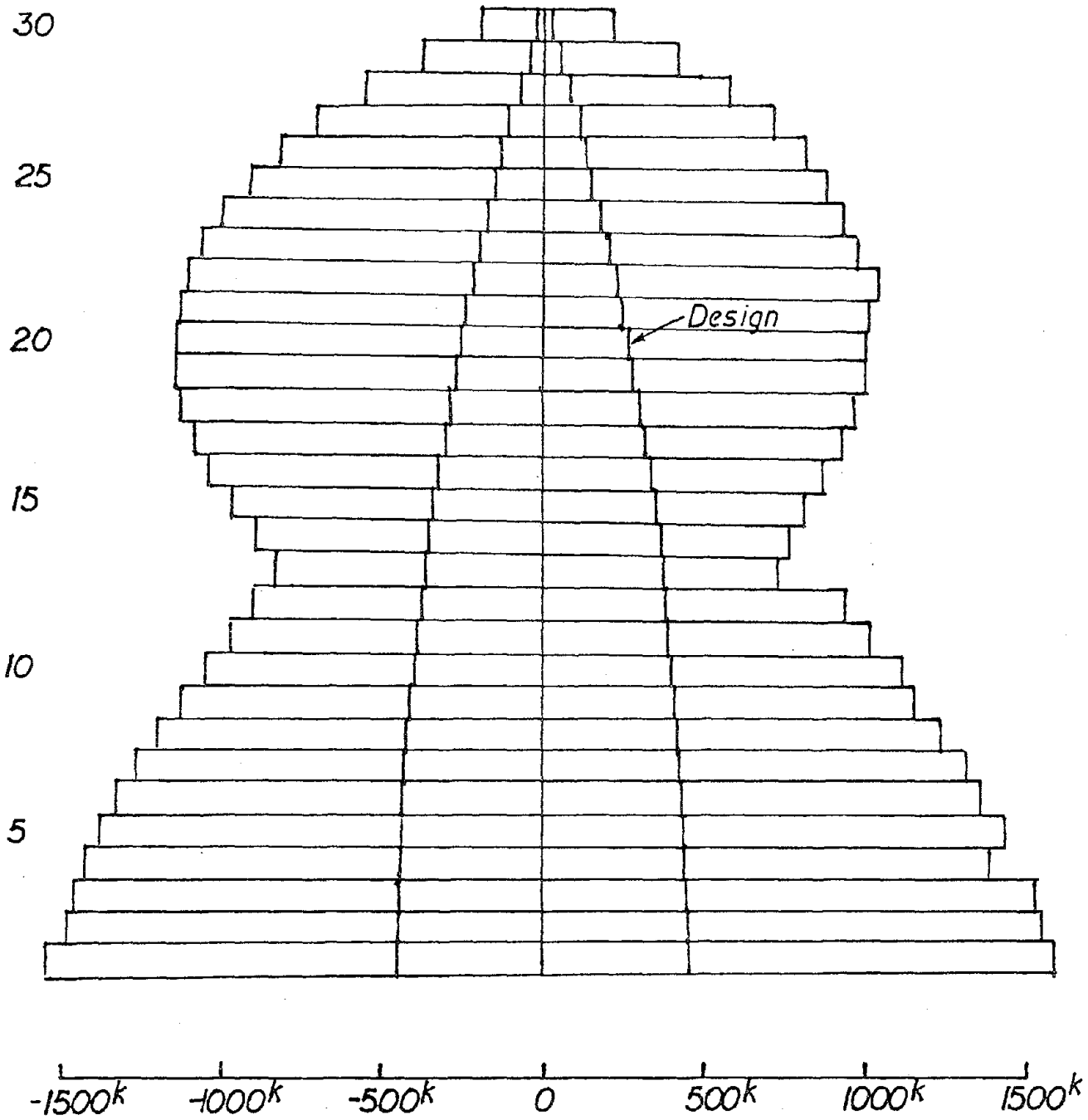

5.4.5. Story Shear Envelopes; Pacoima S16E
(Linear Superstructure)

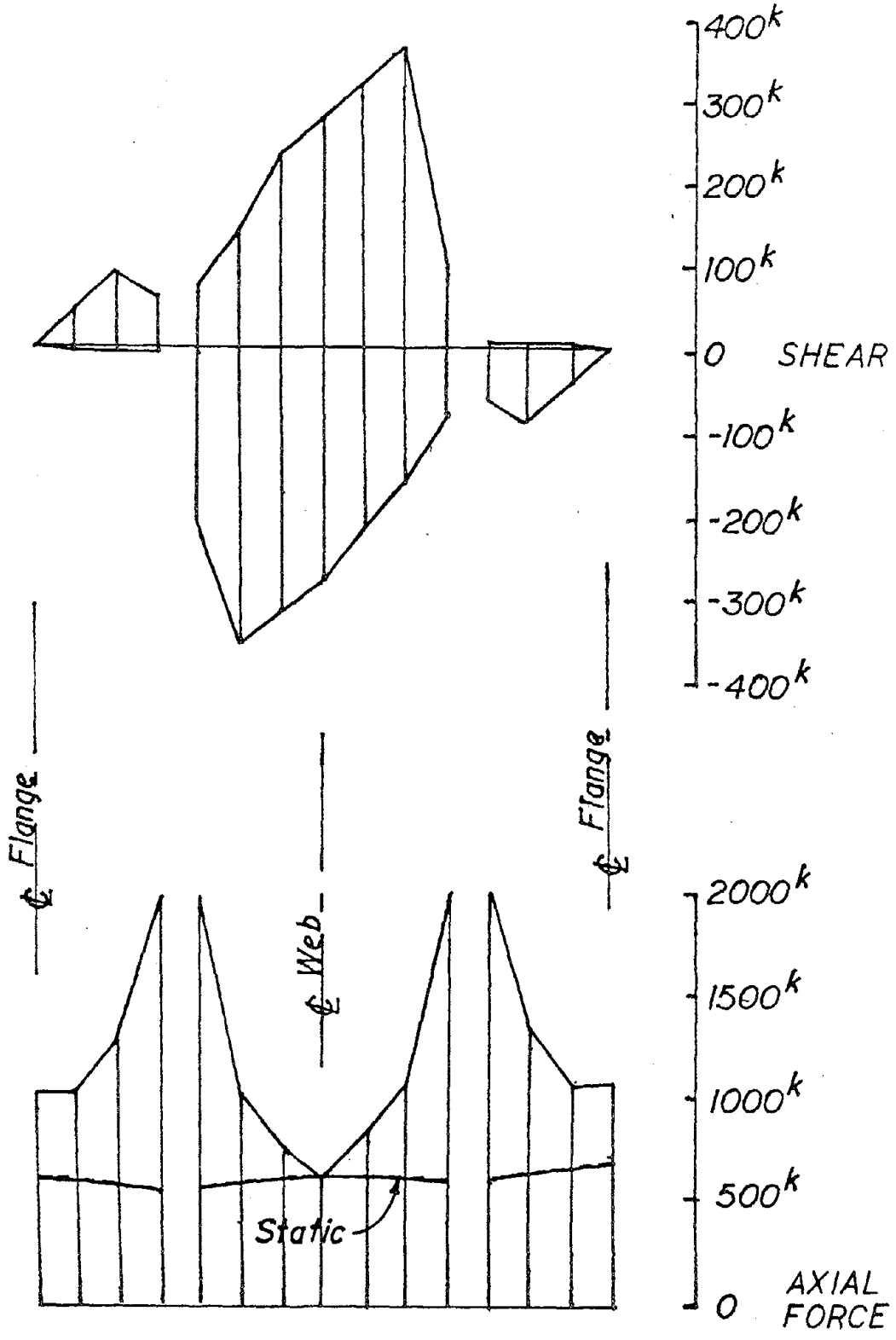

5.4.6. 1st Floor Column Force Envelopes; Pacoima S16E (Linear Superstructure)

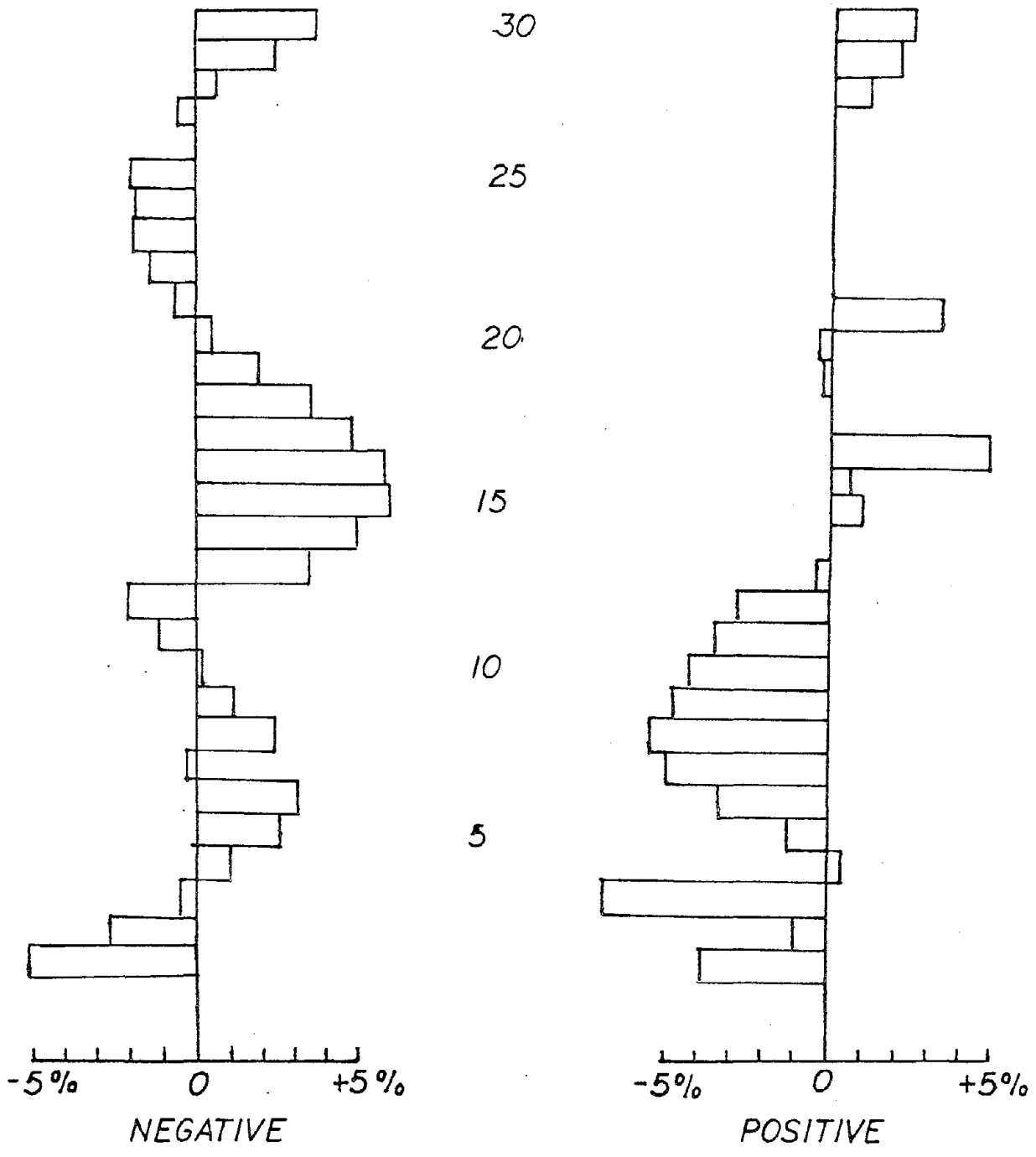

5.4.7. Discrepancy in Story Shear Envelopes; Substructured vs. Non-substructured Analyses

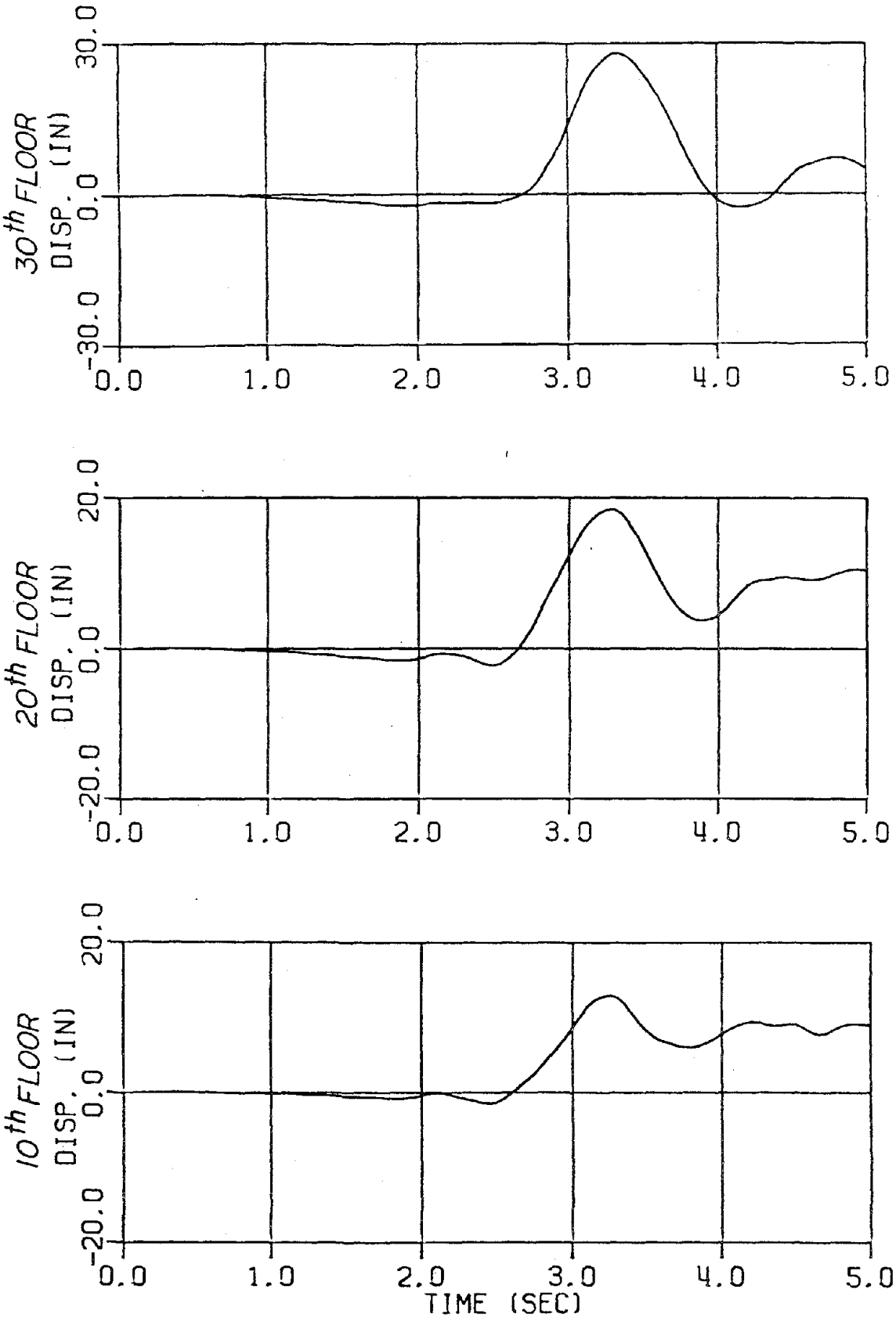

5.4.8. Lateral Floor Displacements: Pacoima S16E
(Nonlinear Superstructure)

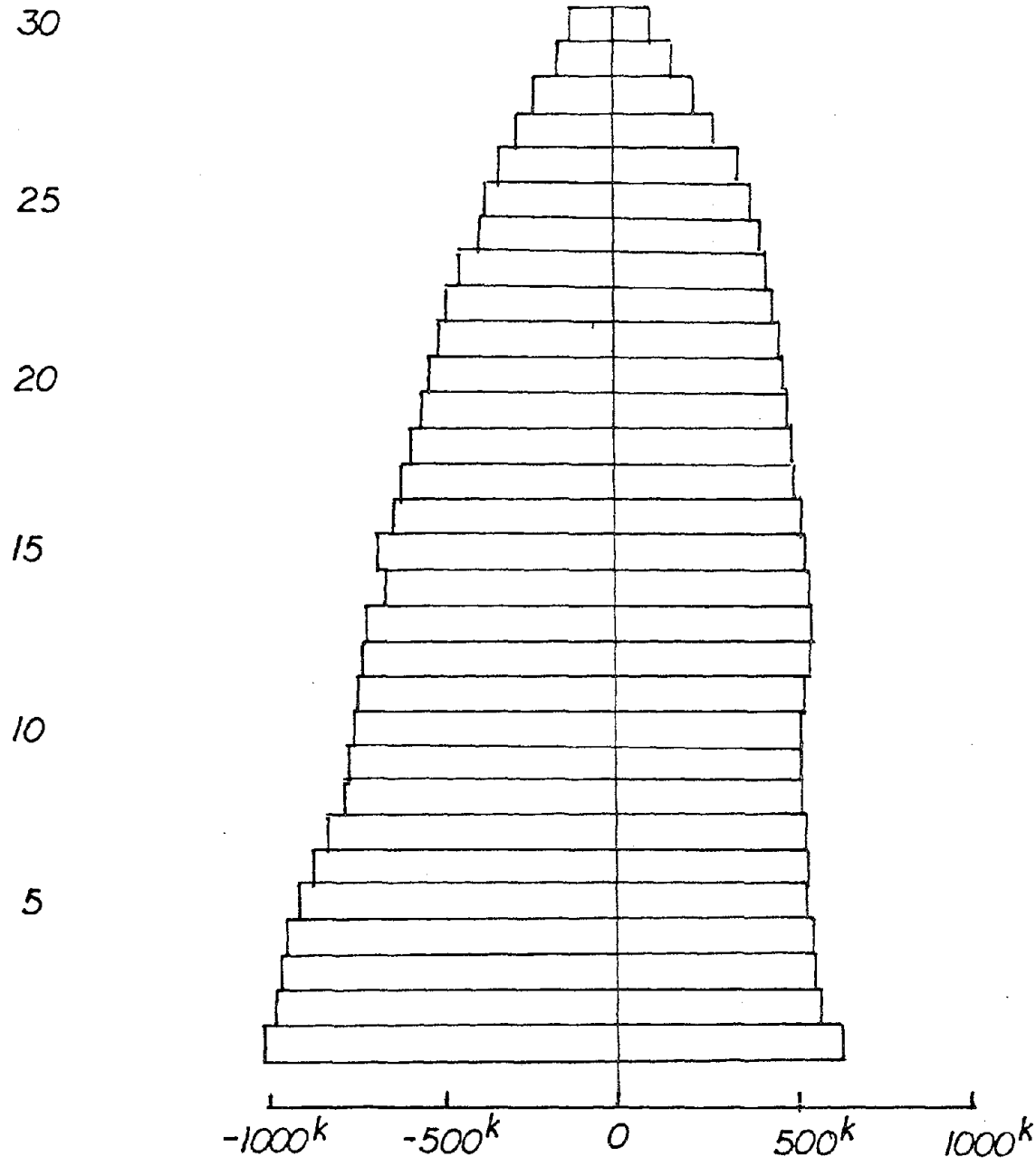

5.4.9 Story Shear Envelopes; Pacoima S16E
(Nonlinear Superstructure)

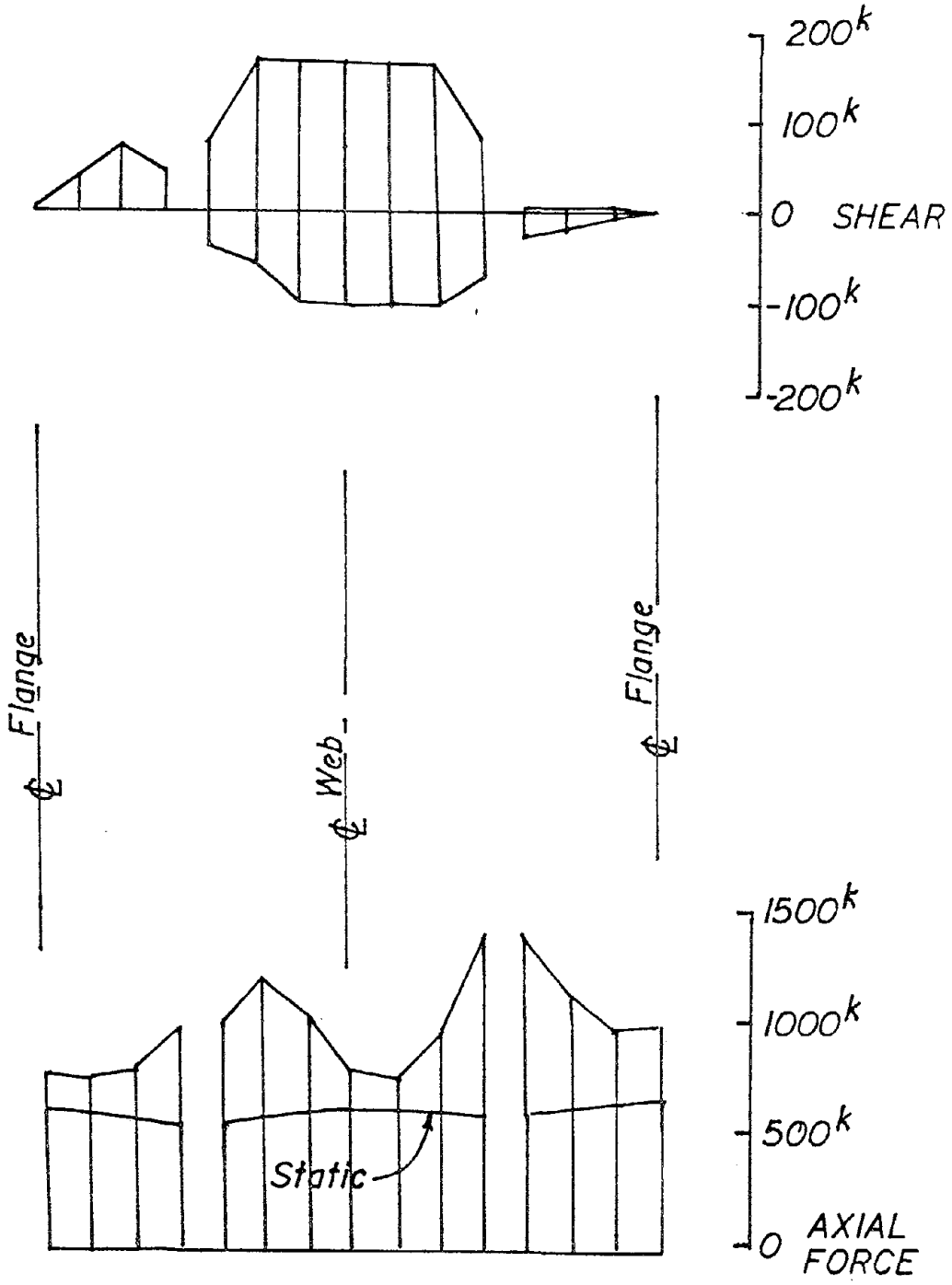

5.4.10. 1st Floor Column Force Envelopes; Pacoima S16E
(Nonlinear Superstructure)

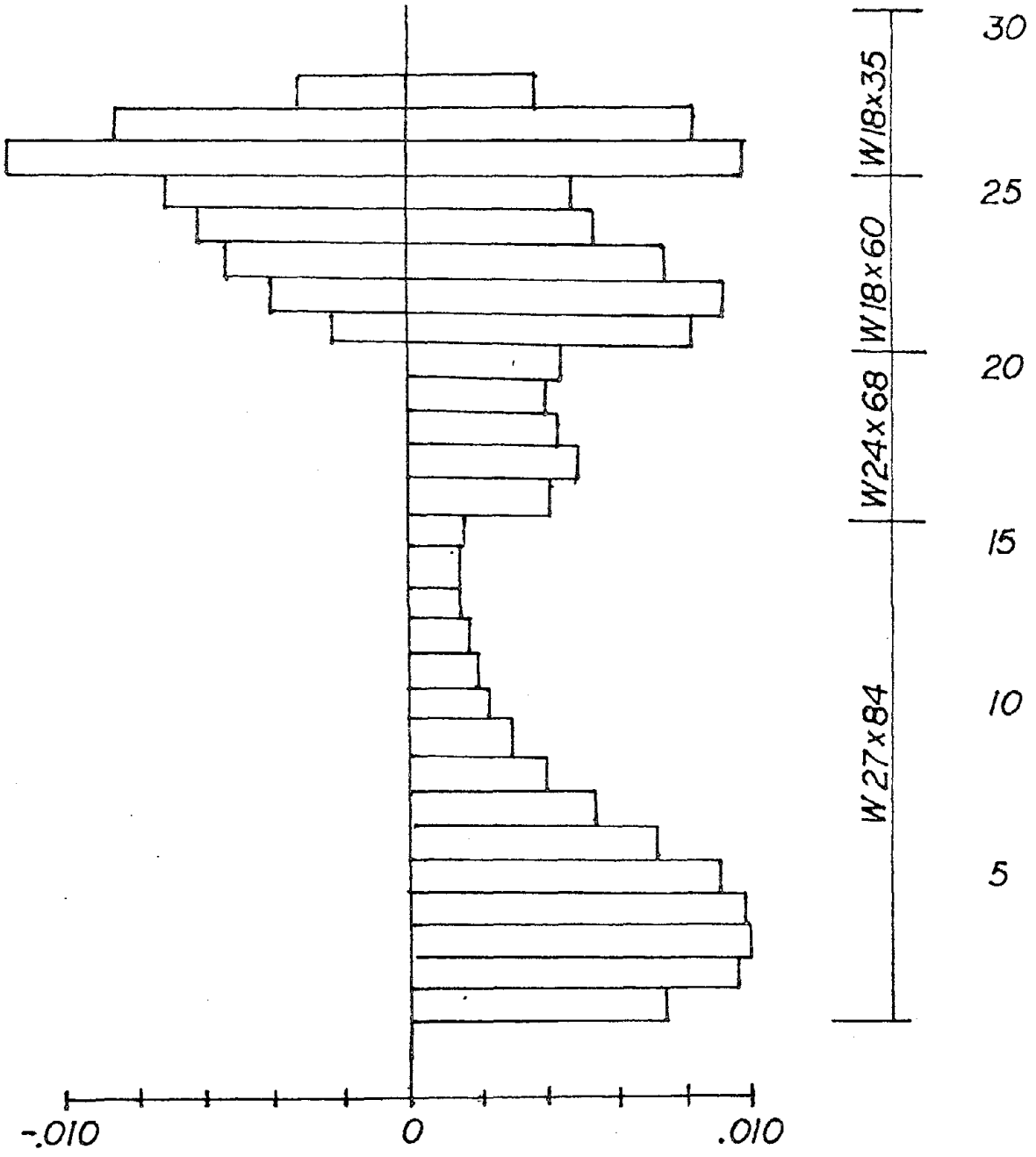

5.4.11. Girder Plastic Hinge Rotation Envelopes; Pacoima S16E (Nonlinear Superstructure)

6. DESIGN CONSIDERATIONS

If a structure is to be designed with intentioned transient uplift capability, this behavior should be considered explicitly in the detailing of the foundation/superstructure interface, as well as in critical service connections. Obviously adequate resistance to any "constant" lateral loading such as mean wind pressure must be provided.

6.1 Required Wind Restraint

As indicated in the introductory section, normal design wind loading is usually low enough that for most structures gravity overturning resistance alone is adequate to ensure stability. The design lateral wind load resultant will commonly fall within the equivalent seismic spectral acceleration range of .02 g to .10 g. Lateral load levels required to initiate rigid body uplift response are usually considerably higher than this amount, i.e. transient uplift response can justifiably be considered an "extreme event" load phenomenon as opposed to a "serviceability" load phenomenon.

6.2 Foundation Details

If a structure is to successfully exhibit transient uplift the separation between foundation and superstructure should satisfy certain criteria:

1. Provide a definite shear transfer to prevent migration of the superstructure.
2. Provide relatively little "tensile" stiffness, i.e. little restraint to vertical base separation.
3. Provide adequate impact capacity (strength and toughness).
4. Provide sufficient compliance to protect the superstructure from any harmful effects of impact.

5. Exhibit behavior which is sufficiently elastic to ensure the superstructure's return to a plumb position after the earthquake.
6. Be economically viable.

One column detail which would seem to meet the above criteria is a steel flexure plate, schematically shown in Figure 6.2.1. The flexure plate readily provides a shear key while allowing nearly free uplift motion. If deemed desirable, an impact layer of neoprene or other material could be provided beneath the column base. This detail was demonstrated to function quite satisfactorily in shaking table tests. [7] If a greater degree of rotational fixity is required for column bases, the baseplate dimensions could be increased or a grade beam could be employed between columns. (The latter approach was taken with the example 20 story frame discussed in the previous section of the report.)

The same flexure plate concept can be extended to a shear wall, as shown for the example core wall system in Figure 6.2.2. The rebar-flexure plate connection can be designed utilizing the principle of "shear friction" as suggested in current ACI provisions.

Figure 6.2.3 shows schematically a foundation interface detail for the framed tube example structure. Providing for the separation at the junction of foundation with the superstructure in this manner allows one complete freedom in choosing the type of foundation; i.e., deep foundations are not precluded from consideration for uplifting structures. Another distinct advantage of providing intentive weak planes is the elimination of potential soil failure resulting from pulling the foundation structure free from the bearing stratum.

It should be noted that, depending upon the degree of restraint present, the flexure plates discussed in the previous paragraphs may develop substantial second order membrane tensile stresses under extreme uplift amplitudes. These large displacement effects should be considered in the design of such details, both with regard to connection requirements and potential effects upon overall structural response.

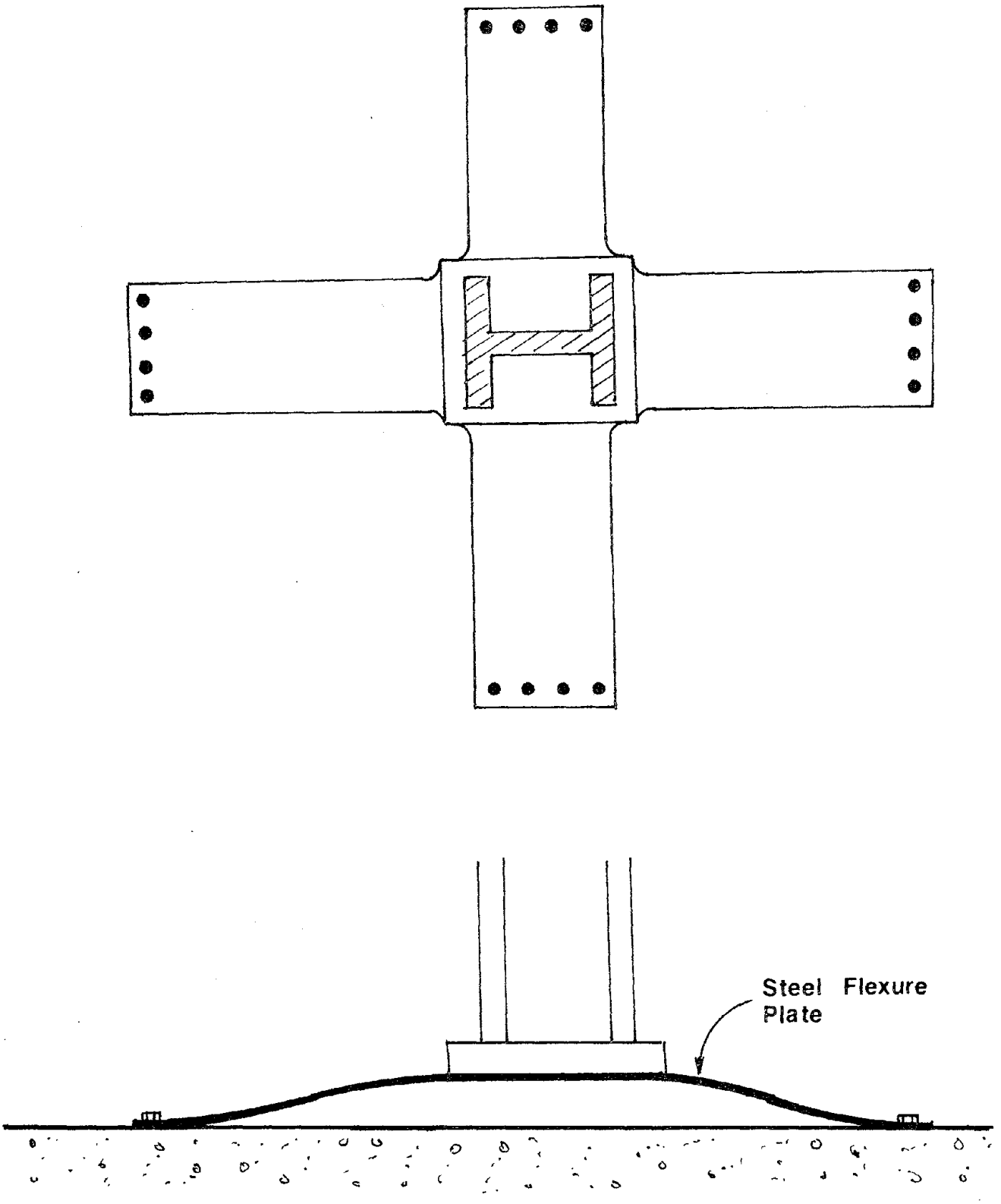

Figure 6.2.1. Typical Column Base Detail

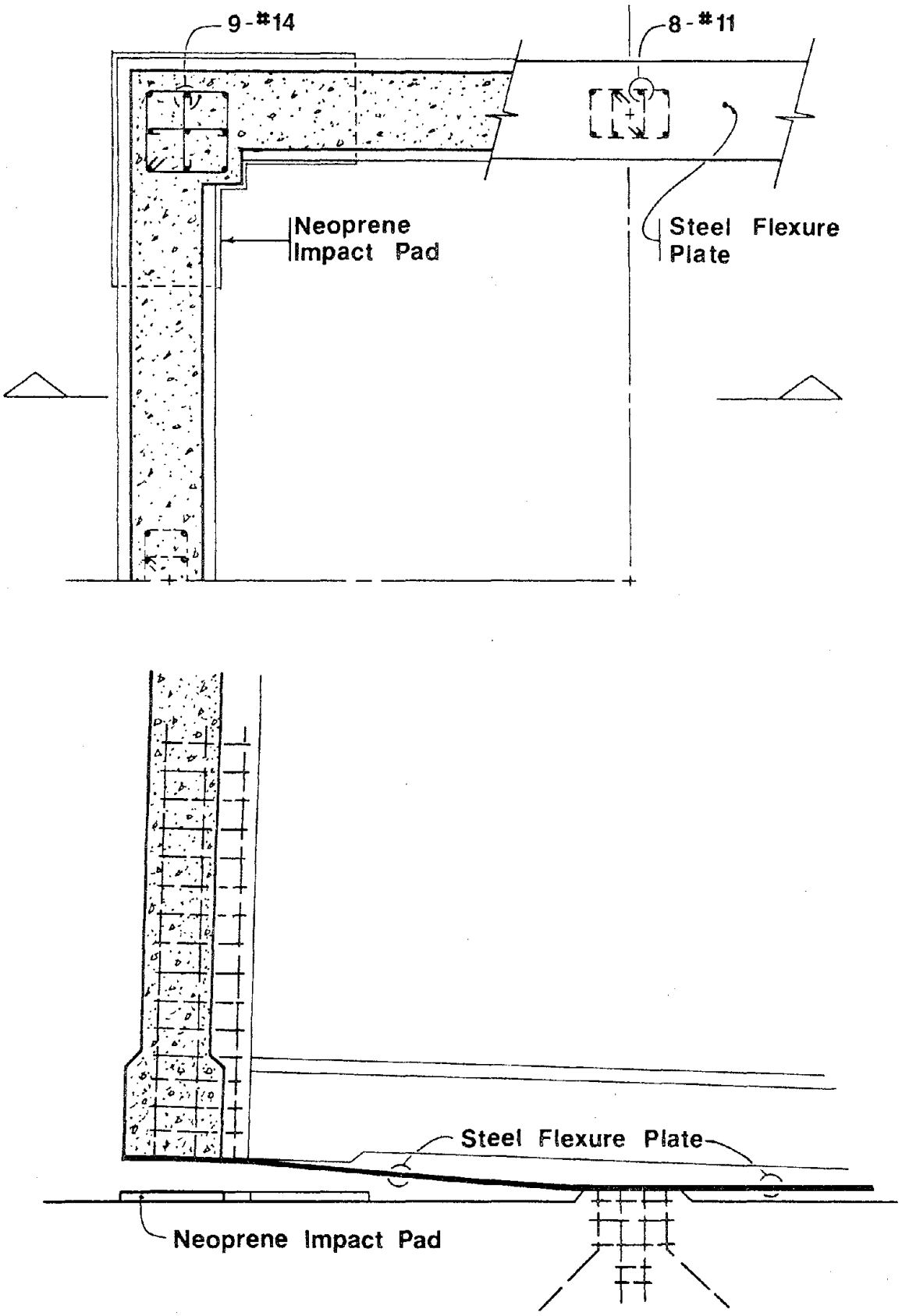

Figure 6.2.2. Cove Wall Base Detail

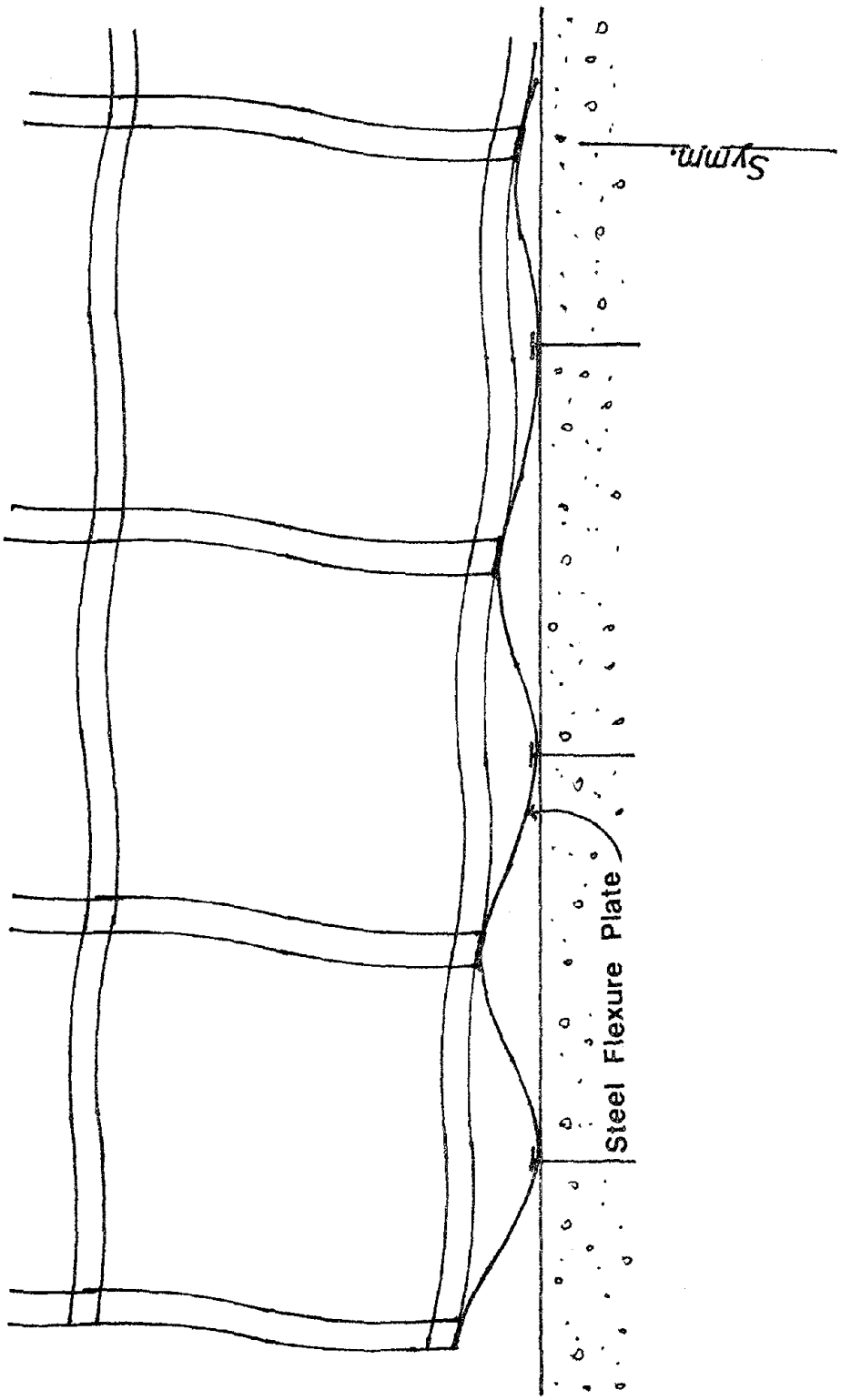

Figure 6.2.3. Framed Tube Base Detail

7. CONCLUSIONS

The analytical work described in this report consistently demonstrated an enhanced "extreme event" seismic response resulting from intentional transient foundation uplift. Overturning resistance provided by gravity alone, for common building structures, will be more than adequate to prevent uplift during extreme wind loading and levels of seismic loading currently specified in most codes. For the popular structural forms examined, namely moment frames, braced frames, shear walls (core wall and coupled wall) and framed tubes, transient uplift resulted in generally lower stress resultants and ductility demands. Although some loss in drift control resulted for those cases with little inherent superstructure energy dissipation, considering the levels of seismic loading drift levels remained within reasonable limits.

An analysis technique incorporating linear substructures coupled to a nonlinear base structure was shown to accurately predict locally nonlinear response with a substantial advantage in computational effort when compared to a fully nonlinear analysis. It was demonstrated quite clearly, as well, that the assumption of linearity deserves close scrutiny; ignoring any significant nonlinearity drastically alters the resulting response.

The phenomenon of transient foundation was also demonstrated to have a mitigating effect only on those modes associated with a significant base overturning effect. For usual building structures this implies that modes higher than the fundamental one will not be affected to any significant degree. Depending upon the structural characteristics and the frequency content of the ground motion the second and even higher

modes may contribute substantially to the seismic response of a building. Particularly for tall slender structures located in close proximity to causative faults, the designer should be cognizant of higher mode effects.

In summary, it would seem there is little structural justification for requiring overturning capability in excess of that required for wind effects. Even if a deep foundation is required for reasons other than excessive overturning capacity, there are distinct structural advantages in providing intended uplift capability during extreme seismic response. The required foundation details need not be elaborate nor costly, but should be carefully considered as an important part of the overall structural design. By carefully considering extreme event response, in addition to the normal serviceability requirements, the safety as well as the long term economy of the structure can be greatly enhanced.

REFERENCES

1. Bathe, K.J. and Wilson, E.L., Numerical Methods in Finite Element Analysis, Prentice-Hall, 1976.

2. Beck, J.L. and Skinner, R.I., "The Seismic Response of a Reinforced Concrete Bridge Pier Designed to Step," Earthquake Engineering and Structural Dynamics, Vol. 2, No. 4, 1974.

3. Clough, R.W. and Huckelbridge, A.A., "Preliminary Experimental Study of the Seismic Uplift of a Steel Frame," EERC Report No. 77-22, University of California, Berkeley, Aug. 1977.

4. Clough, R.W. and Penzien, J., Dynamics of Structures, McGraw-Hill, 1975.

5. Clough, R.W. and Wilson, E.L., "Dynamic Analysis of Large Structural Systems with Local Nonlinearities," Computer Methods in Applied Mechanics and Engineering, Vol. 17/18, Part 1, Jan. 1979.

6. Guyan, R., "Reduction of Stiffness and Mass Matrices," AIAA Journal, Vol. 3, No. 2, Feb. 1965.

7. Huckelbridge, A.A., "Earthquake Simulation Tests of a Nine-Story Steel Frame with Columns Allowed to Uplift," EERC Report No. 77-23, University of California, Berkeley, Aug. 1977.

8. Huckelbridge, A.A. and Christ, R.A., "Nonlinear Overturning Effects in a Core-Stiffened Building," Proceedings, 2nd U.S. National Conference on Earthquake Engineering, Stanford University, 1979.

9. Huckelbridge, A.A. and Ferencz, R.M., "Overturning Effects in Stiffened Building Frames," Earthquake Engineering and Structural Dynamics, Awaiting publication.

10. Kanaan, A. and Powell, G.H., "Drain-2D: A General Purpose Program for Inelastic Dynamic Response of Plane Structures," EERC Report No. 73-6/22, University of California, Berkeley, Revised Aug. 1975.

11. Kron, G., "Solving Highly Complex Elastic Structures in Easy Stages," Journal of Applied Mechanics, ASME, Vol. 22, No. 2, June 1955.

12. Meek, J.W., "Effects of Foundation Tipping on Dynamic Response," Journal of the Structural Division, ASCE, Vol. 101, No. ST 7, July 1975.

13. Meek, J.W., "Dynamic Response of Tipping Core Buildings," Earthquake Engineering and Structural Dynamics, Vol. 6, No. 4, 1978.

14. Muto, K., Umemura, H. and Sonobe, Y., "Study of the Overturning Vibration of Slender Structures," Proceedings, 2nd World Conference on Earthquake Engineering, Tokyo, Japan, Vol. 2, 1960.

15. Newmark, N.M., "A Method of Computation for Structural Dynamics," Journal of the Engineering Mechanics Division, ASCE, Vol. 85, No. EM 3, July 1959.

16. Popov, E.P. and Bertero, V.V., "Seismic Analysis of Some Steel Building Frames," Journal of the Engineering Mechanics Division, ASCE, Vol. 106, No. EM 1, Jan. 1980.

17. Przemieniecki, J.S., "Matrix Structural Analysis of Substructures," AIAA Journal, Vol. 1, No. 1, Jan. 1963.

18. Row, D.G. and Powell, G.H., "A Substructure Technique for Non-linear Static and Dynamic Analysis," EERC Report No. 78-15, University of California, Berkeley, Aug. 1978.

19. Rutenberg, Avigdor, Jennings, Paul and Housner, George, "The Response of Veterans Hospital Building 41 in the San Fernando Earthquake", EERL Report No. 80-03, California Institute of Technology, Pasadena, May, 1980.

20. Trifunac, M.D. and Lee, V., "Routine Processing of Strong-Motion Accelerograms," EERL Report No. 73-03, California Institute of Technology, Oct. 1973.

21. Wilson, E.L., "A Method of Analysis for the Evaluation of Foundation-Structure Interaction," Proceedings, Fourth World Conference on Earthquake Engineering, Santiago, Chile, Vol. 3, 1969.

22. Wolf, J.P. and Skikerud, P.E., "Seismic Excitation with Large Overturning Moments: Tensile Capacity, Projecting Base Mat or Lifting Off?," Nuclear Engineering and Design, Vol. 50, No. 2, 1978.

23. _____, "General Design Requirement," Art. 23, Title 17, Safety of Construction of Hospitals, California Administrative Code, Revised March 1974.

24. _____, "Tentative Provisions for the Development of Seismic Regulations for Buildings," ATC 3-06, Applied Technology Council, 1978.

25. _____, Uniform Building Code, International Conference of Building Officials, Whittier, California, 1979.

APPENDIX I

INTEGRATION CONSTANTS FOR INCREMENTAL DYNAMIC ANALYSIS

For the step-by-step integration scheme utilized in DRAIN-2D, it is assumed the nodal acceleration is constant within each time step:

$$\ddot{u} = \frac{1}{2} (\ddot{u}_{i-1} + \ddot{u}_i) \tag{A1.1}$$

The nodal velocity and displacement are calculated by successive integrations:

$$\dot{u} = \dot{u}_{i-1} + \int_o^t \ddot{u}\, dt \tag{A1.2}$$

$$u = u_{i-1} + \int_o^t \dot{u}\, dt \tag{A1.3}$$

These expressions can be evaluated to determine these response quantities at the time t_i:

$$\dot{u}_i = \dot{u}_{i-1} + \frac{\Delta t}{2}(\ddot{u}_{i-1} + \ddot{u}_i) \tag{A1.4}$$

$$u_i = u_{i-1} + \Delta t\, \dot{u}_{i-1} + \frac{1}{4} \Delta t^2 (\ddot{u}_{i-1} + \ddot{u}_i) \tag{A1.5}$$

The incremental nodal displacement can be found from Eqn. A1.5

$$\Delta u = u_i - u_{i-1} = \Delta t\, \dot{u}_{i-1} + \frac{\Delta t^2}{4}(\ddot{u}_{i-1} + \ddot{u}_i) \tag{A1.6}$$

which can be manipulated using equations A1.4 to find:

$$\Delta\dot{u} = \frac{2}{\Delta t}\ \Delta u - 2\dot{u}_{i-1} \qquad \text{(A1.7)}$$

subtracting the quantity $\frac{\Delta t^2}{2}\ \ddot{u}_{i-1}$ from (A1.6) leads to the other desired equality

$$\Delta\ddot{u} = \frac{4}{\Delta t^2}\ \Delta u - \frac{4}{\Delta t}\ u_{i-1} - 2\ddot{u}_{i-1} \qquad \text{(A1.8)}$$

Substitution of Eqns. A1.7 and A1.8 into the incremental dynamic equilibrium expression (Eqn. 3.4) results in a single variable, the incremental nodal diplacement. Upon solution of this system of equations for $\{\Delta u\}$, the change in nodal velocity and acceleration can be computed using Eqns. A1.7 and A1.8. The response state at the t_i is then found by summation of the incremental changes to the response state at time t_{i-1}.

APPENDIX 2

SUMMARY OF DRAINSUB-2D OPERATIONS

In the following outline of the computational procedure utilized in DRAINSUB-2D, starred items refer to operations performed by the base program DRAIN-2D.

(1)* Problem control information, structure geometry, geometric constraints and boundary conditions specified.

(2) Number of substructure modal coordinates and substructure boundary nodes specified.

(3)* Inertial properties, static loads, acceleration record and damping characteristics specified.

(4)* Element properties specified, global stiffness matrix assembled. Static analysis and geometric stiffness modifications performed if required.

(5) Specified number of substructure natural frequencies $[\Omega^2]$ and modes of vibration $[\Phi]$ of substructure calculated.

(6) The substructure interior dof $K_{\ell\ell}$ are eliminated to determine effective boundary node stiffnesses.

$$K'_{bb} = K_{bb} - K_{b\ell}\, K_{\ell\ell}^{-1}\, K_{\ell b}$$

(7) Compute skyline location matrix for reduced effective dynamic stiffness matrix $[\gamma M_r + K_r]$

(8) Backward eliminate substructure quadrant to calculate $K_{\ell\ell}^{-1} K_{\ell b}$ and calculate mass interaction terms:

$$\left[\begin{array}{c} -\phi_{m\ell}^T M_{\ell\ell} K_{\ell\ell}^{-1} K_{\ell b} \\ \hline K_{b\ell} K_{\ell\ell}^{-1} M_{\ell\ell} K_{\ell\ell}^{-1} K_{\ell b} \end{array}\right]$$

(9) Assemble reduced effective dynamic stiffness matrix $[\gamma M_r + K_r]$.

(10) Compute effective modal and boundary node load array:

$$\left[\begin{array}{c} -\phi_{m\ell}^T M_{\ell\ell} B_{\ell j} \\ \hline -K_{b\ell} K_{\ell\ell} M_{\ell\ell} B_{\ell j} \end{array}\right]$$

(11)* Forward reduce $[\gamma M_r + K_r]$.

(12) For each time step of the desired integration the following operations are performed and response envelopes updated:

(a) Assemble effective load vector

(b)* Reduce load vector and back substitute to determine $\{\Delta u_{ri}\}$

(c) Compute $\{\Delta \dot{u}_{ri}\}$ and $\{\Delta \ddot{u}_{ri}\}$, substructure incremental displacements

$$\{\Delta u_\ell\} = [\Phi_{\ell m}]\{\Delta u_m^*\} - [K_{\ell\ell}^{-1} K_{\ell b}]\{\Delta u_b\}$$

and current response state $\{u_i\}, \{\dot{u}_i\}, \{\ddot{u}_i\}$

(d)* Compute incremental and total element response; test for change of state of nonlinear elements; update $[\gamma M_r + K_r]$ and repeat forward reduction if change of state occurs.

(13) At end of integration print envelope values and time histories.

APPENDIX 3

DRAINSUB-2D USER'S MANUAL

This manual is a revision of the DRAIN-2D User's Guide (A3.1). All features of the original program have been retained, and the corresponding data input specifications remain unchanged. A limited amount of additional data input is required to utilize the sub-structuring capabilities added to DRAIN-2D to produce DRAINSUB-2D.

Developed on a DEC VAX/VMS 11 computer, the present version of DRAINSUB-2D utilizes a double precision global stiffness matrix and load/displacement vector. Additionally, the subspace iteration eigenproblem routine has also been converted to double precision. Conversions to machines with sufficient accuracy at single precision should be easily accomplished. The minimum storage requirements, excluding the element data, will not exceed

$$2 \times NSTEPS + NHOUT + NVOUT + NROUT + 13 \times NEQ + 2 \times KDUP \times NEQ \times MBAND + NELTOT + KFREQ \times NEQ \times [4 \times NROOT + 7] + KSUB \times [LMAX \times (IWDTH + NCOMP) + (2 + IWDTH)(IWDTH + NCOMP)]$$

where

NJTS = number of nodes in structure;

NEQ = number of structure degrees of freedom (conservatively NJTS x 3);

MBAND = maximum half bandwidth of structure stiffness matrix;

NMASS = number of nodes with lumped masses;

NSTEPS = number of integration time steps;

NELTOT = total number of elements in the structure;

NHOUT, NVOUT, NROUT = numbers of nodes for which time history prints of horizontal, vertical and rotational displacements, respectively, are required;

KDUP = 2 if a duplicate structure stiffness matrix is to be held in core, and = 1 if this duplicate matrix is to be held in secondary scratch storage. (See Section B1 of this guide for explanation);

KFREQ = 1 if frequency analysis of the entire structure is to be performed, zero if no frequency analysis desired.

NROOT = number of frequencies and modes of vibration to be found if KFREQ = 1.

KSUB = 2 if linear substructure is to be utilized, else 0.

NCOMP = number of assumed modal vibration patterns to be used to model substructure.

LMAX = number of interior degrees of freedom associated with substructure.

IWDTH = number of substructure boundary degrees of freedom.

References

A3.1 Kanaan, A. and Powell, G.H., "Drain-2D: A General Purpose Program for Inelastic Dynamic Response of Plane Structures," EERC Report No. 73-6/22, University of California, Berkeley, Revised Aug. 1975.

INPUT DATA

The following punched cards define the problem to be solved. Consistent units must be used throughout.

A. PROBLEM INITIATION AND TITLE (A5,3X,18A4) - One Card

Columns 1 - 5: Punch the word START

6 - 8: Blank

9 - 80: Problem title, to be printed with output.

B. STRUCTURE GEOMETRY INFORMATION

B1. CONTROL INFORMATION (9I5,I10,3I5) - One Card

Columns 1 - 5: Number of nodes in structure.

6 - 10: Number of "control nodes" for which coordinates are specified directly. See Section B2.

11 - 15: Number of node coordinate generation commands. See Section B3.

16 - 20: Number of commands for specifying nodes with zero displacements. See Section B4.

21 - 25: Number of commands for specifying nodes with identical displacements. See Section B5.

26 - 30: Number of commands specifying lumped masses at nodes. See Section B6.

31 - 35: Number of different groups of elements in structure. See Section E.

36 - 40: Data checking code. Punch 1 if only a data checking run is required. Leave blank or punch zero if the problem is to be executed. Punch -1 if the problem is to be executed provided the number of element information blocks does not

exceed one. This last option prevents execution, with excessive input/output costs, in cases where in-core operation is intended but errors are made in specifying the required storage.

45: Structure stiffness storage code. A duplicate stiffness matrix must be retained and periodically updated. Leave blank or punch zero if this matrix is to be retained in core. Punch 1 if the matrix is to be saved on secondary scratch storage.

46 - 55: Blank COMMON length to be assumed; if zero or blank, the value compiled into the program will be used.

60: Punch 1 if generated data and element specification output is to be suppressed.

65: Punch 1 if linear substructure is to be utilized for dynamic analysis.

70: Substructure frequency analysis storage code. Punch 1 if analysis is to be written to permanent storage on unit 9. Punch -1 if analysis is to be read from unit 9. If left blank, no action is taken.

B2. CONTROL NODE COORDINATES (I5,2F10.0) - One card for each control node.

See NOTE 1 for explanation.

Columns 1 - 5: Node number, in any sequence.

6 - 15: X coordinate of node.

16 - 25: Y coordinate of node.

B3. COMMANDS FOR STRAIGHT LINE GENERATION OF NODE COORDINATES (4I5,F10.0) - One card for each generation command.

Omit if there are no generation commands. See NOTE 1 for explanation.

Columns 1 - 5: Node number at beginning of generation line.

6 - 10: Node number at end of generation line.

11 - 15: Number of nodes to be generated along line.

16 - 20: Node number difference (constant) between any two successive nodes on the line. If blank or zero, assumed to be equal to 1.

21 - 30: Spacing between successive generated nodes. If greater than or equal to 1.0, assumed to be the actual spacing. If less than 1.0, assumed to be the actual spacing divided by the length of the generation line. If zero or blank, the nodes are automatically spaced uniformly along the generation line.

B4. COMMANDS FOR NODES WITH ZERO DISPLACEMENTS (6I5) - One card for each command.

Omit if no nodes are constrained to have zero displacement. See NOTE 2 for explanation.

Columns 1 - 5: Node number, or number of first node in a series of nodes covered by this command.

10: Code for X displacement. Punch 1 if constrained to be zero, otherwise leave blank or punch zero.

15: Code for Y displacement.

20: Code for rotation.

21 - 25: Number of last node in series. Leave blank for a single node.

26 - 30: Node number difference (constant) between successive nodes in series. If blank or zero, assumed to be equal to 1.

B5. COMMANDS FOR NODES WITH IDENTICAL DISPLACEMENT (16I5) - One card for each command.

Omit if no nodes are constrained to have identical displacements. See NOTE 3 for explanation.

Columns 5: Displacement code, as follows:

Punch 1 for X displacement.

Punch 2 for Y displacement.

Punch 3 for rotation.

6 - 10: Number of nodes covered by this command (maximum 14 - See NOTE 3 for procedure when more than 14 nodes have identical displacements).

11 - 80: Up to 14 fields, each I5. List of nodes, in increasing numerical order.

B6. SUBSTRUCTURE SPECIFICATION (16I5)

Omit if linear substructure is not utilized. See Note 4 for explanation.

Columns 1 - 5: Number of substructure vibration modes to be used as assumed displacement patterns.

10: Substructure output code. Punch 1 for printing of substructure frequency analysis. Punch 2 to include printing of $[K_{\ell\ell}^{-1}K_{\ell b}]$ transformation matrix and mass coupling arrays. Punch 3 to include reduced and unreduced global mass, stiffness and location matrices. Punch zero to prevent output.

11 - 15: Number of boundary nodes.

21 - 80: List of boundary nodes in any order. If more than 13 nodes need to be specified, continue list on additional cards as needed.

B7. COMMANDS FOR LUMPED MASSES AT NODES (I5,3F10.0,2I5,F10.0) - One card for each command.

See NOTE 5 for explanation.

Columns 1 - 5: Node number, or number of first node in a series of nodes covered by this command.

6 - 15: Mass associated with X displacement. May be zero.

16 - 25: Mass associated with Y displacement. May be zero.

26 - 35: Rotary inertia. May be zero.

36 - 40: Number of last node in series. Leave blank for a single node.

41 - 45: Node number difference between successive nodes in series. If blank or zero, assumed to be equal to 1.

46 - 55: Modifying factor by which masses are to be divided. If blank or zero, the factor from the preceding command is assumed, so that if the same factor applies for all commands, it needs to be specified for the first command only. This factor will typically be g, in which case the mass values will be given as weights.

C. LOAD INFORMATION

C1. LOAD CONTROL INFORMATION (3I5,6F10.0,I5) - ONE CARD

Columns 5: Static load code. Punch 1 if static loads are to be applied before the dynamic loads. Leave blank or punch zero if there are no static loads.

6 - 10: Number of commands specifying static loads applied directly at the nodes. See Section C2. Leave blank or punch zero if there are no static loads applied directly at the nodes.

11 - 15: Number of integration time steps to be considered in the dynamic analysis.

16 - 25: Integration time step, Δt.

26 - 35: Magnification factor to be applied to ground accelerations specified for the X direction. See NOTE 6 for explanation.

36 - 45: Magnification factor to be applied to time scale of the acceleration record specified for the X direction. See NOTE 6.

46 - 55: Magnification factor for ground accelerations in Y direction.

56 - 65: Magnification factor for time scale in Y direction.

66 - 75: Absolute value of the maximum displacement permitted before the structure can be assumed to have collapsed. The execution is terminated if this value is exceeded at any step. If zero or blank, assumed to be very high.

76 - 80: Number of lowest squared radial frequencies and corresponding mode shapes to be determined.

C2. COMMANDS FOR STATIC LOADS APPLIED DIRECTLY AT NODES (I5,3F10.0, 2I5) - ONE CARD FOR EACH COMMAND.

Omit if there are no static loads applied directly at nodes. If the static load code (Card C1) is zero or blank the loads will be read and printed, but are otherwise ignored.

Columns 1 - 5: Node number, or number of first node in a series of nodes covered by this command.

6 - 15: Load in X direction, the same on all nodes in the series.

16 - 25: Load in Y direction, the same on all nodes in the series. Note that the Y direction will normally be positive upwards.

26 - 35: Moment load (right hand screw rule about the Z axis - hence counterclockwise positive as normally viewed).

36 - 40: Number of last node in series. Leave blank for a single node.

41 - 45: Node number difference (constant) between successive nodes in series. If blank or zero, assumed to be equal to 1.

Note: A single node may appear in two or more commands if desired. In such a case, the total loads applied at the node will be the sum of the loads from the separate commands.

C3. ACCELERATION RECORDS

C3(a) CONTROL INFORMATION (4I5, 10A6) - ONE CARD

Columns 1 - 5: Number of time-acceleration pairs defining ground motion in X direction (NPTH). Punch zero or leave blank for no ground motion in this direction.

6 - 10: Number of time-acceleration pairs defining ground motion in Y direction (NPTV). Punch zero or leave blank for no ground motion in this direction.

15: Code for printing accelerations as input. Leave blank or punch zero for no output. Punch 1 to get listing of acceleration record.

20: Code for printing of acceleration as interpolated at intervals of Δt. Leave blank or punch zero for no output. Punch 1 to get listing of acceleration record.

21 - 80 Title to identify records, to be printed with output.

C3(b) GROUND ACCELERATION TIME HISTORY IN X DIRECTION (12F6.0)

As many cards as needed to specify NPTH time-acceleration pairs, 6 pairs to a card, assumed to be in acceleration units (not multiples of the acceleration due to gravity). Omit if NPTH equals zero. Note that both the acceleration and time scales may be magnified if desired (see Section C1). If the record is input in terms of the acceleration due to gravity, an acceleration magnification factor equal to g may be used to convert to acceleration units.

The first specified time must be zero, and the first ground acceleration must also be zero.

C3(c) GROUND ACCELERATION TIME HISTORY IN Y DIRECTION (12F6.0)

As many cards as needed to specify NPTV time-acceleration pairs. Omit if NPTV equals zero.

C4. DAMPING INFORMATION (4F10.0) - ONE CARD

See NOTE 7 for explanation.

Columns 1 - 10: Mass proportional damping factor, α.

11 - 20: Stiffness proportional damping factor, β, for current tangent stiffness.

21 - 30: Stiffness proportional damping factor, β_o, for original elastic stiffness.

31 - 40: "Structural" damping factor, δ, not compatible with substructured analysis.

D. TIME HISTORY OUTPUT SPECIFICATION

Printed time histories of selected nodal displacements and element results at selected time intervals may be obtained if desired. Envelope values of all nodal displacements and element results are automatically printed at the end of the computation and if the specified maximum displacement should be exceeded. Intermediate results envelopes may be printed at selected time intervals.

Time history values may be printed as the computation progresses, at the end of the computation only, or in both of these forms. The printouts at the end of the computation are ordered element by element and node by node, rather than time step by time step, and hence are both more compact and more convenient for use in plotting time history graphs. These re-ordered time histories may also be saved on tape for subsequent machine plotting or other processing

D1. CONTROL INFORMATION (13I5) - ONE CARD

Columns 1 - 5: Time interval for printout of nodal displacement time histories, expressed as a multiple of the time step Δt. Leave blank for no printout. The nodes for which time histories are required are specified in Sections D2 through D6.

6 - 10: Time interval for printout of time histories of element results, expressed as a multiple of the time step Δt. Leave blank for no printout. The elements for which time histories are required are specified in Section E.

11 - 15: Time interval for intermediate printout of envelope values, expressed as a multiple of the time step Δt. Leave blank for no intermediate printout. Envelope values are automatically printed at the end of the response period.

16 - 20: Number of nodes (NHOUT) for which X displacement time histories are required.

21 - 25: Number of nodes (NVOUT) for which Y displacement time histories are required.

26 - 30: Number of nodes (NROUT) for which rotation time histories are required.

31 - 35: Number of pairs of nodes (NHR) for which time histories of relative X displacement are required.

36 - 40: Number of pairs of nodes (NVR) for which time histories of relative Y displacement are required.

45: Time history print code for nodal displacement time histories, as follows:

(a) Zero or blank: time history printout only as the computation progresses.

(b) 1: both a printout as the computation progresses and a re-ordered printout at the end of the computation.

(c) 2: only a re-ordered printout at the end of the computation.

50: Time history print code for relative nodal displacement time histories. Zero, 1 or 2 as for the preceding code.

55: Time history print code for element results time histories. Zero, 1 or 2 as for the preceding code.

56 - 60: Tape storage code for saving re-ordered time histories of nodal displacements and relative displacements, as follows:

(a) Zero or blank: The re-ordered time histories are printed but not saved on tape.

(b) Nonzero: The re-ordered time histories are printed and also written on output unit TAPE7. See Note following for further explanation.

61 - 65: Tape storage code for saving re-ordered time histories of element results. Zero or nonzero, as for preceding code.

Note: If the tape storage code is nonzero, each printed line of time history data in the re-ordered time history (i.e., the printed output excluding any headings) is written, non-formatted, on I/O

unit TAPE 7, one record per printed line. That is, the printed time histories are directly reproduced on the file TAPE7.

This option will be used if routines are to be developed for computer plotting of the time history data. In such a case, TAPE7 will usually be equivalenced to a physical tape unit, so that the results will be saved on magnetic tapes for future processing.

At the beginning of any computer run, TAPE7 is rewound. If more than one problem is executed in the run, the time histories will appear sequentially on TAPE7, in the same sequence as the printed time histories.

The program does not write any problem identification data on TAPE7, nor does it explicitly place an end-of-file mark after the last record. To provide a record of the library number of the physical tape which has been used for any results set, it is suggested that the tape storage codes be set equal to the library number. The printed value of the code will then provide a record of the tape assigned to the subsequent time history output.

D2. LIST OF NODES FOR X DISPLACEMENT TIME HISTORIES (10I5)

As many cards as needed to specify NHOUT node numbers, punched ten to a card. Omit if NHOUT equals zero.

D3. LIST OF NODES OF Y DISPLACEMENT TIME HISTORIES (10I5)

As many cards as needed to specify NVOUT node numbers, punched ten to a card. Omit if NVOUT equals zero.

D4. LIST OF NODES FOR ROTATION TIME HISTORIES (10I5)

As many cards as needed to specify NROUT node numbers, punched ten to a card. Omit if NROUT equals zero.

D5. LIST OF NODES FOR RELATIVE X DISPLACEMENT TIME HISTORIES (10I5)

As many cards as needed to specify NHR pairs of node numbers, 5 pairs to a card. Omit if NHR equals zero. The printed displacement is the displacement of the first node of any pair minus the displacement of the second node.

D6. LIST OF NODES FOR RELATIVE Y DISPLACEMENT TIME HISTORIES (10I5)

As may cards as needed to specify NVR pairs of node numbers, 5 pairs to a card. Omit if NVR equals zero.

E. ELEMENT SPECIFICATION

For input and output, the elements must be divided into groups. All elements in any group must be of the same type, and typically all elements of a single type will be included in a single group. However, elements of the same type may be subdivided into separate groups if desired.

Elements may be input in any convenient sequence. Within any group, the elements must be numbered in sequence beginning with 1.

The total number of element groups may not exceed 10.

All flexural members within a linear substructure must be designated as linear beam elements. All truss bars are specified using the nonlinear truss element, but those within the substructure are automatically forced to behave linearly by the revised element subroutines. Presently, the semi-rigid connection and infill panel elements can not be used within a linear substructure.

All figures and appendices referenced in the element input instructions are contained in Reference A3.1, which should be consulted for more detailed information.

E1. TRUSS ELEMENTS

See Appendix B1 for description of element. Number of words of information per element = 35.

E1(a) CONTROL INFORMATION FOR GROUP (4I5) - ONE CARD

5: Punch 1 (to indicate that group consists of truss elements).

6 - 10: Number of Elements in group.

11 - 15: Number of different element stiffness types (max 40). See Section E1(b).

16 - 20: Number of different fixed end force patterns (max 40). See Section E1(c).

E1(b) STIFFNESS TYPES (I5, 5F10.0,I5) - ONE CARD FOR EACH STIFFNESS TYPE.

Columns 1 - 5: Stiffness type number, in sequence beginning with 1.

6 - 15: Young's modulus of elasticity.

16 - 25: Strain hardening modulus, as a proportion of Young's modulus.

26 - 35: Average cross sectional area.

36 - 45: Yield stress in tension.

46 - 55: Yield stress or elastic buckling stress in compression.

60: Buckling code. Punch 1 if element buckles elastically in compression. Punch zero or leave blank if element yields in compression, without buckling.

E1(c) FIXED END FORCE PATTERNS (2I5,4F10.0) - ONE CARD FOR EACH FIXED END FORCE PATTERN.

Omit if there are no fixed end forces. See Fig. B1.5.

Columns 1 - 5: Pattern number, in sequence beginning with 1

10: Axis code, as follows:

Code = 0: Forces are in the element coordinate system, as in Fig.B1.5a.

Code = 1: Forces are in the global coordinate system, as in Fig.B1.5b.

11 - 20: Clamping force F_i.

21 - 30: Clamping force V_i.

31 - 40: Clamping force F_j.

41 - 50: Clamping force V_j.

E1(d) ELEMENT GENERATION COMMANDS (9I5,2F5.0,F10.0) - ONE CARD FOR EACH GENERATION COMMAND.

Elements must be specified in increasing numerical order Cards for the first and last elements must be included. See NOTE 8 for explanation of generation procedure.

Columns 1 - 5: Element number, or number of first element in a sequentially numbered series of elements to be generated by this command.

6 - 10: Node number at element end i.

11 - 15: Node number at element end j.

16 - 20: Node number increment for element generation. If zero or blank, assumed to be equal to 1.

21 - 25: Stiffness type number.

30: Code for including geometric stiffness. Punch 1 if geometric stiffness is to be included. Leave blank or punch zero if geometric stiffness is to be ignored.

35: Time history output code. If a time history of element results is not required for the elements covered by this command, punch zero or leave blank. If a time history printout, at the intervals specified on card D1, is required, punch 1.

36 - 40: Fixed end force pattern number for static dead loads on element. Leave blank if there are no dead loads. See Note below.

41 - 45: Fixed end force pattern number for static live loads on element. Leave blank if there are no live loads.

46 - 50: Scale factor to be applied to fixed end forces due to static dead loads. Leave blank if there are no dead loads.

51 - 55: Scale factor to be applied to fixed end forces due to static live loads. Leave blank if there are no live loads.

56 - 65: Initial axial force on element, tension positive.

Note: If the static load code, Card C1, is zero but fixed end forces are still specified for some elements, an inconsistency results. In effect, any such fixed end forces will be treated as initial element forces.

E2. BEAM-COLUMN ELEMENTS

See Appendix B2 for description of element. Number of words of information per element - 141.

E2(a) CONTROL INFORMATION FOR GROUP (7I5) - ONE CARD

Columns 5: Punch 2 (to indicate that group consists of beam column elements).

6 - 10: Number of elements in group.

11 - 15: Number of different element stiffness types (max. 40). See Section E2(b).

16 - 20: Number of different end eccentricity types (max. 15). See Section E2(c).

21 - 25: Number of different yield interaction surfaces for cross sections (max. 40).

26 - 30: Number of different fixed end force patterns (max. 35). See Section E2(e).

31 - 35: Number of different initial element force patterns (max. 30). See Section E2(f).

E2(b) STIFFNESS TYPES (I5,4F10.0,3F5.0,2F10.0) - ONE CARD FOR EACH STIFFNESS TYPE.

Columns 1 - 5: Stiffness type number, in sequence beginning with 1.

6 - 15: Young's modulus of elasticity.

16 - 25: Strain hardening modulus, as a proportion of Young's modulus.

26 - 35: Average cross sectional area.

36 - 45: Reference moment of inertia.

46 - 50: Flexural stiffness factor k_{ii}.

51 - 55: Flexural stiffness factor k_{jj}.

56 - 60: Flexural stiffness factor K_{ij}.

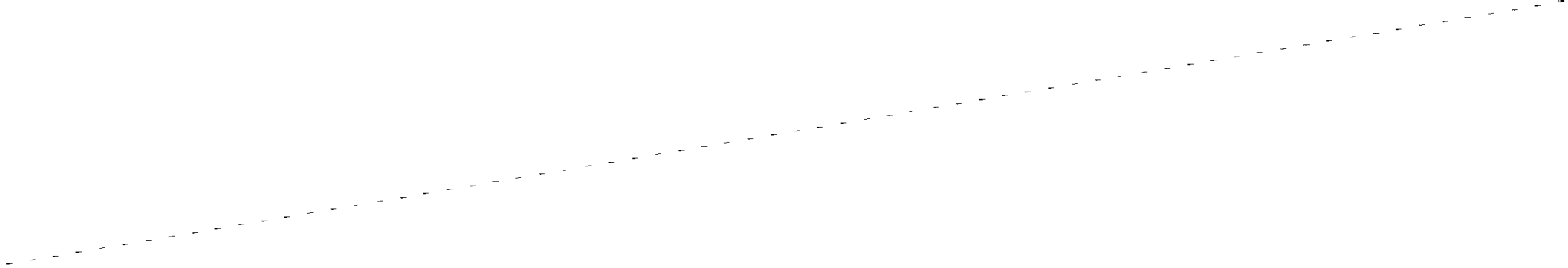

61 - 70: Effective shear area. Leave blank or punch zero if shear deformations are to be ignored, or if shear deformations have already been taken into account in computing the flexural stiffness factors.

71 - 80: Poisson's ratio (used for computing shear modulus, and required only if shear deformations are to be considered).

E2(c) END ECCENTRICITIES (I5,4F10.0) - ONE CARD FOR EACH END ECCENTRICITY TYPE.

Omit if there are no end eccentricities. See Fig. B2.6 for explanation. All eccentricities are measured from the node to the element end.

Columns 1 - 5: End eccentricity type number, in sequence beginning with 1.

6 - 15: X_i = X eccentricity at end i.

16 - 25: X_j = X eccentricity at end j.

26 - 35: Y_i = Y eccentricity at end i.

36 - 45: Y_j = Y eccentricity at end j.

E2(d) CROSS SECTION YIELD INTERACTION SURFACES (2I5,4F10.0,4F5.0) - ONE CARD FOR EACH YIELD SURFACE.

See Fig. B2.3 for explanation.

Columns 1 - 5: Yield surface number, in sequence beginning with 1.

10: Yield surface shape code, as follows:

Punch 1: Beam type, without P-M interaction.

Punch 2: Steel I-beam type.

Punch 3: Reinforced concrete column type.

11 - 20: Positive (sagging) yield moment, M_{y+}.

21 - 30: Negative (hogging) yield moment, M_{y-}.

31 - 40: Compression yield force, P_{yc}. Leave blank if shape code = 1.

51 - 55: M - coordinate of balance point A, as a proportion of M_{y+}. Leave blank if shape code = 1.

56 - 60: P - coordinate of balance point A, as a proportion of P_{yc}. Leave blank if shape code = 1.

61 - 65: M - coordinate of balance point B, as a proportion of M_{y-}. Leave blank if shape code = 1.

66 - 70: P - coordinate of balance point B, as a proportion of P_{yc}. Leave blank if shape code = 1.

E2(e) FIXED END FORCE PATTERNS (2I5,7F10.0) - ONE CARD FOR EACH FIXED END FORCE PATTERN.

Omit if there are no fixed end forces. See Fig. B2.5.

Columns 1 - 5: Pattern number, in sequence beginning with 1.

10: Axis code, as follows:

Code = 0: Forces are in the element coordinate system, as in Fig. B2.5a.

Code = 1: Forces are in the global coordinate system, as in Fig. B2.5b.

11 - 20: Clamping force, F_i.

21 - 30: Clamping force, V_i.

31 - 40: Clamping moment, M_i.

41 - 50: Clamping force, F_j.

51 - 60: Clamping force, V_j.

61 - 70: Clamping moment, M_j.

71 - 80: Live load reduction factor, for computation of live load forces to be applied to nodes. See Section B2.5, Appendix B2 for explanation.

E2(f) INITIAL ELEMENT FORCE PATTERNS (I5,6F10.0) - ONE CARD FOR EACH INITIAL FORCE PATTERN.

Omit if there are no initial forces: See Fig. B2.5a.

Columns 1 - 5: Pattern number, in sequence beginning with 1.

6 - 15: Initial axial force, F_i.

16 - 25: Initial shear force, V_i.

26 - 35: Initial moment, M_i.

36 - 45: Initial axial force, F_j.

46 - 55: Initial shear force, V_j.

56 - 65: Initial moment, M_j.

E2(g) ELEMENT GENERATION COMMANDS (12I5,2F5.0,I5,F5.0) - ONE CARD FOR EACH GENERATION COMMAND.

Elements must be specified in increasing numerical order. Cards for the first and last elements must be included. See NOTE 8 for explanation of generation procedure.

Columns 1 - 5: Element number, or number of first element in a sequentially numbered series of elements to be generated by this command.

6 - 10: Node number at element end i.

11 - 15: Node number at element end j.

16 - 20: Node number increment for element generation. If zero or blank, assumed to be equal to 1.

21 - 25: Stiffness type number.

26 - 30: End eccentricity type number. Leave blank or punch zero if there is no end eccentricity.

31 - 35: Yield surface number for element end i.

36 - 40: Yield surface number for element end j.

45: Code for including geometric stiffness. Punch 1 if geometric stiffness is to be included. Leave blank or punch zero if geometric stiffness is to be ignored.

50: Time history output code. If a time history of element results is not required for the element covered by this command, punch zero or leave blank. If a time history printout, at the intervals specified on card D1, is required, punch 1.

51 - 55: Fixed end force pattern number for static dead loads on element. Leave blank or punch zero if there are no dead loads. See Note below.

56 - 60: Fixed end forces pattern number for static live loads on element. Leave blank or punch zero there are no live loads.

61 - 65: Scale factor to be applied to fixed end forces due to static dead loads.

66 - 70: Scale factor to be applied to fixed end forces due to static live loads.

71 - 75: Initial force pattern number. Leave blank or punch zero if there are no initial forces.

76 - 80: Scale factor to be applied to initial element forces.

Note: If the static load code, Card C1, is zero but fixed end forces are still specified for some element, an inconsistency results. In effect, any such fixed end forces will be treated as initial element forces.

E3. INFILL PANEL ELEMENTS

See Appendix B3 for description of element. Number of words of information per element = 42.

E3(a) CONTROL INFORMATION FOR GROUP (3I5) - ONE CARD

Columns 5: Punch 3 (to indicate that group consists of infill panel elements).

6 - 10: Number of elements in group.

11 - 15: Number of different element stiffness types (max. 40). See Section E3(b).

E3(b) STIFFNESS TYPES (I5,5F10.0,I5) - ONE CARD FOR EACH STIFFNESS TYPE.

Columns 1 - 5: Stiffness type number, in sequence beginning with 1.

6 - 15: Shear modulus of elasticity.

16 - 25: Strain hardening shear modulus, as a proportion of shear modulus of elasticity.

26 - 35: Average thickness of panel.

36 - 45: Yield stress in shear.

46 - 55: Strain at complete failure, as a proportion of strain at yield. This must not be less than 1.0.

60: Failure code, governing type of behavior after failure. Punch 1 if strength and stiffness are to be reduced to zero after failure. Punch zero or leave blank if strength and stiffness of elastic (strain hardening) component is to be retained after failure.

E3(c) ELEMENT GENERATION COMMANDS (8I5,F10.0) - ONE CARD FOR EACH GENERATION COMMAND

Elements must be specified in increasing numerical order. Cards for the first and last elements must be included. See NOTE 8 for explanation of generation procedure.

Columns	1 - 5:	Element number, or number of first element in a sequentially numbered series of elements to be generated by this command.
	6 - 10:	Node number i. See Note below.
	11 - 15:	Node number j.
	16 - 20:	Node number k.
	21 - 25:	Node number ℓ.
	26 - 30:	Node number increment for element generation. If zero or blank assumed to be equal to 1.
	31 - 35:	Stiffness type number.
	40:	Time history output code. If a time history of element results is not required for elements covered by this command, punch zero or leave blank. If a time history printout, at the intervals specified on Card D1, is required, punch 1.
	41 - 50:	Initial shear stress in element.

Note: Node numbers i, j, k, ℓ must be in sequence clockwise around each element when viewed in the positive Z direction (that is, counter-clockwise as normally viewed).

E4. SEMI-RIGID CONNECTION ELEMENTS

See Appendix B4 for description of element. Number of words of information per element = 25.

E4(a) CONTROL INFORMATION FOR GROUP (3I5) - ONE CARD

Columns 5: Punch 4 (to indicate that group consists of semi-rigid connection elements).

6 - 10: Number of elements in Group.

11 - 15: Number of different element stiffness types (max. 40). See Section E4(b).

E4(b) STIFFNESS TYPES (I5,4F10.0) - ONE CARD FOR EACH STIFFNESS TYPE.

Columns 1 - 5: Stiffness type number, in sequence beginning with 1.

6 - 15: Initial rotational stiffness (moment per radian).

16 - 25: Strain hardening stiffness, as a proportion of initial rotational stiffness.

26 - 35: Positive yield moment. See Note below.

36 - 45: Negative yield moment.

Note: Positive rotation is rotation of node i clockwise relative to node j when viewed in the positive Z direction (that is, counter-clockwise as normally viewed). A positive moment in the connection tends to produce positive rotation.

E4(c) ELEMENT GENERATION COMMANDS (6I5),F10.0) - ONE CARD FOR EACH GENERATION COMMAND.

Elements must be specified in increasing numerical order. Cards for the first and last elements must be included. See NOTE 8 for explanation of generation procedure.

Columns 1 - 5: Element number or number of first element in a sequentially numbered series of elements to be generated by this command.

6 - 10: Node number i.

11 - 15: Node number j.

16 - 20: Node number increment for element generation. If zero or blank, assumed to be equal to 1.

21 - 25: Stiffness type number.

30: Time history output code. If a time history of element results is not required for elements covered by this command, punch zero or leave blank. If a time history printout, at the intervals specified on Card D1, is required, punch 1.

31 - 40: Initial moment in connection.

E5. BEAM ELEMENTS

The beam element is identical to the beam column element described in Appendix B2, except that only a beam type yield code is permitted.

The input data is identical to that for the beam column element (Section E2), except as follows:

(1) Punch 5 in column 5 of Card E2(a), to indicate that the group consists of beam elements.

(2) The term "yield moment values" is substituted for "yield interaction surfaces".

(3) The yield surface data on Cards E2(d) is unchanged. However, any data in columns 5 - 10 and 31 - 80 are ignored, and a beam type yield surface is automatically assumed.

Number of words of information per element = 97.

E6. BEAM ELEMENTS WITH DEGRADING STIFFNESS

See Report text for description of element. Number of words of information per element - 165.

E6(a) CONTROL INFORMATION FOR GROUP (7I5) - ONE CARD

5: Punch 6 (to indicate that group consists of beam elements with degrading stiffness).

6 - 10: Number of elements in group.

11 - 15: Number of different element stiffness types (max. = 40). See Section E6(b).

16 - 20: Number of different end eccentricity types (max. = 15). See Section E2(c).

21 - 25: Number of different yield moment values for cross sections (max. = 40). See Section (E2(d).

26 - 30: Number of different fixed end force patterns (max. = 34). See Section E2(e).

31 - 35: Number of different initial element force patterns (max. = 30). See Section E2(f)

E6(b) STIFFNESS TYPES - TWO CARDS FOR EACH STIFFNESS TYPE.

CARD 1: BEAM PROPERTIES CARD (I5,3F10.0,3F5.0,2F10.0)

Columns 1 - 5: Stiffness type number, in sequence beginning with 1.

6 - 15: EI, reference flexural stiffness.

16 - 25: EA, effective axial stiffness.

26 - 35: GA', effective shear stiffness, If blank or zero, shear deformations are neglected.

36 - 40: Flexural stiffness factor k_{ii}.

41 - 45: Flexural stiffness factor k_{jj}.

46 - 50: Flexural stiffness factor k_{ij}.

51 - 60: Strain hardening ratio for inelastic flexure at node i. If a nonzero hinge stiffness is specified for node i on CARD 2, columns 6-15, then this strain hardening ratio will apply

directly to the hinge moment-rotation relationship. Otherwise, this ratio will apply to the overall beam end moment-rotation relationship or cantilever P-δ relationship.

61 - 70: Strain hardening ratio for inelastic flexure at node j. As with node i, a zero or nonzero hinge stiffness for node j on CARD 2, columns 16-25 will control whether this ratio is directly applied to the hinge alone or to the beam as a whole.

CARD 2: HINGE PROPERTIES CARD (I5,7F10.0)

Leave blank to obtain Takeda model.

Columns 1 - 5: Stiffness type number, in sequence beginning with 1 and corresponding to the stiffness type number on the preceding BEAM PROPERTIES CARD.

6 - 15: Hinge stiffness at node j. Leave blank or zero if hinge properties are to be determined by the program (these properties are marked with * in the output). If blank or zero, the following field for node j must also be blank or zero. If nonzero, the following field must also be nonzero.

16 - 25: Hinge stiffness at node j.

26 - 35: α_i, unloading stiffness parameter for end i. Leave blank or zero for unloading according to Takeda model.

36 - 45: α_j, unloading stiffness parameter for end j. Leave blank or zero for unloading according to Takeda model.

46 - 55: β_i, loading parameter for end i. Leave blank or zero for reloading according to Takeda model.

56 - 65: β_j, loading parameter for end j. Leave blank or zero for reloading according to Takeda model.

66 - 75: N, loading exponential parameter.

E6(c) through E6(g) These sections are identical to section E2(c) through E2(g).

NOTE ON SIGN CONVENTION

The sign convention used for output of bending moments for the reinforced concrete beam element differs from that for the other beam elements.

(1) Other elements:

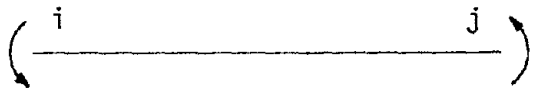

as noted in the report

(2) RC beam elements:

E7. LINEAR BEAM ELEMENTS

The linear beam element is identical to the beam element except that it is assumed to have unlimited elastic load capacity.

The input data is identical to that for the beam column element (Section E2), except as follows.

(1) Punch 7 in column 5 of Card E2(a), to indicate that the group consists of linear beam elements.

(2) Although yield interaction surface information will be read if specified, it is not needed and will be subsequently ignored.

Number of words of information per element = 72

All flexural members within a linear substructure must be designated as linear beam elements.

F. NEXT PROBLEM

The data for a new problem may follow immediately, starting with card A.

G. TERMINATION CARD (A4) - One card to terminate the complete data deck.

Columns 1 - 4: Punch the work STOP

NOTES

NOTE 1. NODE COORDINATE SPECIFICATION

The "control node" coordinates must be defined with respect the X, Y coordinate system. The coordinates of the remaining nodes may be generated using straight line generation commands (Section B3). The number of nodes generated by each command may be one or any larger number. The coordinates of the two nodes at the beginning and end of the generation line must have been previously defined, either by direct specification or by previous straight line generation.

It is not necessary to provide generation commands for nodes which are (a) sequentially numbered between the beginning and end nodes of any straight line, and (b) equally spaced along that line. After all generation commands have been executed, the coordinates for each group of unspecified nodes are automatically generated assuming sequential numbering and equal spacing along lines joining the specified nodes immediately preceding and following the group. That is, any generation command with equal spacing and a node number difference of one is superfluous.

NOTE 2. NODES WITH ZERO DISPLACEMENTS

Each node of the structure may have up to three degrees of freedom, namely X displacement, Y displacement and rotation. These are all displacements relative to the ground.

Initially the program assumes that all three degrees of freedom are present at all nodes (code = 0), and initializes the data arrays accordingly. If this assumption is correct, the cards of Section B4 should be omitted. In some cases, however, either (a) certain nodes may be fixed relative to the ground in certain directions or (b) it may be reasonable to assume zero displacement. Any degree of freedom which is fixed is to be assigned a code = 1, and cards must be included in Section B4 to specify those nodes and degrees of freedom for which the codes are equal to 1.

If there is any doubt, it should be assumed that all nodes can displace with all three degrees of freedom (i.e. all codes = 0). If however, certain degrees of freedom can be eliminated, the computer time may be significantly reduced.

NOTE 3. NODES WITH IDENTICAL DISPLACEMENTS

It may often be reasonable to assume that certain nodes displace identically in certain directions. Identical displacements may be specified by the commands of Section B5. The input format for this section limit to 14 the number of nodes covered by any single command. If more than 14 nodes are to be assigned identical displacements, two or more commands should be used, with the nodes in increasing numerical order in each command, and with the smallest numbered node common to all commands.

As with displacements which are constrained to be zero, greater computational efficiency may be achieved by specifying identical displacements. However, whereas the specification of zero

displacements will always decrease the structure stiffness band width or leave it unchanged, specification of identical displacements may increase this band width. The effect may be to increase the required structure stiffness storage and/or the computational effort required to solve the equilibrium equations. Identical displacements should therefore be specified with caution, and their effects on storage requirements and execution times should be investigated. It should be noted that the equation solver used in the program is much less sensitive to local increases in stiffness matrix band width than solvers based on a banded storage scheme.

NOTE 4. SUBSTRUCTURE SPECIFICATION

The user must specify the number of assumed modal displacement patterns to be utilized and the number of boundary nodes. The boundary of the substructure is specified by listing the node numbers in any order. The structure's nodes must be numbered so that the linear degrees of freedom will have the lowest dof numbers. A single identical displacement command should not include nodes on opposite sides of the substructure boundary.

NOTE 5. SPECIFICATION OF LUMPED MASSES

The specification commands for lumped masses will generally permit the user to input the nodal masses with only a few cards. Any node may, if desired, appear in more than one specification command. In such cases the mass associated with any degree of freedom will be the sum of the masses specified in the separate commands. If

certain nodes are constrained to have an identical displacement, the mass associated with this displacement will be the sum of the masses specified for the individual nodes.

Note that the masses are to be input in units of mass rather than weight, but that values numerically equal to the weight may be input if an appropriate modifying factor is specified.

NOTE 6. SCALING OF EARTHQUAKE RECORDS

The acceleration scale factors may be used to increase or decrease the ground accelerations, or to convert from multiples of the acceleration due to gravity to acceleration units, or both. Modification of the earthquake intensity by scaling the acceleration values is a common practice in research investigations, but should be undertaken cautiously in practical applications. When the accelerations are scaled, the ground velocities and displacements are scaled in the same proportion.

Provision is also made to modify the time scale. If a time scale factor equal to, say, f, is specified, all input times are multiplied by f before obtaining the interpolated accelerations at intervals equal to the integration time step. If the ground accelerations remain unchanged, the effect is to increase the ground velocities by f and the ground displacements by f^2, and to alter the frequency content of the earthquake. Time scale modifications should not be made without carefully considering their influence on the ground motion.

NOTE 7. DAMPING

Damping of four different types may be specified, singly or in any combination. These are as follows:

(1) Mass-proportional damping, in which a viscous damping matrix $C = \alpha M$ is assumed, where M = mass matrix. The procedure for calculating α is reviewed in Reference A3.1.

(2) Stiffness proportional damping, in which a viscous damping matrix $C = \beta K_T$ is assumed, where K_T = current tangent stiffness matrix at any time, including any geometric stiffnesses.

(3) Stiffness proportional damping, in which a viscous damping matrix $C = \beta_0 K_0$ is assumed, where K_0 = original elastic stiffness matrix ignoring the geometric stiffness.

(4) "Structural" damping, in which damping forces are assumed such that (a) the magnitudes of the damping forces originating within any element are a multiple, δ, of the absolute values of the element actions (axial forces, end moments, etc.), and (b) the direction of each damping action is such that it opposes the rate of change of the corresponding element deformation. No viscous damping matrix is assumed. Instead, damping forces in any time step are applied, based on the number actions and rates of deformation existing at the end of the previous step. The member actions used to calculate the damping forces are the total actions, including both static and dynamic effects. The damping forces are first applied in the second time step.

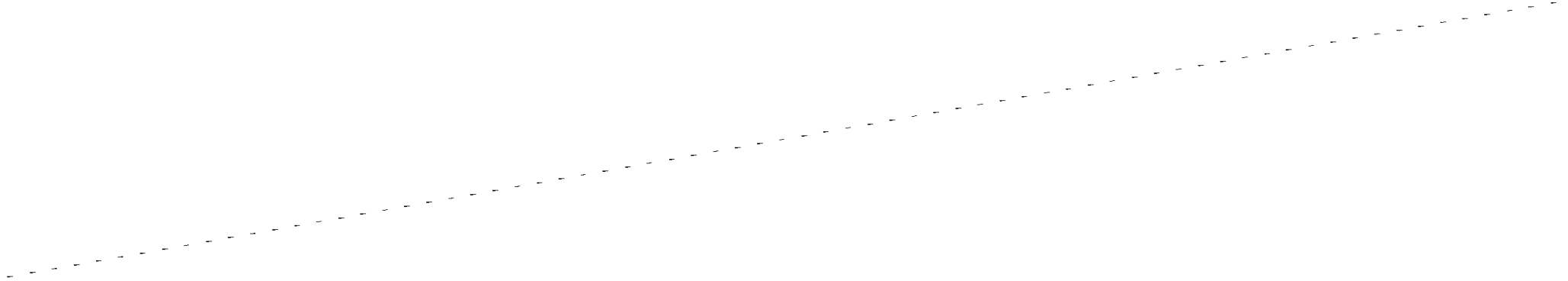

Little use appears to have been made of the "structural" damping concept, and hence little experience is available, especially for inelastic structures. A possible problem is that the damping forces may tend to accentuate small oscillations in the numerical computations, because the damping forces in any step are always based on the state at the end of the previous step. Until experience is gained, this option should be used cautiously. It is included in the program primarily for research reasons.

NOTE 8. ELEMENT DATA GENERATION

In the element generation commands, the elements must be specified in increasing numerical order. Cards may be provided for sequentially numbered elements, in which case each card specifies one element and the generation option is not used. Alternatively, the cards for a group of elements may be omitted, in which case the data for the missing group is generated as follows:

1. All elements are assigned the same stiffnesses, strengths, element load data, output codes, etc., as the element preceding the missing group.
2. The numbers of the nodes for each missing element are obtained by adding the specified node number increment to the node numbers for the preceding element. The node number increment is that specified for the element preceding the missing group.

In the printout of the element data, generated data is identified by an asterisk at the beginning of the printed line.